UNIVERSITY OF CALIFORNIA
SANTA CRUZ

PROBING GAMMA RAYS FROM MEV-SCALE DARK MATTER WITH EFFECTIVE FIELD THEORY

A dissertation submitted in partial satisfaction of the
requirements for the degree of

DOCTOR OF PHILOSOPHY

in

PHYSICS

by

Adam Coogan

September 2018

The Dissertation of Adam Coogan
is approved:

Stefano Profumo, Chair

Michael Dine

Tesla Jeltema

Lori Kletzer
Vice Provost and Dean of Graduate Studies

Table of Contents

List of Figures

List of Tables

Abstract

Probing Gamma Rays from MeV-Scale Dark Matter with Effective Field Theory

by

Adam Coogan

Experiments have recently placed stringent constraints on the most natural incarnations of weakly interacting massive particles (WIMPs), which motivates exploring alternative dark matter (DM) candidates. One interesting possibility is that DM has mass at the MeV scale. Indirect detection of gamma rays produced in its self-annihilations is a particularly timely subject since proposed telescopes such as e-ASTROGAM are poised to revolutionize our understanding of the MeV gamma ray spectrum.

This thesis presents a comprehensive analysis of how existing and future gamma ray detectors can probe three realistic simplified models of MeV DM. After employing chiral perturbation theory to write down effective Lagrangians for the DM's interactions with mesons, the relevant strongly interacting degrees of freedom at the MeV scale, the gamma-ray spectra for DM annihilation are computed in detail. The final state radiation from annihilation into leptons and charged pions is calculated exactly, and contributions to the charged pion decay spectrum are accounted for at each step of the decay chain. The electron and positron spectra are also determined in these models and used to derive accurate cosmic microwave background (CMB) constraints. A common concern is that CMB constraints rule out the possibility of detecting photons from MeV DM. This is found not to be the case over most of the parameter space of the simplified models, with e-ASTROGAM providing stronger constraints even when the DM annihilates in an s-wave. For p-wave DM, e-ASTROGAM will place bounds approaching the thermal relic cross section.

To my parents, Jay and Kathleen,

for their love and for showing me how to live full lives.

Acknowledgments

I am so thankful to the people and opportunities I have been surrounded with that have helped me become a physicist.

My advisor, Stefano Profumo, has been a font of ideas and a strong supporter since I first met him on the visit day to UC Santa Cruz. In our group meetings I learned to determine what is worth working on as well as how to clarify and present a project's central lessons. I will especially remember his encouragement to "converge". Aside from suggesting the project that turned into this thesis, Francesco D'Eramo has also been a great mentor, with a focus on being "correct" rather than "first". Thanks to Michael Dine for always being willing to take an hour to talk about research roadblocks at any given time.

I am lucky to have struck up a wonderful physics partnership with Logan Morrison, a tireless collaborator on the research in this thesis. I admire his measured, thoughtful approach to physics and programming. Working closely with him (often texting until late in the night) has pushed me to refine my thinking, write cleaner code, and generally be a better physicist.

Many other astro/particle theory graduate students, postdocs and office mates at UC Santa Cruz have been a source of great physics conversations, support and friendship throughout the years: Nicolas Fernandez, Eric Carlson, Jonathan Cornell, Benjamin Lehmann, Di Xu, Laurel Haskin-Stephenson, Emma Storm, Laura Fava, William Shepherd and Patrick Draper.

I have had the privilege of being a student at excellent schools throughout my life. The teachers and students at my middle and high school, Moses Brown, created a culture where learning and creativity were deeply valued. Ruth Breindel, Ransom Griffin, Bruce Shaw, Dr Moss, Jamie German and George Tsakraklides particularly encouraged me to pursue my wide-ranging interests ranging from

Latin history to building a working trebuchet to making up physics problems with my friend Dylan Rankin in the back of my calculus class.

Brown University was an incredible intellectual community where I learned equally from my professors and peers. Special thanks to my fellow physics majors and life-long friends Michael Wagman, Thomas Iadecola and Matthew Dodelson for ignoring prerequisites and soldiering through long nights. My work style has been shaped by each of them, and I am excited to see each of them continuing in their promising physics careers. I am also grateful to my research mentors Ian Dell'Antonio, Meenakshi Narain, and particularly Richard Gaitskell for giving me the opportunity to work on the LUX detector and reminding me to always look at the raw data carefully before doing complicated analyses.

During graduate school I benefited from classes taught by Anthony Aguirre, Michael Dine, Howie Haber. Other graduate students have been friends, housemates and homework buddies over the years: Alice Durand, Natasha Woods, Adam Reyes, Brendan Wells, Caitlin Johnson, Devon Hollowood, Sheena Scheer and Stephen Martin. Ram Akella, Francesco Avanzi, Zeshi Zheng and Martha Conklin provided me the unique opportunity to live a double life as a machine learning/hydrology researcher. This experience played a key role in helping me secure my upcoming postdoctoral research position.

Most of all I want to thank my parents, Jay and Kathleen, and sister, Eliza, for their unending love and support. They have constantly nurtured my love of learning and passions for science, art, culture and travel. One especially important moment was in fourth grade when we found Brian Greene's excellent popular science book *The Elegant Universe* in an airport bookstore: reading it made me decide to become a physicist. Words do not do justice to how thankful I am to them for everything.

Last but not least, thanks so much to my partner Laura Henn for her support through the highs and lows of graduate school, the many adventures we have had together, giving me a different perspective on life, and joining me for the next adventure in Amsterdam.

Chapter 1

Introduction

While weakly interacting massive particles (WIMPs) have been the favorite dark matter candidate since the 1980s, they are facing increasing pressure from experiments. There are good reasons for the WIMP's popularity. Assuming thermal production via freeze-in [66], dark matter (DM) with a weak-scale mass m_χ and self-annihilation cross section $\sigma_{\bar{\chi}\chi}$ gives the correct relic density. The perturbative unitarity bound $m_\chi \lesssim 100$ TeV suggests DM should not be much heavier than the weak scale. If the DM really does interact via the weak interaction analogously to a heavy neutrino, m_χ must be greater than roughly 1 GeV [95].[1] While m_χ and $\sigma_{\bar{\chi}\chi}$ need not be electroweak-scale to give the correct relic density, new physics is expected between the weak and TeV scales in any case to solve the hierarchy problem. Supersymmetry (SUSY) achieves this elegantly and furthermore provides a WIMP in the form of the neutralino [104].

However, concerted experimental efforts at colliders and related experiments, direct detection experiments, and in astrophysical searches for features in gamma rays and cosmic ray antimatter have found signatures of neither the most straightforward WIMP models nor SUSY [11]. As an example of one of the many stringent

[1] This fact is known as the Lee-Weinberg limit after its discoverers.

bounds, under the assumption that DM is thermally produced the Fermi-LAT telescope's non-detections of dwarf spheroidal galaxies have ruled out WIMPs with mass 1 GeV $\lesssim m_\chi \lesssim$ 100 GeV [3].

An interesting possibility is that the DM instead has a mass at the MeV scale.[2] Detecting MeV-scale DM is challenging. Direct detection experiments, for example, are typically insensitive to nuclear recoils below $\sim$ 1 GeV since the recoil energy scales as m_χ^2, though novel detectors have recently been proposed to address this issue [89]. Numerous existing terrestrial, cosmological and astrophysical constraints apply to MeV-scale dark matter [90, 49, 89].

As with WIMPs, the annihilation of MeV-scale DM can produce features in the electromagnetic spectrum. Gamma rays from this process would lie predominantly in the range $\mathcal{O}(100\text{ keV} - 1\text{ GeV})$, which includes the neutral pion decay peak centered at $\sim$ 70 MeV. This energy window was last explored by COMPTEL [132] and EGRET [76] in the 1990s, leading to a couple order of magnitude sensitivity gap relative to the $\gtrsim$ 1 GeV and x-ray portions of the electromagnetic spectrum. Several experiments have been proposed to close this gap: GAMMA-400 [60], GRIPS [68], Advanced Compton Telescope (ACT) [25], Advanced Energetic Pair Telescope (AdEPT) [77], PINGU [144], AMIGO[3]. The most mature proposal is e-ASTROGAM's [135], which is aiming to fly in the 2030s.[4] Its projected point-source continuum sensitivity is compared to other experiments in Figure 1.1.

In this thesis, I address the major problem of constructing realistic particle physics models of MeV-scale dark matter and accurately computing the resulting gamma ray spectra from self-annihilation, with a focus on hadronic final states.

The analysis will focus on three simplified models consisting of Dirac fermion

[2]Note that while the DM mass could be as low as a few keV before it becomes a warm relic and affects structure formation [24], I will not consider DM below the MeV scale in this thesis.

[3]See `https://pcos.gsfc.nasa.gov/physpag/probe/AMEGO_probe.pdf`

[4]Also see `http://eastrogam.iaps.inaf.it/`.

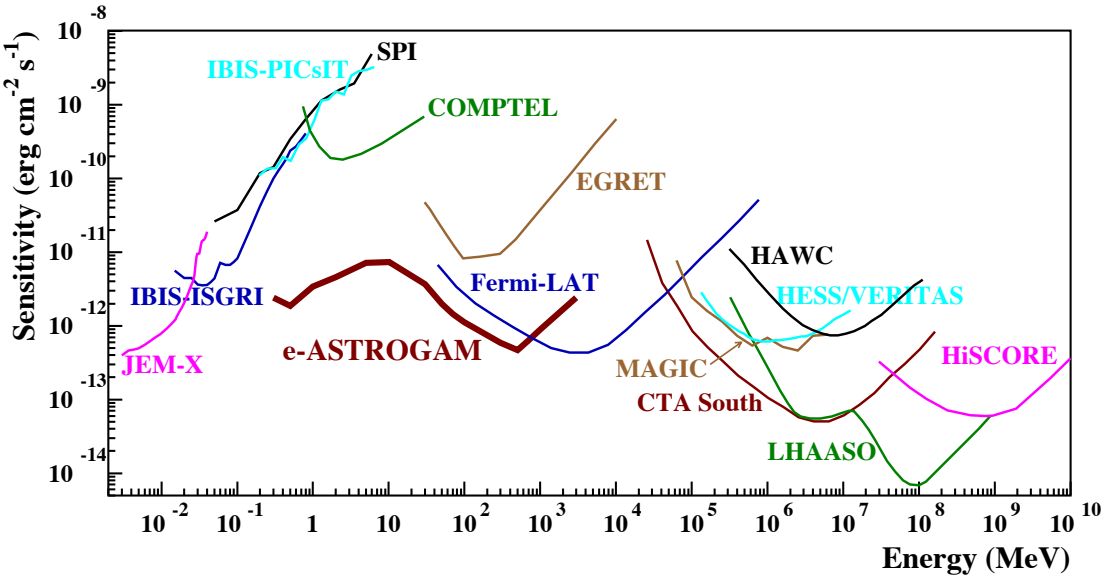

Figure 1.1: The point source continuum sensitivity for e-ASTROGAM and several other gamma- and x-ray instruments. The sensitivity was computed at 3σ assuming an effective exposure time of 1 year for a source at high galactic latitude. The plot is taken from the e-ASTROGAM whitebook [135].

dark matter χ along with a new particle mediating its interactions with the Standard Model, including quarks and gluons. Since QCD confines below $\Lambda_{\rm QCD} \sim 1$ GeV perturbative QCD is invalid in this regime, where the relevant degrees of freedom are mesons, a substantial difference compared to the WIMP case. In Chapter 3 I describe in detail how the effective theory of mesons, chiral perturbation theory (chiPT), is constructed, and apply this to the simplified models of MeV DM. While dimensional analysis suggests the range of the validity for chiPT is $2m_\chi \lesssim \Lambda_{\rm QCD}$, resonances such as the ρ and the exotic $f_0(500)$ scalar spoil this, so I restrict to $2m_\chi < 500$ MeV throughout this thesis. Approaches that can extend this analysis to higher DM masses are discussed in sec. 6.2 of the conclusion.

After constructing the effective field theory for MeV-scale dark matter, gamma ray spectra are computed in detail in Chapter 4. The final state radiation (FSR) spectrum for leptons is computed exactly, and for the first time the FSR spectrum

for the charged pion final state is included. Contributions to the radiative charged pion decay spectrum are analyzed in detail. The resulting DM annihilation spectra are utilized to determine constraints on the DM self-annihilation cross section from COMPTEL, EGRET, Fermi-LAT and e-ASTROGAM in Chapter 5.

As discussed in section 5.4, various features of the CMB can be modified by energy injected by residual DM annihilations if the self-annihilation cross section is large enough. Since a critical concern is that CMB constraints rule of the possibility of indirectly detecting MeV DM, the e^+/e^- spectra from DM annihilation are also derived and used to accurately compute this bound. An interesting result of this thesis is that the constraints derived for e-ASTROGAM are often stronger than those from CMB, even for DM annihilating in an s-wave. The e^+/e^- spectra are also important inputs for accounting for secondary gamma ray emission, which is not treated in this work.

Before launching into the analysis, I will briefly summarize related work on indirect detection of MeV-scale DM, and how the analysis herein differs.

- Gonzalez-Morales et al [67] discuss CMB bounds and indirect detection, but focus on annihilation into individual final states. The Altarelli-Parisi approximation for the muon FSR spectrum employed is not valid for $\mathcal{O}(100$ MeV) center of mass energies (this is discussed in sec. 4.2), and it is unclear whether the muon's subsequent radiative decay was accounted for. Myself and Logan Morrison provided the code to compute the gamma ray and positron spectra from DM annihilating into $\pi^+\pi^-$ followed by pion decay, but FSR was not included. They find that CMB constraints rule out indirect detection of $\bar{\chi}\chi \to \pi^+\pi^-$ in dwarf spheroidals but possibly not in the Galactic Center.

- Bartels et al [17] studied the channels $\gamma\gamma$, $\pi^0\gamma$, $\pi^0\pi^0$, $\bar{\ell}\ell$, again making the assumption that DM annihilates only into one of these states. The lepton

spectra were also computed with the Altarelli-Parisi approximation. Unlike this thesis they include secondary gamma ray emission, and use a more detailed statistical analysis. In chapter 5 their background model is used in determining the expected limits from e-ASTROGAM. I have checked that I obtain comparable limits to them when restricting my analysis to individual final states.

- Essig et al [54] performed a thorough analysis of the discovery prospects for final states including electrons and photons, but not hadrons, focusing primarily on lower DM masses.

- Boddy and Kumar [22] considered the $\gamma\gamma$, $\pi^0\gamma$ and $\pi^0\pi^0$ final states. Their background model is a power law fit to existing MeV gamma ray data and they use the dwarf spheroidal Draco as the target for computing projected limits for several proposed telescopes. Substituting this model for the one adopted in this thesis leads to slightly weaker projected limits.

Chapter 2

Microscopic Models

The starting point for this analysis is a set of microscopic models that include the dark matter particle χ, taken to be a Dirac fermion, and a mediator that interacts with χ and Standard Model (SM) fields. The mediator particle is required since renormalizable, gauge-invariant interactions involving only the SM fields and χ are forbidden. Additionally, in accordance with the Lee-Weinberg bound, the mediator is requisite for χ's self-annihilation cross section to be large enough to avoid overclosing the universe. In this chapter Lagrangians are presented for the cases where the mediator is a real scalar, vector and pseudoscalar mediator are considered here; the axial vector mediator can be analyzed using similar techniques and is left for future work. UV completions are also described to motivate each model, and connected to the parameterizations chosen here.

In each of the models, χ and the mediator fields are taken to be singlets under the SM gauge group $\mathrm{SU}(3)_C \times \mathrm{SU}(2)_L \times \mathrm{U}(1)_Y$. The models are defined by a Lagrangian just above the confinement scale ($\sim$ 1 GeV), where the SM fields c, b, t, τ, h, $W^{\pm}$ and Z have been integrated out. Effective interactions with mass dimension up to five are considered, with mass scales proportional to the Higgs vacuum expectation value (vev) $v_h = 246$ GeV.

2.1 Scalar Simplified Model

Letting S be the scalar mediator, the Lagrangian is taken to be

$$\mathcal{L}_{>1\text{ GeV}}|_S = \frac{3\alpha_s}{4\pi v_h} g_{SG} S G^a_{\mu\nu} G^{a\mu\nu} - g_{Sf} S \sum_{q=u,d,s} \frac{m_q}{v_h} \bar{q} q \tag{2.1}$$

$$+ \mathcal{L}_{S,\text{free}} + \mathcal{L}_{\chi,\text{free}} + \mathcal{L}_{\text{QED}} + \mathcal{L}^{(2)}_{\text{chiPT+EM}} + \mathcal{L}_{S,\text{int}} \tag{2.2}$$

$$\mathcal{L}_{S,\text{free}} = \frac{1}{2}(\partial_\mu S)^2 - \frac{1}{2} m_S^2 S^2 \tag{2.3}$$

$$\mathcal{L}_{\chi,\text{free}} = \bar{\chi}(i\not{\partial} - m_\chi)\chi \tag{2.4}$$

$$\mathcal{L}_{\text{QED}} = -\frac{1}{4} F_{\mu\nu} F^{\mu\nu} + \sum_{\ell=e,\mu} \bar{\ell}(i\not{D} - m_\ell)\ell \tag{2.5}$$

$$\mathcal{L}_{S,\text{int}} = -g_{S\chi} S \bar{\chi}\chi - \frac{5\alpha_{\text{EM}}}{24\pi v_h} g_{SF} S F_{\mu\nu} F^{\mu\nu} - g_{Sf} S \sum_{\ell=e,\mu} \frac{m_f}{v_h} \bar{\ell}\ell. \tag{2.6}$$

The Lagrangian is written in this form to highlight the terms in the first line, which will be the ones matched onto the chiral Lagrangian. The Lagrangians for the other simplified models will be presented in a similar manner. I have assumed minimal flavor violation (MFV), which is the hypothesis that all flavor violation originates from the SM Yukawa matrices Y_U, Y_D and Y_e [39, 46]. Without this assumption, flavor changing neutral currents (FCNC) processes such as the rare decays $B^+ \to SK^+$ and $K^+ \to S\pi^+$ can proceed at rates inconsistent with observations. The same constant of proportionality was chosen for all the Yukawas to avoid inducing shifts in the mesons' masses that are challenging to compute.

2.1.1 UV Completions

This model's couplings arise in the most natural UV completion of this Lagrangian: the Higgs portal model, which is one of the simplest ways of coupling a hidden sector to the Standard Model [120]. The scalar sector of the renormalizable

electroweak-scale Lagrangian for the Higgs portal model is

$$\mathcal{L}_{\text{HP,int}} = \frac{1}{2}|D_\mu \tilde{H}|^2 + \frac{1}{2}(\partial_\mu \tilde{S})^2 + V_{\text{HP}}(\tilde{S}, \tilde{H}), \tag{2.7}$$

$$V_{\text{HP}}(\tilde{S}, \tilde{H}) \equiv -\mu^2 \tilde{H}^\dagger \tilde{H} + \lambda(\tilde{H}^\dagger \tilde{H})^2 + \frac{1}{2}\mu_{\tilde{S}}^2 + \epsilon_1(\tilde{H}^\dagger \tilde{H})\tilde{S} + \epsilon_2(\tilde{H}^\dagger \tilde{H})\tilde{S}^2 + V(S). \tag{2.8}$$

The tildes denote that the fields are interaction eigenstates. After electroweak symmetry breaking $\tilde{H} \to \frac{1}{\sqrt{2}}(0, v_h + \tilde{h})$, and the quadratic part of the potential becomes

$$V_{\text{HP}} \supset -\frac{1}{2}\begin{pmatrix}\tilde{h} & \tilde{S}\end{pmatrix}\begin{pmatrix} m_{\tilde{H}}^2 & \epsilon_1 v_h \\ \epsilon_1 v_h & m_{\tilde{S}}^2 \end{pmatrix}\begin{pmatrix}\tilde{h} \\ \tilde{S}\end{pmatrix}, \qquad m_{\tilde{H}}^2 \equiv 2\mu^2,\ m_{\tilde{S}}^2 \equiv \mu_S^2 + \epsilon_2 v_h^2. \tag{2.9}$$

The eigenvalues of the mass matrix are

$$m_\pm = \frac{1}{2}\left[m_{\tilde{H}}^2 + m_{\tilde{S}}^2 \pm \sqrt{A}\right], \qquad A \equiv (m_{\tilde{H}}^2 - m_{\tilde{S}}^2)^2 + 4\epsilon_1^2 v_h^2, \tag{2.10}$$

and the mass eigenstates are

$$\begin{pmatrix} h \\ S \end{pmatrix} = \begin{pmatrix} \cos\theta & \sin\theta \\ -\sin\theta & \cos\theta \end{pmatrix}\begin{pmatrix}\tilde{h} \\ \tilde{S}\end{pmatrix}, \qquad \tan 2\theta = \frac{2 v_h \epsilon_1}{m_{\tilde{S}}^2 - m_{\tilde{H}}^2}. \tag{2.11}$$

The parameters in the potential can be adjusted to give an arbitrary mass to S. Diagonalizing the mass matrix gives rise to couplings between S and matter fields equal to the Higgs couplings rescaled by $\sin\theta$; the term $\mathcal{L} \supset -h g_{S\chi} \sin\theta \bar{\chi}\chi$ is induced as well. While this latter term gives rise to invisible Higgs decays that were recently constrained at the LHC to $\Gamma_{h\to\text{invis.}} \lesssim 0.23$ [87], it is irrelevant at MeV energy scales since the Higgs decouples. The Higgs portal matches onto

$\mathcal{L}_{>1\text{ GeV}}|_S$ with[1]

$$g_{Sff} = g_{SG} = g_{SF} = -\sin\theta, \qquad g_{S\chi} = \tilde{g}_{S\chi}\cos\theta, \tag{2.12}$$

where $\tilde{g}_{S\chi}$ is the coupling between the interaction eigenstate $\bar{S}$ and the dark matter.

Another simple UV-completion for $\mathcal{L}_{>1\text{ GeV}}|_S$ is to couple S to a heavy quark Q:

$$\mathcal{L}_{\text{h.q.,int}} = \bar{Q}(i\not{D} - m_Q)Q - g_{SQ}S\bar{Q}Q. \tag{2.13}$$

Q could be taken to be t or a new colored fermion with $m_Q \gtrsim 5$ TeV to avoid LHC constraints. The main difference between these scenarios is that rare meson decay constraints depend substantially on the coupling between S and the top quark, which is generated at loop-order in this theory [89]. In either scenario $m_Q \gg 1$ GeV and so Q can be integrated out, giving

$$g_{SG} = \frac{g_{SQ}v_h}{3m_Q}, \; g_{Sq} = g_{SF} = 0. \tag{2.14}$$

While g_{Sf} becomes nonzero due to renormalization group evolution from m_Q to 1 GeV, we ignore its value, which is roughly

$$\frac{g_{SQ}v_h}{16\pi^2 m_Q}\alpha_s^2(1\text{ GeV})\log\frac{1\text{ GeV}}{m_Q}. \tag{2.15}$$

Since $m_Q \gtrsim v_h$, this coupling is about a factor of 100 smaller than g_{SG} and can thus be ignored.

[1]The couplings to gluons and photons were computed by integrating out τ, c, b, t, W, h and Z [101].

2.2 Pseudoscalar Simplified Model

The Lagrangian for this model is similar to $\mathcal{L}_{>1\text{ GeV}}|_S$ with S replaced by the pseudoscalar mediator P:

$$\mathcal{L}_{>1\text{ GeV}}|_P = -\frac{g_s^2 g_{PG}}{32\pi^2 v_h} P G^a_{\mu\nu}\tilde{G}^{a\mu\nu} + i g_{Pu} P \frac{m_u}{v_h}\bar{u}\gamma^5 u + i g_{Pd} P \sum_{q=d,s}\frac{m_q}{v_h}\bar{q}\gamma^5 q \quad (2.16)$$

$$\mathcal{L}_{P,\text{free}} = \frac{1}{2}(\partial_\mu P)^2 - \frac{1}{2}m_P^2 P^2 \quad (2.17)$$

$$\mathcal{L}_{\chi,\text{free}} = \bar{\chi}(i\partial\!\!\!/ - m_\chi)\chi \quad (2.18)$$

$$\mathcal{L}_{\text{QED}} = -\frac{1}{4}F_{\mu\nu}F^{\mu\nu} + \sum_{\ell=e,\mu}\bar{\ell}(i\not{D} - m_\ell)\ell \quad (2.19)$$

$$\mathcal{L}_{P,\text{int}} = i g_{P\chi} P\bar{\chi}\gamma^5\chi - \frac{e^2 g_{PF}}{16\pi^2 v_h} P F_{\mu\nu}\tilde{F}^{\mu\nu} + i g_{P\ell} P \sum_{\ell=e,\mu}\frac{m_\ell}{v_h}\bar{\ell}\gamma^5\ell. \quad (2.20)$$

I have again assumed MFV, but kept the couplings of P to leptons, up-type and down-type quarks independent to focus on its hadronic interactions. If $g_{Pu} = g_{Pd} = g_{P\ell}$, $\bar{\chi}\chi \to \mu^+\mu^-$ dominates the branching fractions and spectrum, which is quite uninteresting. The first term was chosen to match the QCD theta term with $\theta = g_{PG}P/v_h$. Assuming the same MFV-type couplings hold for P's interactions with τ, c, b and t, integrating them out gives $g_{PG} = 2g_{Pu} + g_{Pd}$ and $g_{PF} = g_{P\ell} + (8g_{Pu} + g_{Pd})/9$.

$$g_{PG} = 2g_{Pu} + g_{Pd} \quad (2.21)$$

$$g_{PF} = g_{P\ell} + \frac{1}{9}(8g_{Pu} + g_{Pd}). \quad (2.22)$$

2.2.1 UV Completions

The pseudoscalar simplified model appears in variants of the two Higgs doublet model (2HDM) that have been augmented with another pseudoscalar singlet $\tilde{P}$ [18,

65]. The 2HDM is one of the simplest and most important generalizations of the Standard Model. It is required in well-motivated theories such as supersymmetry as well as in some axion solutions to the strong CP problem, and has been used to construct models for baryogenesis [27, 7].

The basic idea in adding a pseudoscalar singlet to the 2HDM, which will be reviewed below in more detail, is that the interaction eigenstate $\tilde{P}$ couples to the dark matter and the two Higgs doublets through a special mixing term. The CP-odd scalar $\tilde{A}$ from the 2HDM thus combines with $\tilde{P}$ to form mass eigenstates P and A. Taking $m_A \gg m_P$ for simplicity, the state P thus acquires couplings to fermions equal to $\tilde{A}$'s, rescaled by sine of the mixing angle θ. The parameters g_{Pq} and $g_{P\ell}$ above arise by choosing a variant of the 2HDM where one of the Higgs doublets couples only to leptons and the other couples just to quarks. This is called the type III or lepton-specific 2HDM [59], and has been used to build models for anomalies such as the muon $(g-2)$ [1, 97].

This type of mixing appears naturally in the next-to-minimal supersymmetric Standard Model (NMSSM) [7]. It has been used to construct SUSY and non-SUSY models for the Galactic Center GeV gamma ray excess [79, 36, 35, 137], since the DM self-annihilation cross section is s-wave while the direct detection cross section is spin-dependent. The mixing is also produced in so-called "axion portal" models, where the pseudoscalar arises as the phase of a complex scalar field associated with a U(1) symmetry [111, 59].

In the rest of this subsection I will derive expressions for the simplified model couplings $g_{P\chi}$, g_{Pq}, $g_{P\ell}$, g_{PG} and g_{PF} in the UV completion just summarized. The

starting point is the 2HDM scalar potential, which is given by [65]

$$V_{\rm 2HDM} = \mu_1^2|H_1|^2 + \mu_2^2|H_2|^2 - \mu^2[H_1^\dagger \cdot H_2 + \text{h.c.}] + \frac{\lambda_1}{2}|H_1|^4 + \frac{\lambda_2}{2}|H_2|^4 \tag{2.23}$$

$$+ \lambda_3|H_1|^2|H_2|^2 + \lambda_4|H_1^\dagger \cdot H_2|^2 + \frac{\lambda_5}{2}\left[(H_1^\dagger \cdot H_2)^2 + \text{h.c.}\right], \tag{2.24}$$

where I have assumed CP conservation and imposed a $\mathbb{Z}_2$ symmetry $H_1 \to H_1$, $H_2 \to -H_2$ to suppress flavor-changing neutral currents which is softly broken by the μ^2 term. The part of the Lagrangian containing the dark matter, $\tilde{P}$ and the mixing piece is

$$\mathcal{L} \supset \mathcal{L}_{\tilde{P}} + \mathcal{L}_\chi + \mathcal{L}_{\rm mix} + i\tilde{g}_{P\chi}\tilde{P}\bar{\chi}\gamma^5\chi \tag{2.25}$$

$$\mathcal{L}_{\tilde{P}} = \frac{1}{2}(\partial_\mu \tilde{P})^2 - \frac{1}{2}m_{\tilde{P}}^2\tilde{P}^2 \tag{2.26}$$

$$\mathcal{L}_\chi = \bar{\chi}(i\partial\!\!\!/ - m_\chi)\chi \tag{2.27}$$

$$\mathcal{L}_{\rm mix} = i\kappa\tilde{P}(H_1^\dagger H_2 - H_2^\dagger H_1). \tag{2.28}$$

Taking the vacuum to be the normal, CP-conserving one, the Higgs doublets can be expanded in component fields as

$$H_i = \begin{pmatrix} \phi_i^+ \\ \frac{1}{\sqrt{2}}(v_i + h_i + ia_i) \end{pmatrix}. \tag{2.29}$$

The doublets' vevs v_1 and v_2 satisfy $v_h = \sqrt{v_1^2 + v_2^2}$ and the angle β is defined by $\tan\beta \equiv v_2/v_1$.

The component fields with the same CP and charge quantum numbers in the two doublets mix. It is straightforward to expand $V_{\rm 2HDM}$ to isolate the (a_1, a_2) mass matrix. The mass eigenstates are $(G^0, \tilde{A})$, where $\tilde{A} = \cos\beta a_2 - \sin\beta a_1$, G^0

is the Goldstone eaten by the Z^0, and $\tilde{A}$'s mass is

$$m_{\tilde{A}}^2 = \left(\frac{2\mu^2}{v_h^2} \csc(2\beta) - \lambda_5 \right) v_h^2. \tag{2.30}$$

Substituting into the mixing Lagrangian gives

$$\mathcal{L}_{\text{mix}} = -\kappa v_h \tilde{A} \tilde{P}. \tag{2.31}$$

As in Sec. 2.1.1, the $(\tilde{A}, \tilde{P})$ mass matrix is straightforward to diagonalize, with the mixing angle θ found to be

$$\tan 2\theta = \frac{2\kappa v_h}{m_{\tilde{A}}^2 - m_{\tilde{P}}^2}. \tag{2.32}$$

The 2HDM Yukawa interactions are

$$\mathcal{L}_{Y,\text{2HDM}} = -\sum_{i=1,2} \left[Y_d^i (\bar{Q}_L \cdot H_i) d_R + Y_u^i (\bar{Q}_L \cdot \tilde{H}_i) u_R + Y_l^i (\bar{L}_L \cdot H_i) e_R + \text{h.c.} \right], \tag{2.33}$$

where I dropped the sum over fermion generations for simplicity and $\tilde{H}_i \equiv \epsilon \cdot H_i^*$ and ϵ is the antisymmetric 2×2 matrix. Substituting for the mass eigenstates and taking $m_A \gg m_P$ to decouple the pseudoscalar gives

$$\mathcal{L}_{Y,\text{2HDM}} \supset i \frac{m_u}{v_h} \cot\beta \sin\theta P \bar{u} \gamma^5 u - i \frac{m_d}{v_h} \cot\beta \sin\theta P \bar{d} \gamma^5 d \tag{2.34}$$

$$+ i \frac{m_l}{v_h} \tan\beta \sin\theta P \bar{e} \gamma^5 e. \tag{2.35}$$

Upon integrating out fermions heavier than 1 GeV, these interactions contribute to the $PF\tilde{F}$, while the interactions between P, gauge bosons and the charged Higgs do not. Integrating out the c, b and t quarks also gives the $PG\tilde{G}$ interaction, with

the c and t contributing with the opposite sign of the b (up to small corrections from the couplings' runnings). Finally, the DM interaction with P is weakened by a factor of $\cos\theta$ to $\mathcal{L} \supset i\tilde{g}_{P\chi} \cos\theta P\bar{\chi}\gamma^5\chi$. To summarize, the couplings in this extension of the type III 2HDM are related to those in $\mathcal{L}_{>1\text{ GeV}}|_P$ by

$$g_{Pu} = \sin\theta \cot\beta \tag{2.36}$$

$$g_{Pd} = -g_{Pu} \tag{2.37}$$

$$g_{P\ell} = \sin\theta \tan\beta \tag{2.38}$$

$$g_{PG} = 2g_{Pu} + g_{Pd} = g_{Pu} \tag{2.39}$$

$$g_{PF} = 2g_{Pu}\left(\frac{2}{3}\right)^2 + g_{Pd}\left(\frac{1}{3}\right)^2 + g_{P\ell}(-1)^2 = \left(g_{P\ell} + \frac{7}{9}g_{Pu}\right) \tag{2.40}$$

$$g_{P\chi} = g_{\tilde{P}\chi}\cos\theta. \tag{2.41}$$

By taking β to be small, $g_{Pu}/g_{P\ell}$ can be made large, decoupling the leptons.

Coupling $\tilde{P}$ to other variants of the 2HDM would lead to different relations between the couplings of P with leptons and up- and down-type quarks. For example, using a type II 2HDM in which one of the doublets couples to up-type quarks while the other couples to down-type quarks and leptons gives

$$g_{Pu} = \sin\theta \cot\beta \tag{2.42}$$

$$g_{Pd} = -\sin\theta \tan\beta \tag{2.43}$$

$$g_{P\ell} = \sin\theta \tan\beta. \tag{2.44}$$

2.3 Vector Simplified Model

The microscopic Lagrangian for the vector simplified model is

$$\mathcal{L}_{>1\text{ GeV}}|_V = \sum_{q=u,d,s} g_{Vq} V_\mu \bar{q}\gamma^\mu q \tag{2.45}$$

$$\mathcal{L}_{V,\text{free}} + \mathcal{L}_{\chi,\text{free}} + \mathcal{L}_{\text{QED}} + \mathcal{L}_{V,\text{int}} + \mathcal{L}_{\text{WZW}}|_V \tag{2.46}$$

$$\mathcal{L}_{V,\text{free}} = -\frac{1}{4} V_{\mu\nu} V^{\mu\nu} + \frac{1}{2} m_V^2 V_\mu V^\mu \tag{2.47}$$

$$\mathcal{L}_{\chi,\text{free}} = \bar{\chi}(i\partial\!\!\!/ - m_\chi)\chi \tag{2.48}$$

$$\mathcal{L}_{\text{QED}} = -\frac{1}{4} F_{\mu\nu} F^{\mu\nu} + \sum_{\ell=e,\mu} \bar{\ell}(iD\!\!\!/ - m_\ell)\ell \tag{2.49}$$

$$\mathcal{L}_{V,\text{int}} = g_{V\chi} V_\mu \bar{\chi}\gamma^\mu \chi + V_\mu \sum_{\ell=e,\mu} g_{V\ell} \bar{\ell}\gamma^\mu \ell, \tag{2.50}$$

where V_μ is the vector mediator. As I will explain below, no kinetic mixing term was include since it can be rotated away through a field redefinition. Note also that there are no dimension 5 operators. While dipole terms such as $V_{\mu\nu}\bar{q}\sigma^{\mu\nu}q$ appear to be dimension 5, they flip chirality, requiring an insertion of the Higgs doublet. The resulting operator is thus dimension 6. Since we are assuming minimal flavor violation, the dipole operators are suppressed by the light quark Yukawa couplings, making them irrelevant to this thesis.

One remarkable feature of quantum electrodynamics is that the ratios of particles' electric charges are not modified by loop diagrams. If this were not the case and (for example) the electron charge Q_e and up quark charge Q_u were renormalized differently, charge conservation would be violated at higher orders in perturbation theory, violating the Ward identity and thus gauge invariance. This discussion begs the question of whether this same property holds for the ratios between g_{Vu}, g_{Vd} and g_{Vs}. Surprisingly, it does, even though the vector's mass term seems to break gauge invariance. The reason is that $\mathcal{L}_{V,\text{free}}$ can be

modified by making V_μ a gauge boson for a $\mathrm{U}(1)'$ symmetry with a Stuckelberg mass term:

$$\mathcal{L}'_{V,\text{free}} = -\frac{1}{4}V_{\mu\nu}V^{\mu\nu} + \frac{1}{2}(\partial_\mu\sigma - m_V V_\mu)(\partial^\mu\sigma - m_V V^\mu) - \frac{1}{2}m_\sigma^2\sigma^2. \tag{2.51}$$

The fermions have charges g_{Vf} under $\mathrm{U}(1)'$. The transformation laws for V_μ and the Stuckelberg field σ are taken to be

$$V_\mu \to V_\mu + \partial_\mu\alpha, \qquad \sigma \to \sigma + \alpha, \tag{2.52}$$

which makes the mass term and thus the whole Lagrangian gauge-invariant. This formulation makes it clear that the ratios between V_μ's couplings to fermion fields as well as composite fields like the pions are equal to their tree-level values to all orders. In this limit $m_\sigma \to \infty$ the Stuckelberg field decouples, $\mathcal{L}'_{V,\text{free}} \to \mathcal{L}_{V,\text{free}}$ and the statement about coupling ratios still holds.

2.3.1 UV Completions

While $\mathcal{L}_{>1\text{ GeV}}|_V$ is already a renormalizeable Lagrangian, it is worth mentioning how it relates to other frameworks. One of the simplest DM models is to couple χ to the SM through a dark photon A'^μ, which is the gauge boson of a new $\mathrm{U}(1)'$ symmetry particle that couples to the SM fermions proportionally to their electric or hypercharges [123]. The simplest example of this is

$$\mathcal{L}_{\text{d.p.}} = \mathcal{L}_{\chi,A'} - \frac{\epsilon}{2}F'_{\mu\nu}F^{\mu\nu} + \mathcal{L}_{\text{SM}} \tag{2.53}$$

$$\mathcal{L}_{\chi,A'} = -\frac{1}{4}F'_{\mu\nu}F'^{\mu\nu} + \frac{1}{2}m_{A'}^2 A'_\mu A'^\mu + \bar{\chi}(i\partial\!\!\!/ - g'A\!\!\!/' - m_\chi)\chi, \tag{2.54}$$

where g' is the gauge coupling for $\mathrm{U}(1)'$, ϵ is the mixing angle and the FF' interaction is called kinetic mixing since it looks like a gauge kinetic term. The field strength F can be that of the photon or hypercharge gauge boson [123]. The mass term can either be put in explicitly, in which case it is protected from additive renormalization and is thus technically natural, or it can be produced by breaking $\mathrm{U}(1)'$ with a new Higgs or the Stuckelberg mechanism [7].

The dark photon Lagrangian can be cast in the form above by shifting $A^\mu \to A^\mu - \epsilon A'^\mu$ or using the equations of motion of the photon $\partial_\mu F^{\mu\nu} = eJ^\nu_{\mathrm{EM}} - \epsilon \partial_\mu F'^{\mu\nu}$. Either way, making the substitution and dropping terms of order ϵ^2, the kinetic mixing term becomes

$$-\frac{\epsilon}{2} F'_{\mu\nu} F^{\mu\nu} = \epsilon e A'_\mu J^\mu_{\mathrm{EM}}. \tag{2.55}$$

This matches onto $\mathcal{L}_{>1\ \mathrm{GeV}}|_V$ with

$$V_\mu = A'_\mu, \qquad g_{Vff} = \epsilon e Q_f. \tag{2.56}$$

A less minimal possibility is to gauge the SM fermions under a new group. A well-motivated example is $\mathrm{U}(1)_{B-L}$ where B (L) is baryon (lepton) number, since it is anomaly free when the SM is augmented with right-handed neutrinos [94]. Individual lepton flavors can also be given different anomaly-free gauge charges. The same can be done with different quark flavors, though new Higgs may be required and flavor-changing neutral currents are produced at tree level [7]. More generally, the SM fermions can be gauged under an arbitrary new $\mathrm{U}(1)'$ even if it is anomalous by treating $\mathcal{L}_{>1\ \mathrm{GeV}}|_V$ as an effective theory, where the UV model contains new fermions rendering it non-anomalous whose masses can easily be taken to be outside the reach of current experiments [122]. Later in this work,

I will explore the gamma ray spectra, branching fractions and indirect detection constraints that result from different choices of the couplings.

Chapter 3

Matching onto the Theory of Mesons

The next step is to understand how the mediators from the simplified models in the previous chapter interact with mesons.

Meson physics can be described using an effective field theory (EFT) called chiral perturbation theory (chiPT). The key idea of effective field theory is to find a simple QFT for capturing physics at an energy scale of interest such that quantities can be computed at successive levels of approximation. Top-down EFTs are the simplest kind: starting with a UV Lagrangian $\mathcal{L}$ containing particles ϕ and Φ, the heavy particle Φ is "integrated out" of the path integral[1] to study processes at energies $Q^2 \ll m_\Phi$. This results in a Lagrangian $\mathcal{L}_{\text{EFT}} = \sum_{n=0}^{\infty} \mathcal{L}_{\text{EFT}}^{(n)}$ such that the generating functions in the underlying and effective theories are equal:

$$\int [\mathcal{D}\phi][\mathcal{D}\Phi] e^{i\int d^4x\ \mathcal{L}} = \int [\mathcal{D}\phi] e^{i\int d^4x\ \left[\mathcal{L}_{\text{EFT}}^{(0)} + \mathcal{L}_{\text{EFT}}^{(1)} + \mathcal{L}_{\text{EFT}}^{(2)} + \ldots\right]}. \tag{3.1}$$

The Fermi theory of the weak interactions is an example of a top-down EFT. The

[1] This can be done by simplifying the Lagrangian using the W's equation of motion.

expansion parameter is the Fermi constant G_F, and the theory is very successful at describing processes below $G_F^{-1/2} \approx 300$ GeV such as muon and β decay.

To construct chiPT, the goal is to find an expansion in the meson momentum $\mathcal{L}_{\text{chiPT}} = \sum_{n=1}^{\infty} \mathcal{L}_{\text{chiPT}}^{(2n)}$ (where $\mathcal{L}_{\text{chiPT}}^{(n)} \sim \mathcal{O}(p^{2n})$) such that

$$\int [\mathcal{D}G_\mu^a][\mathcal{D}\bar{q}_i][\mathcal{D}q_i] e^{i\int d^4x\ \mathcal{L}_{\text{QCD}}} = \int [\mathcal{D}\pi^a] e^{i\int d^4x\ \left[\mathcal{L}_{\text{chiPT}}^{(2)} + \mathcal{L}_{\text{chiPT}}^{(4)} + \ldots\right]}, \tag{3.2}$$

where products over the indices are implied and $\{\pi^a\}$ stands for the meson fields. The path integral cannot be performed analytically in this case since QCD is non-perturbative below $\Lambda_{\text{QCD}} \sim 4\pi f_\pi$. Instead, the guiding principle is to construct $\mathcal{L}_{\text{chiPT}}$ by writing down all terms compatible with the symmetries of QCD, in accordance with a "theorem" of Weinberg [141]. Understanding the power counting scheme controlling the accuracy of chiPT calculations is also important, since the effective Lagrangian contains an infinite number of terms, each with its own low energy constant.

Much of this chapter is dedicated to summarizing the aspects of chiral perturbation theory relevant for this thesis, along the lines of [125]. While the leading order chiral Lagrangian is described briefly in many quantum field theory textbooks [118, 127], the physics is quite elegant, and some more obscure features are required for this thesis. First I describe chiral symmetry, a spontaneously broken symmetry of QCD that will be used to carry out Weinberg's procedure. After identifying the mesons as Goldstones associated with chiral symmetry breaking, I explain the Coleman-Callan-Wess-Zumino (CCWZ) procedure and apply it to construct $\mathcal{L}_{\text{chiPT}}$. A thorough explanation of the theta term and anomalies in the chiral Lagrangian is also provided.[2]

[2]Further information on chiral symmetry breaking, chiral perturbation theory, the CCWZ procedure and effective field theory can be found in [141, 125, 100, 96, 138, 84, 45, 6, 72, 91].

With this machinery in place, I apply it to the novel situation at hand: matching the scalar, vector and pseudoscalar simplified models onto chiral Lagrangians. A reader well-versed in chiral perturbation theory is invited to skip to sections 3.5, 3.7 and 3.8, where the matching is performed in detail. The branching fractions for dark matter self-annihilation are also discussed in these sections, and are key outputs from this chapter, along with the matched Lagrangians.

3.1 Chiral Symmetry and Goldstone's Theorem in QCD

At 1 GeV where the simplified model Lagrangians of the previous chapter were defined, the QCD part of the SM Lagrangian is given by[3]

$$\mathcal{L}_{\text{QCD}} = \bar{\mathbf{q}}(i\not{D} - M_q)\mathbf{q} - \frac{1}{4}G^a_{\mu\nu}G^{a\mu\nu}, \tag{3.3}$$

where $\mathbf{q} \equiv (u, d, s)^T$, $M_q = \text{diag}(m_u, m_d, m_s)$ is the matrix of light quark masses, the QCD covariant derivative is

$$D_\mu \equiv \partial_\mu - ig_s\frac{\lambda^a}{2}A^a_\mu \tag{3.4}$$

and g_s is the strong coupling constant. In the so-called chiral limit $m_u, m_d, m_s \to 0$, the Lagrangian splits into terms containing particles with distinct chirality:

$$\mathcal{L}_{\text{QCD},0} = \bar{\mathbf{q}}_R(i\not{D})\mathbf{q}_R + \bar{\mathbf{q}}_L(i\not{D})\mathbf{q}_L - \frac{1}{4}G^a_{\mu\nu}G^{a\mu\nu}, \tag{3.5}$$

[3]This expression does not include the theta term, which will be discussed in sec. 3.6.

where $q_L \equiv P_L q$, $q_R \equiv P_R q$, and $P_{R,L} = (1 \pm \gamma^5)/2$ are the usual chiral projectors. This Lagrangian is manifestly invariant under $\mathrm{U}(3)_L \times \mathrm{U}(3)_R$, which consists of independent rotations of the left and right-handed quark flavors:

$$\mathbf{q}_R \to e^{i\alpha_R^a \lambda^a/2} e^{i\alpha_R} \mathbf{q}_R, \tag{3.6}$$

$$\mathbf{q}_L \to e^{i\alpha_L^a \lambda^a/2} e^{i\alpha_L} \mathbf{q}_L, \tag{3.7}$$

where I have chosen the Gell-Mann matrices $\lambda^1, \ldots, \lambda^8$ as the SU(3) generators. However, the subgroup $\mathrm{U}(1)_A$ (where the left and right-handed quarks are rotated by opposite phases) is anomalous, and thus not a symmetry of $\mathcal{L}_{\mathrm{QCD},0}$ at the quantum level, so the true symmetry group of $\mathcal{L}_{\mathrm{QCD},0}$ is $\mathrm{SU}(3)_L \times \mathrm{SU}(3)_R \times \mathrm{U}(1)_V$. I return to $\mathrm{U}(1)_A$ to Sec. 3.6. As shown in Appendix B, $\mathrm{U}(1)_V$ is associated with baryon number; the remaining $\mathrm{SU}(3)_L \times \mathrm{SU}(3)_R$ symmetry is called chiral symmetry.

It turns out that chiral symmetry is broken spontaneously in QCD. To understand this requires reviewing some general features of symmetries. Let G be a symmetry group, and let the fields ϕ_i live in a representation of G's Lie algebra with generators t^a. Then the change in the field under an infinitesimal transformation with parameters ϵ_a is $\delta\phi_i = i\epsilon^a t^a_{ij} \phi_j$. Since the Noether currents J^a_μ are obey the continuity equation $\partial^\mu J^a_\mu = 0$, the associated charges

$$Q^a(t) \equiv \int d^3x \; J^0(x) = \int d^3x \; \sum_i \frac{\partial \mathcal{L}}{\partial \dot{\phi}_i} \frac{\delta \phi_i}{\delta \epsilon^a} \tag{3.8}$$

are conserved ($\dot{Q}^a(t) = 0$ or equivalently $[H, Q^a] = 0$ where H is the Hamiltonian).

In QCD, $G = \mathrm{SU}(3)_L \times \mathrm{SU}(3)_R$ or equivalently $\mathrm{SU}(3)_V \times \mathrm{SU}(3)_A$, where $Q^a_V \equiv Q^a_R + Q^a_L$ and $Q^a_A \equiv Q^a_R - Q^a_L$. Assuming that this symmetry is unbroken, we should expect to see parity doublets for mesons with the same J. Given a positive-parity

eigenstate of H, $|\lambda\rangle$, there is a corresponding negative-parity state $Q_A^a|\lambda\rangle$ with the same mass since Q_A^a commutes with the Hamiltonian. However, we don't see this parity doubling in the hadron spectrum. The pions do not have similarly light partners, and the vectors mesons are significantly lighter than the axial vector ones ($m_\rho \sim 770$ MeV while $h_1(1170)$ is one of the lightest axial vector mesons). Another important piece of the puzzle is that along with the requirement that $\mathrm{SU}(3)_C$ confines, the 't Hooft anomaly matching condition is impossible to satisfy for $\mathrm{SU}(N_f)_L \times \mathrm{SU}(N_f)_R \times \mathrm{U}(1)_V$ for $N_f \geq 3$, implying that chiral symmetry must be broken [134]. While this result does not specify the nature of the symmetry breaking, the low masses of the pseudoscalar mesons are an indicator that they are (pseudo)Nambu-Goldstone bosons (NGBs) caused by the spontaneous breaking of $\mathrm{SU}(3)_A$. The kaons and η are heavier than the pions ($m_\pi \sim 140$ MeV, $m_K \sim 490$ MeV, $m_\eta \sim 540$ MeV) since they contain a strange quark and thus feel the impact of explicit chiral symmetry breaking.

Let's understand the NGB nature of the pions and examine the mechanism for chiral symmetry breaking. Turning back to the general case, using that $\partial\mathcal{L}/\partial\dot{\phi}_i$ is the canonical momentum π_i and using the canonical commutation relations gives

$$[Q^a, \phi_i] = \sum_j \int d^3x \; [\pi_j(\vec{x}), \phi_i(\vec{y})] \frac{\delta\phi_i(\vec{x})}{\delta\epsilon^a} = t^a_{ij}\phi_j. \tag{3.9}$$

In other words, the charge operators form a representation of G's Lie algebra. Now suppose that the symmetry leaves the vacuum $|\Omega\rangle$ invariant so that $\exp(i\epsilon^a Q^a)|\Omega\rangle$; then $Q^a|\Omega\rangle = 0$. Taking the vev of the above expression gives

$$\langle [Q^a, \phi_i] \rangle = 0 = t^a_{ij}\langle\phi_j\rangle, \tag{3.10}$$

so all the fields' vevs must be zero.

The other possibility is that there is an operator ϕ_i with nonzero vev (which is assumed to be constant in time), in which case

$$t^a_{ij}\langle\phi_j\rangle = \langle[Q^a, \phi_i]\rangle \neq 0. \tag{3.11}$$

This means that $Q^a|\Omega\rangle \neq 0$: in other words, while the Lagrangian obeys the symmetry, the vacuum state does not. By inserting a complete set of states

$$1 = \sum_X \int \frac{d^3p}{(2\pi)^3 2E_X} |X\rangle\langle X|, \tag{3.12}$$

where the integral is over the state's total momentum and the sum is over all other momenta and quantum numbers, we can work out the implications of eq. 3.11:[4]

$$\langle[Q^a(x^0), \phi_i(0)]\rangle = \int d^3x \ \langle[J^a_0(x), \phi_i(0)]\rangle \tag{3.13}$$

$$= \sum_X \int \frac{d^3p}{(2\pi)^3 2E_X} \int d^3x \ \left[c^a_{Xi}(\mathbf{p}, x) - {c^a_{Xi}}^*(\mathbf{p}, x)\right], \tag{3.14}$$

where $c^a_{Xi}(\mathbf{p}, x) \equiv \langle\Omega|J^a_0(x)|X(p)\rangle\langle X(p)|\phi_i(0)|\Omega\rangle$. Since the vacuum is translation-invariant, this function can be simplified:

$$\langle\Omega|J^a_0(x)|X(p)\rangle = \langle\Omega|e^{i\hat{P}\cdot x}J^a_0(0)e^{-i\hat{P}\cdot x}|X(p)\rangle = e^{-ip\cdot x}\langle\Omega|J^a_0(0)|X(p)\rangle, \tag{3.15}$$

[4]Since $Q^a|\Omega\rangle \neq 0$, Q does not actually exist in the Hilbert space by the Fabri-Picasso theorem, which says that its value is proportional to the volume of space [57]. However, its commutator with other operators can still be defined.

so $c^a_{Xi}(\mathbf{p},x) = c^a_{Xi}(\mathbf{p},0)e^{-ip\cdot x} \equiv c^a_{Xi}(\mathbf{p})e^{-ip\cdot x}$. Eq. 3.13 then becomes

$$\langle [Q^a(x^0), \phi_i(0)] \rangle = \sum_X \int \frac{d^3p}{(2\pi)^3 2E_X} \int d^3x \ \left[c^a_{Xi}(\mathbf{p})e^{-ip\cdot x} - {c^a_{Xi}}^*(\mathbf{p})e^{ip\cdot x} \right] \tag{3.16}$$

$$= \sum_X \int \frac{d^3p}{2E_X} \delta^{(3)}(\mathbf{p}) \left[c^a_{Xi}(\mathbf{p})e^{-iE\cdot t} - {c^a_{Xi}}^*(\mathbf{p})e^{iE\cdot t} \right] \tag{3.17}$$

$$= \sum_X \frac{1}{2m_X} \left[c^a_{Xi}(\mathbf{0})e^{-im_X t} - {c^a_{Xi}}^*(\mathbf{0})e^{im_X t} \right] \tag{3.18}$$

$$= \text{const.} \tag{3.19}$$

The constant on the RHS of eq. 3.16 is called the order parameter for the spontaneous symmetry breaking. Letting $c^a_{Xi}(\mathbf{0}) \equiv |c^a_{Xi}(\mathbf{0})| \exp(i\phi_X)$, the $m_X \neq 0$ terms in this sum each contribute

$$\frac{|c^a_{Xi}(\mathbf{0})|}{2m_X} \left[e^{i(\phi_X - m_X t)} - e^{-i(\phi_X - m_X t)} \right] \propto \sin(\phi_X - m_X t); \tag{3.20}$$

since the right hand side of eq. 3.16 is constant, these terms must sum to zero. Therefore only terms that can contribute to the LHS of eq 3.16 are the ones with $m_X = 0$ as well as $c^a_{Xi}(\mathbf{0})/(im_X) \neq 0$ and real. This proves the Nambu-Goldstone theorem, which says that for each Q^a that does not leave the vacuum invariant there is a massless boson that is not annihilated by J^a_0 and ϕ_i [107, 62, 63].

To apply this to QCD, we would now like to find the order parameter for chiral symmetry breaking (an operator with nonzero vev) and confirm our inference from the hadron spectrum that $\mathrm{SU}(3)_A$ is the broken symmetry. Define the scalar and pseudoscalar densitities as

$$\mathcal{S}^a = \bar{q}\lambda^a q, \ a = 0, \ldots, 8 \tag{3.21}$$

$$\mathcal{P}^a = i\bar{q}\gamma^5\lambda^a q, \ a = 0, \ldots, 8. \tag{3.22}$$

Using the equal time anticommutation relations for the quark fields as well as the commutation relations for the Gell-Mann matrices, the transformation laws for the scalar density can be shown to transform as

$$[Q_V^a, \mathcal{S}^0] = 0, a = 1, \ldots, 8 \tag{3.23}$$

$$[Q_V^a, \mathcal{S}^b] = if^{abc}\mathcal{S}^c, a, b = 1, \ldots, 8, \tag{3.24}$$

and similarly for the pseudoscalar densities. Is it possible that the vector-like global symmetries Q_V^a are broken? Vafa and Witten proved a theorem [138] showing that in gauge theories with vector-like forces and no theta term (such as QCD) this cannot happen. Taking the vev of eq. 3.24 and applying this result shows that $\langle \mathcal{S}^a \rangle = 0$ for $a = 1, \ldots, 8$, but does not give any new information about the scalar singlet density $\mathcal{S}^0$.

We can get more information out of eq. 3.24 by judiciously choosing a:

$$a = 3 : \langle \bar{u}u \rangle - \langle \bar{d}d \rangle = 0 \tag{3.25}$$

$$a = 8 : \langle \bar{u}u \rangle + \langle \bar{d}d \rangle - 2\langle \bar{s}s \rangle = 0. \tag{3.26}$$

This implies that for each quark flavor q_i we have

$$\langle \bar{q}q \rangle = 3\langle \bar{q}_i q_i \rangle, \tag{3.27}$$

where i is not summed over, and $\langle \bar{q}q \rangle$ is called the chiral (or quark) condensate. It has been demonstrated conclusively that it is nonzero using lattice QCD (see eg [105]) and experimental data [41]. The chiral condensate, which is generated dynamically from quark-gluon interactions, is the order parameter for chiral symmetry breaking.

The final step is to relate the chiral condensate to the broken generators. Using more Gell-Mann matrix manipulations, it can be shown that

$$i[Q_A^a, \mathcal{P}^a] = \begin{cases} \bar{u}u + \bar{d}d, & a = 1, 2, 3 \\ \bar{u}u + \bar{s}s, & a = 4, 5 \\ \bar{d}d + \bar{s}s, & a = 6, 7 \\ \frac{1}{3}(\bar{u}u + \bar{d}d + 4\bar{s}s), & a = 8 \end{cases} \tag{3.28}$$

$$\implies \langle i[Q_A^a, \mathcal{P}^a] \rangle = \frac{2}{3}\langle \bar{q}q \rangle, \ a = 1, \ldots, 8, \tag{3.29}$$

where I used eq. 3.27 in the last line. This is in complete analogy with Goldstone's theorem (eq. 3.16), and we can therefore see that $\mathrm{SU}(3)_A$ must indeed be spontaneously broken.

To summarize, in QCD the chiral condensate acquires a nonzero vev due to gluon dynamics, which by eq. 3.29 causes the spontaneous symmetry breaking pattern

$$\mathrm{SU}(3)_L \times \mathrm{SU}(3)_R \to \mathrm{SU}(3)_V. \tag{3.30}$$

There are eight NGBs $|\phi^a\rangle$ such that $\langle \Omega | Q_A^a | \phi^a \rangle \neq 0$ and $\langle \Omega | \mathcal{P}^a | \phi^a \rangle \neq 0$. By Lorentz covariance, the matrix element for the axial-vector current between the NGBs states and the vacuum can be written as

$$\langle \Omega | \mathcal{A}_\mu^a(0) | \phi^b(p) \rangle \equiv i p_\mu f_\pi \delta^{ab}, \tag{3.31}$$

where $\mathcal{A}_\mu^a$ is the axial vector current, $f_\pi \approx 92$ MeV is the pion decay constant, and the NGBs must be pseudoscalars.

The NGBs' transformation laws under $\mathrm{SU}(3)_V$ are easy to read off: since the

matrix of NGBs $\Pi \equiv \Pi^a \lambda^a/2$ must transform the same way as $\mathcal{A}_\mu \equiv \mathcal{A}_\mu^a \lambda^a/2$, we have

$$\Pi \to V \Pi V^\dagger \approx \Pi + i\alpha^a [T^a, \Pi] + \mathcal{O}(\alpha) \tag{3.32}$$

for a transformation $V = \exp(i\alpha^a T^a) \in \mathrm{SU}(3)_V$. The correspondence between the mesons and elements of Π can be ascertained by judicious choice of a basis for the algebra of $\mathrm{SU}(3)_V$. The electromagnetic charge and isospin operators can be expressed in terms of the Gell-Mann matrices as

$$Q_{\mathrm{EM}} = \frac{1}{2}\left(\lambda_3 + \frac{1}{\sqrt{3}}\lambda_8\right), \qquad I_3 = \frac{1}{2}\lambda_3. \tag{3.33}$$

These form the Cartan subalgebra of $\mathrm{SU}(3)_V$ and can be used to identify the positions of some of the particles in Π. Defining the rest of the $\mathrm{SU}(3)_V$ generators to be ladder operators produces other states in the meson octet from known ones. For example, consider the pions, which live in an SU(2) subgroup of $\mathrm{SU}(3)_V$ spanned by $\{\lambda_1/2, \lambda_2/2, \lambda_3/2\}$. Taking

$$M_1 = \begin{pmatrix} 0 & 0 & 0 \\ 1 & 0 & 0 \\ 0 & 0 & 0 \end{pmatrix} \tag{3.34}$$

gives $[Q_{\mathrm{EM}}, M_1] = -M_1$ and $[I_3, M_1] = -M_1$, which means π^- lives in this component of Π. Acting with the raising operator $T_+ \equiv (\lambda_1 + i\lambda_2)/(2\sqrt{2})$ on M_1

gives

$$M_2 \equiv T_+ M_1 = \frac{1}{\sqrt{2}} \begin{pmatrix} 1 & 0 & 0 \\ 0 & -1 & 0 \\ 0 & 0 & 0 \end{pmatrix}. \tag{3.35}$$

Since this matrix satisfies $[Q_{\rm EM}, M_2] = 0$ and $[I_3, M_2] = 0$, the neutral pion field must reside in these components. Applying this procedure produces the rest of the entries in the NGBs matrix:

$$\Pi = \begin{pmatrix} \pi^0 + \frac{1}{\sqrt{3}}\eta & \sqrt{2}\pi^+ & \sqrt{2}K^+ \\ \sqrt{2}\pi^- & -\pi^0 + \frac{1}{\sqrt{3}}\eta & \sqrt{2}K^0 \\ \sqrt{2}K^- & \sqrt{2K^0} & -\frac{2}{\sqrt{3}}\eta \end{pmatrix}, \tag{3.36}$$

where the normalization is conventional. The next section examines how Π transforms under general chiral rotations, which do not act in such an obvious way on Π.

3.2 The CCWZ Procedure

Quantum field theories often exhibit symmetry breaking where a group G spontaneously breaks into a subgroup H, producing $N_G - N_H$ NGBs.

This section reviews the Coleman-Callan-Wess-Zumino (CCWZ) procedure [42, 34], which provides a systematic way to construct a Lagrangian for the NGBs that is invariant under G with a vacuum state that is not. The following material is based on the excellent reviews [115, 126]. In the rest of this section, uppercase letters index G's generators, lowercase ones index H's generators and hatted quantities indicate broken generators and their indices.

The starting point for constructing the Lagrangian is to arrange the NGBs $\{\phi^{\hat{a}}\}$ into the exponential field

$$\Phi(x) = U[\Pi]F, \qquad U[\Pi] = \exp\left(i\frac{\sqrt{2}}{f}\Pi_{\hat{a}}(x)\hat{T}^{\hat{a}}\right), \tag{3.37}$$

where $\hat{T}^{\hat{a}}$ are the broken generators of G, F is the vacuum state (potentially a vector or a matrix), f is a constant and $\Pi(x) \equiv \Pi_{\hat{a}}(x)\hat{T}^{\hat{a}}$ is the matrix of NGBs. Two field configurations $\Phi_1(x)$ and $\Phi_2(x)$ are equivalent if $\Phi_1(x) = \Phi_2(x)h$ for $h \in H$, since $hF = F$ for all $h \in H$. This means the NGBs span the coset space G/H.

Let $\Pi^{(g)}(x)$ denote the NGB field obtained by acting on $\Pi(x)$ with $g \in G$: we want to determine what this field is. The most obvious thing to try is looking for a transformation that gives $U[\Pi] \to g \cdot U[\Pi]$. However, $g \cdot U[\Pi]$ is a general element of G and thus cannot be written as the exponential of broken generator. This transformation law cannot be obtained by transforming the NGB fields. The way forward is to use the fact that any group transformation $g_\alpha \in G$ can be written as

$$g_\alpha = e^{i\alpha_A T^A} = e^{i\hat{f}_{\hat{a}}(\alpha)\hat{T}^{\hat{a}}}e^{if_a(\alpha)T^a}, \tag{3.38}$$

where $\hat{f}$ and f are functions of α; this is a consequence of the Baker-Campbell-Hausdorff (BCH) formula. Applying this to $g \cdot U[\Pi]$ gives an implicit definition for the transformed NGBs:

$$g \cdot U[\Pi] = U[\Pi^{(g)}] \cdot h[\Pi; g] \tag{3.39}$$

$$\implies U[\Pi] \to U[\Pi^{(g)}] = g \cdot U[\Pi] \cdot h[\Pi; g]^{-1}. \tag{3.40}$$

Since $h[\Pi; g] \in H$ leaves the vacuum invariant, $\Phi(x) \to g \cdot \Phi(x)$. Thanks to eq. 3.40, applying the transformations $g_1 \in G$ and $g_2 \in G$ gives

$$(g_1 \cdot g_2) \cdot U[\Pi]F = U[\Pi^{(g_1 \cdot g_2)}] \cdot h[\Pi; g_1 \cdot g_2]^{-1} F \tag{3.41}$$

$$g_1 \cdot (g_2 \cdot U[\Pi]F) = g_1 \cdot U[\Pi^{(g_2)}] \cdot h[\Pi; g_2]^{-1} F \tag{3.42}$$

$$= U[(\Pi^{(g_2)})^{(g_1)}] \cdot h[\Pi^{(g_2)}; g_1]^{-1} \cdot h[\Pi; g_2]^{-1} F \tag{3.43}$$

$$\implies U[\Pi^{(g_1 \cdot g_2)}]F = U[(\Pi^{(g_2)})^{(g_1)}]F, \tag{3.44}$$

so this transformation respects the group multiplication law. In other words, eq. 3.39 provides a representation of the group G. Since $\Pi^{(g)}$ depends on Π in a complicated way due to the BCH formula, this is called a nonlinear representation of G.

At this point we should pause and make sure the NGB fields transform properly under H and transformations generated by the broken generators. This requires a few properties of G's structure constants:

$$[T^a, T^b] = i f^{abc} T^c \tag{3.45}$$

$$[T^a, \hat{T}^{\hat{b}}] = f^{a\hat{b}\hat{c}} \hat{T}^{\hat{c}} \equiv (t^a_\pi)_{\hat{b}\hat{c}} \hat{T}^{\hat{c}}. \tag{3.46}$$

The first line follows from $f^{ab\hat{c}} = 0$, since H forms a subgroup. The second line follows from this fact in conjunction with the totally antisymmetric nature of the structure constants. Using the Jacobi identity, it can be shown that

$$[t^a_\pi, t^b_\pi] = i f^{abc} t^c_\pi, \tag{3.47}$$

so the matrices $\{t^a_\pi\}$ furnish a representation of H, which I denote r_π. As the notation suggests, this is exactly the representation of H in which the NGBs

transform. This can be confirmed by considering $g_H = \exp(i\alpha_a T^a) \in H$ and using a nontrivial lemma of the BCH formula:

$$e^{i\alpha_a T^a} \cdot \hat{T}^{\hat{a}} \cdot e^{-i\alpha_a T^a} = \left(e^{i\alpha_a t^a_\pi}\right)_{\hat{a}\hat{b}} \hat{T}^{\hat{b}}. \tag{3.48}$$

Applying this gives

$$\begin{aligned} g_H \cdot U[\Pi] &= g_H \cdot \exp\left[i\frac{\sqrt{2}}{f}\Pi_{\hat{a}}\hat{T}^{\hat{a}}\right] && (3.49)\\ &= \exp\left[i\frac{\sqrt{2}}{f}\Pi_{\hat{a}}\left(g_H \cdot \hat{T}^{\hat{a}} \cdot g_H^{-1}\right)\right] \cdot g_H && (3.50)\\ &= \exp\left[i\frac{\sqrt{2}}{f}e^{i\alpha_a t^a_\pi}\Pi\right] \cdot g_H. && (3.51) \end{aligned}$$

Comparing with eq. 3.39 gives

$$\Pi_{\hat{a}} \to \Pi^{(g_H)}_{\hat{a}} = \left(e^{i\alpha_a t^a_\pi}\right)_{\hat{a}\hat{b}} \Pi_{\hat{b}}, \qquad h[\Pi; g_H] = g_H, \tag{3.52}$$

confirming that the NGBs transform linearly under H in the representation r_π. Another important check of our work is to examine the effect of a small transformation under the broken generators. Letting $g_{G/H} = 1 + i\alpha_{\hat{a}}\hat{T}^{\hat{a}}$ and expanding $U[\Pi]$ for small field values gives

$$\Pi_{\hat{a}} \to \Pi^{(g_{G/H})}_{\hat{a}} = \Pi_{\hat{a}} + \frac{f}{\sqrt{2}}\alpha_{\hat{a}} + \dots. \tag{3.53}$$

This demonstrates the shift symmetry that forbids mass terms for the NGBs.

While we now know how NGBs transform under elements of G and that our work is correct so far, constructing a Lagrangian directly from $U[\Pi]$ would still be challenging. For example, derivatives of $U[\Pi]$ do not transform in a nice way due to the factor of $h[\Pi; g]^{-1}$ on the right in eq. 3.40. Decomposing the Maurer-Cartan

form of G into components along the broken and unbroken generators gives objects with more convenient transformation properties. The Maurer-Cartan form is an element of the Lie algebra of G that can be defined at any point in the group by taking the "logarithmic derivative":

$$iU[\Pi]^{-1} \cdot \partial_\mu U[\Pi] \equiv d_{\mu,\hat{a}}[\Pi]\hat{T}^{\hat{a}} + e_{\mu,a}[\Pi]T^a \equiv d_\mu + e_\mu. \tag{3.54}$$

Under a group transformation $g \in G$, the Maurer-Cartan form behaves as

$$iU[\Pi]^{-1} \cdot \partial_\mu U[\Pi] \to h[\Pi; g] \cdot \Big(iU[\Pi]^{-1} \cdot \partial_\mu U[\Pi]\Big) \cdot h[\Pi; g]^{-1} \tag{3.55}$$

$$+ ih[\Pi; g] \cdot \partial_\mu h[\Pi; g]^{-1}. \tag{3.56}$$

The second line is the Maurer-Cartan form at $h[\Pi; g]$, and therefore only has components along the Lie algebra of H. This means the components of eq. 3.54 transform as

$$d_\mu[\Pi] \to h[\Pi; g] \cdot d_\mu[\Pi] \cdot h[\Pi; g]^{-1} \tag{3.57}$$

$$e_\mu[\Pi] \to h[\Pi; g] \cdot (e_\mu[\Pi] + i\partial_\mu) \cdot h[\Pi; g]^{-1}. \tag{3.58}$$

In components, the transformation law for $d_\mu[\Pi]$ is

$$d_{\mu,\hat{a}} \to d^{(g)}_{\mu,\hat{a}} = \Big(e^{i\zeta_a[\Pi;g]t^a_\pi}\Big)_{\hat{a}\hat{b}}\, d_{\mu,\hat{b}}, \tag{3.59}$$

where ζ is some complicated function.

Now it's clear why all this group theory was worth it: the object d_μ transforms in r_π for all elements in G, instead of just under the subgroup H. Keeping in mind that $h[\Pi; g]$ is local since it depends on the NGB fields, the final result is that the complete invariant Lagrangian for our theory of NGBs can be constructed by

forming locally H-invariant terms from d_μ.[5][6] This is the CCWZ procedure.

The leading order Lagrangian is easily found to be

$$\mathcal{L}^{(2)}_{\text{CCWZ}} = \frac{f^2}{4}\delta^{\hat{a}\hat{b}}\,\text{tr}\left[d_{\mu,\hat{a}}d_{\mu,\hat{b}}\right] \tag{3.60}$$

$$= \frac{f^2}{4}\,\text{tr}\left[\partial_\mu U[\Pi]\cdot\partial^\mu U[\Pi]^\dagger\right] \tag{3.61}$$

$$= \frac{1}{2}\,\text{tr}\left[\partial_\mu\Pi_{\hat{a}}\;\partial^\mu\Pi_{\hat{a}}\right] + \ldots \tag{3.62}$$

where I used $U^{-1} = U^\dagger$ and the Hermiticity of the Maurer-Cartan form to obtain the second line.

3.3 The Leading Order Chiral Lagrangian

The preceding section resulted in an abstract procedure for constructing Lagrangians for theories exhibiting $G \to H$ symmetry breaking. In this section, I demonstrate how to use CCWZ to construct the leading order Lagrangian for the light mesons, where $G = \text{SU}(3)_V \times \text{SU}(3)_A$ and $H = \text{SU}(3)_V$. This will include incorporating the mesons' masses and couplings to external fields.

Applying the CCWZ procedure requires choosing a basis for the set of broken generators of G. I work in the Σ basis, in which the RH transformations are the broken ones. Concretely, let

$$g \equiv \begin{pmatrix} L & 0 \\ 0 & R \end{pmatrix} \in \text{SU}(3)_L \times \text{SU}(3)_R \tag{3.63}$$

[5]There is one important exception: the Wess-Zumino-Witten term cannot be constructed in this manner.

[6]It's clear that e_μ cannot be used in the Lagrangian on its own. Instead, it's used to incorporate gauge fields.

be a general group element. The broken generators are then

$$\hat{T}^{\hat{a}} = \begin{pmatrix} 0 & 0 \\ 0 & \hat{T}_R^{\hat{a}} \end{pmatrix}, \tag{3.64}$$

where $\{\hat{T}_R^{\hat{a}}\}$ are the generators of $\mathrm{SU}(3)_R$. Then the exponential field is

$$U[\Pi] = \exp\left[i\frac{\sqrt{2}}{f_\pi}\Pi_{\hat{a}}\hat{T}^{\hat{a}}\right] \equiv \begin{pmatrix} 1 & 0 \\ 0 & \Sigma \end{pmatrix}, \tag{3.65}$$

where $\Sigma \equiv \exp\left[i\frac{\sqrt{2}}{f_\pi}\pi_{\hat{a}}\hat{T}_R^{\hat{a}}\right]$. Eq. 3.40 gives the result of applying a general chiral transformation:

$$U[\Pi] \to U[\Pi^{(g)}] \equiv g \cdot U[\Pi] \cdot h[\Pi; g]^{-1} \tag{3.66}$$

$$= \begin{pmatrix} L & 0 \\ 0 & R \end{pmatrix} \cdot \begin{pmatrix} 1 & 0 \\ 0 & \Sigma \end{pmatrix} \cdot \begin{pmatrix} h_V[\Pi; g]^{-1} & 0 \\ 0 & h_V[\Pi; g]^{-1} \end{pmatrix} \tag{3.67}$$

$$= \begin{pmatrix} L \cdot h_V[\Pi; g]^{-1} & 0 \\ 0 & R \cdot \Sigma \cdot h_V[\Pi; g]^{-1} \end{pmatrix} \tag{3.68}$$

$$\equiv \begin{pmatrix} 1 & 0 \\ 0 & \Sigma^{(g)} \end{pmatrix}. \tag{3.69}$$

The LH and RH components of $h[\Pi; g]^{-1}$ are the same since it is in the vector subgroup H; the last line follows since the transformed exponential field must also be an exponential of broken generators. To carry out this CCWZ construction, we can see that $h_V[\Pi; g] = L$, and so $\Sigma \to \Sigma^{(g)} = R \cdot \Sigma \cdot L^\dagger$.

Next we need to expand the Maurer-Cartan form to identify d_μ and e_μ, the fundamental building blocks of the effective Lagrangian according to CCWZ. It

is easily found to be

$$iU[\Pi]^{-1} \cdot \partial_\mu U[\Pi] = i \begin{pmatrix} 1 & 0 \\ 0 & \Sigma^\dagger \end{pmatrix} \cdot \begin{pmatrix} 0 & 0 \\ 0 & \partial_\mu \Sigma \end{pmatrix} = \begin{pmatrix} 0 & 0 \\ 0 & i\Sigma^\dagger \cdot \partial_\mu \Sigma \end{pmatrix} \tag{3.70}$$

$$= d_{\mu,\hat{a}} \hat{T}^{\hat{a}} + e_{\mu,a} T^a, \tag{3.71}$$

which means that $d_\mu = i\Sigma^\dagger \cdot \partial_\mu \Sigma$ and $e_\mu = 0$. The leading order chiral Lagrangian is thus

$$\mathcal{L}^{(2)}_{\text{chiPT}} = \frac{f_\pi^2}{4} \operatorname{tr}\left[\partial_\mu \Sigma \cdot \partial^\mu \Sigma^\dagger\right]. \tag{3.72}$$

Higher-order terms in the chiral Lagrangian can be formed by combining more powers of d_μ. As mentioned at the beginning of the chapter, Weinberg derived a power-counting scheme for assessing the relative importance of different diagrams by considering how they scale under rescaling of the external momenta. As explained in [141, 96], under a rescaling $\{p_i \to \lambda p_i\}$ of the momenta, a matrix element $\mathcal{M}(\{p_i\}) \to \lambda^D \mathcal{M}(\{p_i\})$, where

$$D = 2 + \sum_{n=1}^{\infty} 2(n-1) N_{2n} + 2N_L, \tag{3.73}$$

where N_{2n} is the number of vertices from $\mathcal{L}^{(2n)}_{\text{chiPT}}$, N_L is the number of loops and D is called the chiral dimension. For $p_i \lesssim 4\pi f_\pi$, diagrams with low chiral dimensions will dominate.

3.4 Quark Masses and External Fields

Until now I have ignored the fact that chiral symmetry is explicitly broken by the quarks' masses and couplings to other fields. To compute quantities like

$\sigma_{\bar{\chi}\chi\to\pi^+\pi^-\gamma}$ we will need to derive the Lagrangian $\mathcal{L}_{\rm QCD+EM}$ for low-energy QCD with massive quarks and electromagnetism. Understanding how to couple external fields to mesons requires revisiting the definition of an effective field theory. The top-down case is straightforward: correlation functions in the underlying and effective theory must agree. However, in bottom-up EFTs, the degrees of freedom are different. The more general statement is that correlation functions of currents (and their derivatives) must agree in the EFT and underlying theory as these encode the symmetries of the theory. These relations are called chiral Ward identities, and are encoded by requiring the generating functional

$$Z_{\rm QCD}[s,p,v,a] = \int [\mathcal{D}\bar{q}_i][\mathcal{D}q_i][\mathcal{D}G^a_\mu] e^{i\int d^4x\ \mathcal{L}_{\rm QCD}[s,p,v,a]}, \tag{3.74}$$

$$\mathcal{L}_{\rm QCD}[s,p,v,a] = \bar{\mathbf{q}}(i\not{D})\mathbf{q} - \frac{1}{4}G^a_{\mu\nu}G^{a\mu\nu} + \bar{\mathbf{q}}\gamma_\mu(r^\mu(x)P_R + l^\mu(x)P_L)\mathbf{q} \tag{3.75}$$

$$- \bar{\mathbf{q}}(s(x) - i\gamma_5 p(x))\mathbf{q}, \tag{3.76}$$

to be invariant under local $\mathrm{SU}(3)_L \times \mathrm{SU}(3)_R$ transformations [20, 96].[7] This means that the auxiliary scalar, pseudoscalar, right and left-handed fields $s(x)$, $p(x)$, $r(x)$ and $l(x)$ must transform as

$$r_\mu \to R\cdot(r_\mu + i\partial_\mu)\cdot R^\dagger \tag{3.77}$$

$$l_\mu \to L\cdot(l_\mu + i\partial_\mu)\cdot L^\dagger \tag{3.78}$$

$$s + ip \to R\cdot(s+ip)\cdot L^\dagger. \tag{3.79}$$

Correlation functions of currents can be extracted by taking functional derivatives of $Z_{\rm QCD}[s,p,v,a]$.

[7] The left and right-handed vector fields can be exchanged for vector and axial-vector fields $v_\mu = (r_\mu + l_\mu)/2$ and $a_\mu = (r_\mu - l_\mu)/2$. While they have more complicated transformation properties, they map directly onto the mediators in the vector and axial vector simplified models. I will use them when I discuss the chiral anomaly in chiPT in Sec. 3.6.

The goal in constructing the chiral Lagrangian is to find $\mathcal{L}_{\text{chiPT}}[s,p,v,a] = \sum_{n=1}^{\infty} \mathcal{L}^{(2n)}_{\text{chiPT}}[s,p,v,a]$ such that

$$Z_{\text{chiPT}}[s,p,v,a] = \int [\mathcal{D}\pi^a] e^{i\int d^4x \left[\mathcal{L}^{(2)}_{\text{chiPT}}[s,p,v,a]+\ldots\right]} = Z_{\text{QCD}}[s,p,v,a]. \tag{3.80}$$

The chiral Lagrangian is constructed by forming combinations of Σ and the auxiliary fields that are invariant under local $\text{SU}(3)_L \times \text{SU}(3)_R$. While invariants can be constructed directly from Σ and the external fields using the above transformation laws, the CCWZ approach also provides a clear and systematic way forward. As before, the key insight is that we can construct G-invariant objects that transform (nonlinearly) in r_π. Working in the same basis as in the previous section, the right and left-handed auxiliary fields can be arranged into a 6×6 matrix $A_\mu = \text{diag}(l_\mu, r_\mu)$ that transforms as $A_\mu \to g(x) \cdot (A + i\partial_\mu) \cdot g^{-1}(x)$. The Maurer-Cartan form then generalizes to the object

$$\bar{A}_\mu \equiv U[\Pi]^{-1} \cdot (A_\mu + i\partial_\mu) \cdot U[\Pi] \tag{3.81}$$

$$\equiv d_{\mu,\hat{a}}[\Pi, A]\hat{T}^{\hat{a}} + e_{\mu,a}[\Pi, A]T^a \tag{3.82}$$

$$\equiv d_\mu[\Pi, A] + e_\mu[\Pi, A]. \tag{3.83}$$

It is trivial to show that under a chiral transformation $\bar{A}_\mu \to h \cdot (\bar{A}_\mu + i\partial_\mu) \cdot h^{-1}$, just as with the Maurer-Cartan form, and thus d_μ and e_μ again transform as in eq. 3.57. The object $d_\mu[\Pi, A]$ can therefore be used to easily construct a $\text{SU}(3)_L \times \text{SU}(3)_R$-invariant Lagrangian. Furthermore, we can see that l_μ and r_μ should be regarded as $\mathcal{O}(p)$ for the power counting to be consistent. It is straightforward to derive d_μ by decomposing $\bar{A}_\mu$ along the broken and unbroken

generators in the Σ-representation:

$$\bar{A}_\mu = \begin{pmatrix} 1 & 0 \\ 0 & \Sigma^\dagger \end{pmatrix} \cdot \begin{pmatrix} l_\mu & 0 \\ 0 & r_\mu \end{pmatrix} \cdot \begin{pmatrix} 1 & 0 \\ 0 & \Sigma \end{pmatrix} = \begin{pmatrix} l_\mu & 0 \\ 0 & i\Sigma^\dagger \partial_\mu \Sigma + \Sigma^\dagger r_\mu \Sigma \end{pmatrix} \tag{3.84}$$

$$= \begin{pmatrix} 0 & 0 \\ 0 & i\Sigma^\dagger \partial_\mu \Sigma + \Sigma^\dagger r_\mu \Sigma - l_\mu \end{pmatrix} + \begin{pmatrix} l_\mu & 0 \\ 0 & l_\mu \end{pmatrix} \tag{3.85}$$

$$\implies d_\mu = i\Sigma^\dagger \partial_\mu \Sigma + \Sigma^\dagger r_\mu \Sigma - l_\mu. \tag{3.86}$$

We also need to construct invariants out of the scalar and pseudoscalar auxiliary fields, which can be arranged into a 6×6 matrix

$$\Delta \equiv \begin{pmatrix} 0 & s - ip \\ s + ip & 0 \end{pmatrix} \tag{3.87}$$

transforming as $\Delta \to g \cdot \Delta \cdot g^{-1}$. "Dressing" this matrix by conjugating with the exponential fields gives an object that transforms (reducibly) in r_π:

$$\bar{\Delta} = U[\Pi]^{-1} \cdot \Delta \cdot U[\Pi] = \begin{pmatrix} 0 & (s - ip)\Sigma \\ \Sigma^\dagger (s + ip) & 0 \end{pmatrix}. \tag{3.88}$$

This decomposes into two irreducible representations that form two invariants $\mathrm{tr}[(s - ip)\Sigma \pm \Sigma^\dagger (s + ip)]$. Parity is a symmetry of QCD, so the invariant with the minus sign does not contribute. Therefore the leading-order Lagrangian formed from d_μ and this invariant is

$$\mathcal{L}^{(2)}_{\mathrm{chiPT}}[s, p, v, a] = \frac{f_\pi^2}{4} \mathrm{tr}\left[d_{\mu,\hat{a}}[\Pi, A] d^{\mu,\hat{a}}[\Pi, A]\right] + \frac{B f_\pi^2}{2} \mathrm{tr}\left[(s - ip)\Sigma + \mathrm{h.c.}\right] \tag{3.89}$$

$$= \frac{f_\pi^2}{4} \mathrm{tr}\left[(D_\mu \Sigma)(D^\mu \Sigma)^\dagger\right] + \frac{B f_\pi^2}{2} \mathrm{tr}\left[(s - ip)\Sigma + \mathrm{h.c.}\right], \tag{3.90}$$

where it is simple to show that the covariant derivative is

$$D_\mu \Sigma = \partial_\mu \Sigma - i r_\mu \Sigma + i \Sigma l_\mu. \tag{3.91}$$

and B is a constant required to give the right mass dimensions. To ensure that the equations of motion are consistent, the scalar and pseudoscalar fields are counted as $Bs \sim Bp \sim \mathcal{O}(p^2)$. Now that I have derived this Lagrangian and settled on a parameterization for the generalized Maurer-Cartan form, I will work directly with the Σ matrix and external fields.

Quark masses can be incorporated by treating the mass matrix M_q as a so-called spurion. M_q is a constant matrix and thus invariant under chiral transformations, which means it explicitly breaks chiral symmetry. However, if $M_q \to R M L^\dagger$ under chiral transformations, the low-energy QCD Lagrangian would be invariant. The spurion procedure is to use this artificial transformation law to construct the most general invariant Lagrangian, setting M_q equal to its true value at the end to softly break the symmetry [125]. Using the general Lagrangian (eq. 3.89) with $s = M_q$ and the other external fields set to zero gives

$$\mathcal{L}^{(2)}_{\text{chiPT}} = \frac{f_\pi^2}{4} \operatorname{tr}\left[\partial_\mu \Sigma \cdot \partial^\mu \Sigma^\dagger\right] + \frac{B f_\pi^2}{2} \operatorname{tr}\left[M_q \Sigma + \Sigma^\dagger M_q\right]. \tag{3.92}$$

Expanding the Lagrangian out using the NGB matrix from eq. 3.36 gives

$$\begin{aligned}
\mathcal{L}^{(2)}_{\text{chiPT}} \supset\ & B(m_u + m_d)\pi^+\pi^- + \frac{1}{2}B(m_u + m_d)(\pi^0)^2 + B(m_u + m_s)K^+K^- && (3.93)\\
& + B(m_d + m_s)K^0\overline{K^0} + \frac{1}{6}B(m_u + m_d + 4m_s)\eta^2 && (3.94)\\
& + \frac{1}{\sqrt{3}}B(m_u - m_d)\pi^0\eta. && (3.95)
\end{aligned}$$

At lowest order and in the $m_u = m_d = m$ limit, the mesons' masses are

$$m_{\pi^+}^2 = m_{\pi^0}^2 = 2Bm \tag{3.96}$$

$$m_{K^+}^2 = m_{K^0} = B(m + m_s) \tag{3.97}$$

$$m_\eta^2 = \frac{2}{3}B(m + 2m_s) \tag{3.98}$$

These masses satisfy the Gell-Mann-Okubo relation $4m_K^2 = 3m_\eta^2 + m_\pi^2$, which is satisfied by the actual meson masses to about 5%. Substituting in for the meson masses gives $B = 2566$ MeV. It is also related to the chiral condensate through $3f_\pi^2 B = -\langle \bar{q}q \rangle$ [125].

To couple other fields to the mesons, the auxiliary fields can be promoted to dynamical ones. For example, incorporating electromagnetism requires to gauging the $\mathrm{U}(1)_{\mathrm{EM}}$ subgroup of $\mathrm{SU}(3)_L \times \mathrm{SU}(3)_R$. Since $\mathcal{L}^{(2)}_{\mathrm{chiPT}}$ is already invariant under local chiral transformations, we can simply set $l_\mu = r_\mu = eQ_q A_\mu$, where Q_q is the matrix of quark charges, so that $\mathcal{L}_{\mathrm{QCD+EM}}$ matches onto $\mathcal{L}^{(2)}_{\mathrm{chiPT+EM}} = \mathcal{L}^{(2)}_{\mathrm{chiPT}}[M_q, 0, eQ_q A_\mu, eQ_q A_\mu]$.

A particularly important application of this method is matching the Fermi theory onto the chiral Lagrangian. This gives a term coupling the charged pion to the muon and muon neutrino, permitting the width for $\pi^- \to \mu^- \bar{\nu}_\mu$ to be computed. The result is

$$\Gamma_{\pi^- \to \mu^- \bar{\nu}_\mu} = \frac{G_F^2 |V_{ud}|^2}{4\pi} f_\pi^2 m_\pi m_\mu^2 \left(1 - \frac{m_\mu^2}{m_\pi^2}\right)^2 . \tag{3.99}$$

Using the measured width, the pion decay constant f_π is found to be 92.4 MeV.

3.5 Matching for the Scalar Model

There is one term that complicates matching the scalar simplified model Lagrangian (eq. 2.1) onto the chiral Lagrangian:

$$\mathcal{L}_{>1\text{ GeV}}|_S \supset \frac{3g_{SG}\alpha_s}{4\pi v} S G^a_{\mu\nu} G^{a\mu\nu}. \tag{3.100}$$

Luckily, this same roadblock was encountered in the context of computing $\Gamma_{h\to\pi^+\pi^-}$ before the Higgs mass was known to be larger than 1 GeV [38, 50, 139]. The troublesome term can be rewritten using the conformal anomaly. A dilatation (or scale transformation) is defined by

$$\phi(x) \to e^{D\sigma}\phi(e^\sigma x), \tag{3.101}$$

where D is the scaling dimension of the field and $\sigma \in \mathbb{R}$. While $D = 1$ for scalars and vectors and 3/2 for fermions, it is 0 for Goldstone bosons as a consequence of shift symmetry [38]. The dilatation current D^μ associated with this transformation is anomalous. While the Lagrangian containing massless particles gives $\partial_\mu D^\mu = 0$, this is not true at the quantum level, since the coupling constants depend on the energy scale through their β functions. Including quantum corrections gives the relation

$$\partial^\mu D_\mu = \frac{\beta(g_s)}{2g_s} G^a_{\mu\nu} G^{a\mu\nu} + \sum_f (1-\gamma_f) m_f \bar{f} f + \frac{\beta(e)}{2e} F_{\mu\nu} F^{\mu\nu}. \tag{3.102}$$

The sum ranges over all the fermions in the theory (u, d, s, e, μ, χ for $\mathcal{L}_{>1\text{ GeV}}|_S$), and γ_f is the anomalous mass dimension for f.

To utilize this in the matching, we must rewrite $\mathcal{L}_{>1\text{ GeV}}|_S$ and scale from $\mu > 1$ GeV to $\mu < 1$ GeV. It is trivial to match terms involving electrons, muons

and the photon onto the sub-GeV Lagrangian, so I will ignore these terms in what follows. Eq. 3.102 can be rearranged as

$$-\frac{9\alpha_s}{8\pi}G^a_{\mu\nu}G^{a\mu\nu} - \sum_{q=u,d,s}\gamma_q m_q \bar{q}q = \partial^\mu D_\mu - \sum_{q=u,d,s} m_q \bar{q}q. \tag{3.103}$$

I expanded $\beta(g_s)$ to leading order since g_s is small above 1 GeV. An important result is that $\partial^\mu D_\mu$ and $m_q\bar{q}q$ are RGE-invariant, which means the LHS of this expression is as well [71]. This means we can drop the γ_q term (which goes as $\alpha_s(1\text{ GeV})$ and is thus sub-leading) and cast the terms in the Lagrangian containing quarks and gluons as

$$\mathcal{L}_{>1\text{ GeV}}|_S \supset \mathcal{L}_{\text{QCD+EM}} + \frac{3g_{SG}\alpha_s}{4\pi v}SG^a_{\mu\nu}G^{a\mu\nu} - g_{Sf}S\sum_{q=u,d,s}\frac{m_q}{v}\bar{q}q \tag{3.104}$$

$$\approx \mathcal{L}_{\text{QCD+EM}} - \frac{2g_{SG}}{3v}S\partial_\mu D^\mu - \sum_{q=u,d,s}\frac{m_q}{v}S\left(g_{Sf} - \frac{2}{3}g_{SG}\right)\bar{q}q. \tag{3.105}$$

Since the terms in this Lagrangian are RGE-invariant, we can now match onto the chiral Lagrangian using the techniques from the previous section.

Setting the external fields to

$$s = \left[1 + \frac{1}{v}\left(g_{Sf} - \frac{2g_{SG}}{3}\right)S\right]M_q \tag{3.106}$$

$$p = 0 \tag{3.107}$$

$$r_\mu = l_\mu = eQ_q A_\mu, \tag{3.108}$$

the leading order effective sub-GeV Lagrangian is found to be

$$\mathcal{L}^{(2)}_{<1\text{ GeV}}\Big|_S \supset \frac{\tilde{f}_\pi^2}{4}\operatorname{tr}\left[D_\mu\Sigma\cdot D^\mu\Sigma^\dagger\right] + \frac{\tilde{B}\tilde{f}_\pi^2}{2}\operatorname{tr}\left[M_q\Sigma^\dagger + M_q\Sigma\right] \tag{3.109}$$

$$+ \frac{\tilde{B}\tilde{f}_\pi^2}{2}\left(g_{Sf} - \frac{2g_{SG}}{3}\right)\frac{S}{v}\operatorname{tr}\left[M_q\Sigma^\dagger + M_q\Sigma\right] \tag{3.110}$$

$$- \frac{2g_{SG}}{3}\frac{S}{v}\partial_\mu D^\mu + \frac{1}{2}(\partial_\mu S)^2 - \frac{1}{2}\tilde{m}_S^2 S^2, \tag{3.111}$$

where I have only written terms for the fields that directly interact with mesons. Notice that I have written several parameters with tildes. This is because the scalar receives a vev since it couples to the chiral condensate. As a result, the parameter $\tilde{f}_\pi$ is not equal to f_π (and similarly for $\tilde{B}$ and $\tilde{m}_S$), so these parameters need to be fixed by matching onto physical quantities. The dilatation current is obtained by finding the variation of the Lagrangian under a dilatation:

$$\begin{aligned}\partial_\mu D^\mu &= \frac{\delta\,\mathcal{L}^{(2)}_{<1\text{ GeV}}\Big|_S}{\delta\sigma} \\ &= -\frac{\tilde{f}_\pi^2}{2}\operatorname{tr}[D_\mu\Sigma\cdot D^\mu\Sigma^\dagger] \\ &\qquad - \frac{\tilde{B}\tilde{f}_\pi^2}{2}\left[4 + 3\left(g_{Sf} - \frac{2g_{SG}}{3}\right)\frac{S}{v}\right]\operatorname{tr}\left[M_q\Sigma^\dagger + M_q\Sigma\right].\end{aligned} \tag{3.112}$$

Upon substituting this expression, the Lagrangian becomes

$$\mathcal{L}^{(2)}_{<1\text{ GeV}}\Big|_S \supset \frac{\tilde{f}_\pi^2}{4}\operatorname{tr}\left[D_\mu\Sigma\cdot D^\mu\Sigma^\dagger\right] + \frac{\tilde{B}\tilde{f}_\pi^2}{2}\operatorname{tr}\left[M_q\Sigma^\dagger + M_q\Sigma\right] \tag{3.113}$$

$$+ \frac{\tilde{f}_\pi^2 g_{SG}}{3}\frac{S}{v}\operatorname{tr}\left[D_\mu\Sigma\cdot D^\mu\Sigma^\dagger\right] \tag{3.114}$$

$$+ \frac{\tilde{B}\tilde{f}_\pi^2}{2}(g_{Sf} + 2g_{SG})\frac{S}{v}\operatorname{tr}\left[M_q\Sigma^\dagger + M_q\Sigma\right] \tag{3.115}$$

$$+ \frac{\tilde{B}\tilde{f}_\pi^2}{3}(3g_{Sf} - 2g_{SG})g_{SG}\frac{S^2}{v^2}\operatorname{tr}\left[M_q\Sigma^\dagger + M_q\Sigma\right] \tag{3.116}$$

$$+ \frac{1}{2}(\partial_\mu S)^2 - \frac{1}{2}\tilde{m}_S^2 S^2. \tag{3.117}$$

The final step is to determine the scalar vev and relate parameters $\tilde{f}_\pi$, $\tilde{B}$ and $\tilde{m}_S$ to physical parameters. The scalar potential is found by setting $\pi^a = 0 \leftrightarrow \Sigma = 1$:

$$V(S) = -\tilde{B}\tilde{f}_\pi^2 \operatorname{tr}[M_q] - \tilde{B}\tilde{f}_\pi^2(g_{Sf} + 2g_{SG})\frac{S}{v}\operatorname{tr}[M_q] \tag{3.118}$$

$$+ \frac{1}{2}\left[\tilde{m}_S^2 + \frac{4\tilde{B}\tilde{f}_\pi^2}{3v^2}(2g_{SG} - 3g_{Sf})g_{SG}\operatorname{tr}[M_q]\right] S^2. \tag{3.119}$$

The term on the second line must be the scalar's physical mass, m_S. The vev is straightforward to compute:

$$v_S = \frac{\tilde{B}\tilde{f}_\pi^2 \operatorname{tr}[M_q](g_{Sf} + 2g_{SG})}{vm_S^2}. \tag{3.120}$$

Now the tilde parameters can be determined. Upon shifting $S \to S + v_S$, the kinetic and mass terms for the mesons are altered. Requiring the kinetic term to be canonically normalized and the meson masses to take their physical values gives the relations

$$\tilde{f}_\pi^2 = \left(1 + \frac{4g_{SG}}{3}\frac{v_S}{v}\right) f_\pi^2 \tag{3.121}$$

$$\tilde{B}\tilde{f}_\pi^2 = \left[1 - \left(g_{Sf} + \frac{2}{3}g_{SG}\right)\frac{v_S}{v} + \mathcal{O}\left(\frac{v_S^2}{v^2}\right)\right] Bf_\pi^2, \tag{3.122}$$

where I have assumed that $v_S \ll v$. Using these relations, eq. 3.120 can be solved for the vev that minimizes $V(S)$:

$$v_S = \frac{\sqrt{4Bf_\pi^2(g_{Sf} + 2g_{SG})^2 \operatorname{tr}[M_q] + m_S^2 v^2} - m_S v}{2m_S(g_{Sf} + 2g_{SG})}. \tag{3.123}$$

With the couplings both set to 1, the vev exceeds 1 GeV (the scale of the EFT) for $m_S \lesssim 4$ MeV, altering S's couplings to mesons. Since vev appear in the

Lagrangian as v_S/v, it only impacts observables when $g_{S\chi} \ll g_{Sf}, g_{SG}$ (so the DM does not only annihilate mediators), $m_\chi > m_\pi$ (so the $\pi\pi$ final state is accessible) and $m_S \ll 4$ MeV (so the vev is large). This corner of parameter space is not relevant since $g_{S\chi}$ must be undetectably small; I will therefore set $v_S = 0$.

The final result of this section is the leading order effective sub-GeV Lagrangian for the scalar simplified model, which, to reiterate in full, is

$$\mathcal{L}^{(2)}_{<1\text{ GeV}}\Big|_S = \mathcal{L}_{S,\text{free}} + \mathcal{L}_{\chi,\text{free}} + \mathcal{L}_{\text{QED}} + \mathcal{L}^{(2)}_{\text{chiPT+EM}} + \mathcal{L}_{S,\text{int}} \tag{3.124}$$

$$+ \frac{f_\pi^2 g_{SG}}{3}\frac{S}{v}\,\text{tr}\left[D_\mu\Sigma\cdot D^\mu\Sigma^\dagger\right] \tag{3.125}$$

$$+ \frac{Bf_\pi^2}{2}(g_{Sf}+2g_{SG})\frac{S}{v}\,\text{tr}\left[M_q\Sigma^\dagger + M_q\Sigma\right] \tag{3.126}$$

$$+ \frac{Bf_\pi^2}{3}(3g_{Sf}-2g_{SG})g_{SG}\frac{S^2}{v^2}\,\text{tr}\left[M_q\Sigma^\dagger + M_q\Sigma\right] \tag{3.127}$$

$$\mathcal{L}_{S,\text{free}} = \frac{1}{2}(\partial_\mu S)^2 - \frac{1}{2}m_S^2 S^2 \tag{3.128}$$

$$\mathcal{L}_{\chi,\text{free}} = \bar\chi(i\partial\!\!\!/ - m_\chi)\chi \tag{3.129}$$

$$\mathcal{L}_{\text{QED}} = -\frac{1}{4}F_{\mu\nu}F^{\mu\nu} + \sum_{\ell=e,\mu}\bar\ell(iD\!\!\!/ - m_\ell)\ell \tag{3.130}$$

$$\mathcal{L}^{(2)}_{\text{chiPT+EM}} = \frac{f_\pi^2}{4}\,\text{tr}\left[D_\mu\Sigma\cdot D^\mu\Sigma\right] + \frac{Bf_\pi^2}{2}\,\text{tr}\left[M_q\Sigma + \Sigma^\dagger M_q\right] \tag{3.131}$$

$$\mathcal{L}_{S,\text{int}} = -g_{S\chi}S\bar\chi\chi - \frac{5\alpha_{\text{EM}}}{24\pi v}g_{SF}SF_{\mu\nu}F^{\mu\nu} - g_{Sf}S\sum_{\ell=e,\mu}\frac{m_\ell}{v}\bar\ell\ell, \tag{3.132}$$

where the covariant derivatives are

$$D_\mu\ell = (\partial_\mu + ieA_\mu)\ell, \qquad D_\mu\Sigma = \partial_\mu\Sigma + iA_\mu[\Sigma, eQ_q]. \tag{3.133}$$

3.5.1 Branching Fractions

With the effective Lagrangian in hand, it is straightforward to expand the Σ field and determine cross sections for DM annihilation into different final states.

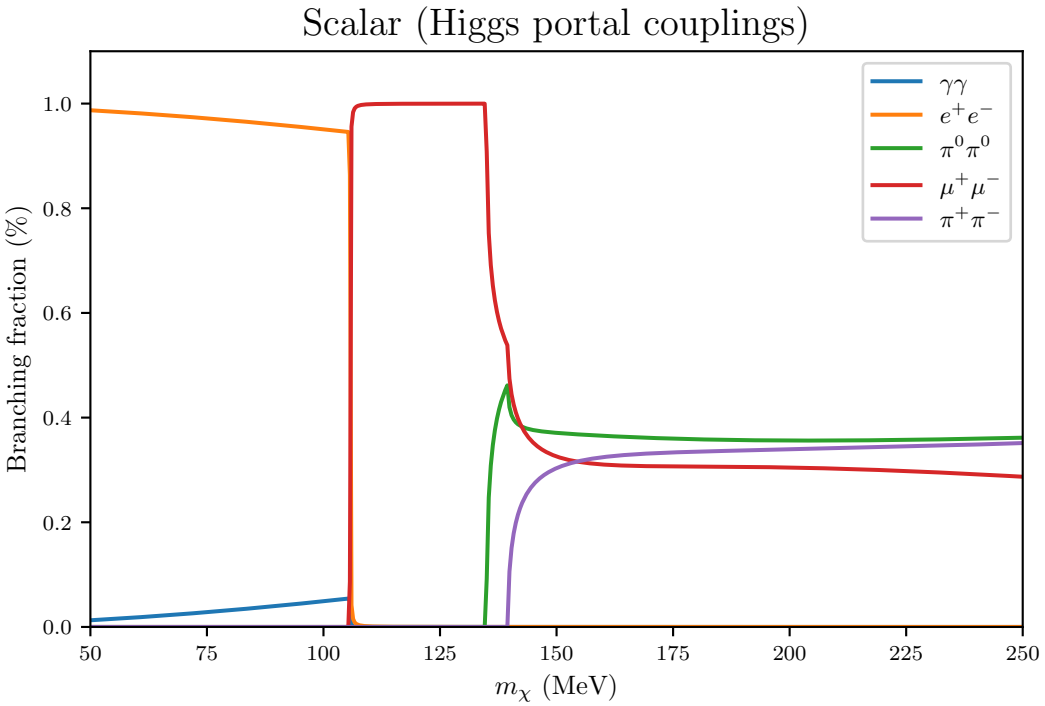

Figure 3.1: Branching fractions for DM annihilation through the scalar mediator, with $g_{S\chi\chi} = g_{Sf} = g_{SG} = g_{SF}$. The mediator's mass is taken to be larger than the dark matter's mass to turn off annihilation into mediators.

The cross sections and computational tools used to derive them are presented in App. D.1.1. The branching fractions for DM annihilation in the scalar simplified model are shown in Figure 3.1 as a function of DM mass, with all couplings set to the same value. The branching fraction is largest into whichever final state is closest to threshold since the coupling between S and each SM state is proportional to the state's Yukawa. The branching fraction into $\gamma\gamma$ is negligibly small, and this final state is generally unimportant for setting constraints on this model when other channels are available. For the coupling relations from the heavy quark UV completion ($g_{Sf} = g_{SF} = 0$, $g_{SG} \neq 0$) only the 2π final states are accessible, and their branching fractions are both 50% due to SU(2) isospin symmetry.

3.6 The Chiral Anomaly

The chiral anomaly plays an important role in the physics of mesons, giving rise to the decay $\pi^0 \to \gamma\gamma$ which sources a great deal of the photons produced in DM annihilation in my simplified models as well as in a variety of astrophysical processes. For all of the simplified models aside from the scalar one, understanding the chiral anomaly is a requirement for performing the matching. In the case of the pseudoscalar, this is clear from the presence of the $PG\tilde{G}$ term. As emphasized by the form I chose for $\mathcal{L}_{>1\text{ GeV}}|_P$, P plays a similar role to the axion, which has long been known to mix with the neutral pion [140]. The $\gamma\gamma$, $3\pi^0$ and $\pi^0\pi^+\pi^-$ final states inherited from this mixing produce significant numbers of photons. The mediator in the vector simplified model plays a similar role to the photon, giving rise the $\pi^0\gamma$ annihilation final state that contributes dominantly or subdominantly to the spectrum, depending on the couplings. The discussion in this section will follow several excellent references: Gasser and Leutwyler's original paper on $\mathrm{U}(3)_L \times \mathrm{U}(3)_R$ chiPT [61], a modern and clear discussion of anomalies in $\mathrm{U}(2)_L \times \mathrm{U}(2)_R$ chiPT [81], and some relevant points from a comprehensive analysis of large-N_c chiPT [82].

3.6.1 The Generating Functional for the Anomaly in QCD

The starting point for this analysis is the QCD Lagrangian, this time with a theta term:

$$\mathcal{L}_{\text{QCD}}[s,p,v,a,\theta] = \bar{\mathbf{q}}(i\not{D})\mathbf{q} - \frac{1}{4}G^a_{\mu\nu}G^{a\mu\nu} + \bar{\mathbf{q}}\gamma_\mu(v^\mu(x) + a^\mu(x)\gamma^5)\mathbf{q} \tag{3.134}$$

$$- \bar{\mathbf{q}}(s(x) - i\gamma_5 p(x))\mathbf{q} + \frac{g_s^2}{32\pi^2}\theta(x)G^a_{\mu\nu}\tilde{G}^{a\mu\nu}, \tag{3.135}$$

where s, p, v_μ and a_μ are 3×3 hermitian matrices. As described above, imposing local $\mathrm{U}(3)_L \times \mathrm{U}(3)_R$ invariance and taking functional derivatives gives the chiral Ward identities for this theory. Similarly to the spurion analysis used above to incorporate quark masses and external fields, we need to extend the chiral Lagrangian to break $\mathrm{U}(1)_A$ in the manner dictated by the anomaly. The transformation law for the action $S_{\mathrm{QCD}}[s, p, v, a, \theta]$ under a small chiral transformation

$$R(x) = 1 + i\beta(x) + i\alpha(x), \qquad L(x) = 1 + i\beta(x) - i\alpha(x), \tag{3.136}$$

where $\alpha(x)$ and $\beta(x)$ are 3×3 Hermitian matrices, is well-known. First, all the terms in $\mathcal{L}_{\mathrm{QCD}}[s, p, v, a, \theta]$ aside from the theta term must be invariant, which is already the case thanks to the transformation laws in eqs. 3.77-3.79. However, the generating function is not invariant due to the fermion determinant, which gives two contributions to the action. The first part comes from the $\mathrm{U}(1)_A$ part of the transformation and gives the familiar $G\tilde{G}$ term, which results in the following transformation law for $\theta(x)$:

$$\theta(x) \to \theta(x) - 2 \operatorname{tr} \alpha(x). \tag{3.137}$$

The generalization to a finite transformation $(\bar{L}, \bar{R}) \in \mathrm{U}(3)_L \times \mathrm{U}(3)_R$ is $\theta \to \theta - \arg\det \bar{R}\bar{L}^\dagger$.[8] The second contribution to the action captures the other anomalous

[8]Since $\mathrm{U}(3)_L \times \mathrm{U}(3)_R$ is not simply connected and log is multivalued, the generating functional must therefore be periodic in $\theta(x)$ with period 2π [61].

triangle, square and pentagon diagrams[9]. It can be written explicitly as [16]

$$\delta S[s,p,v,a,\theta]_{\rm WZW} = \int d^4x \ \ {\rm tr}[\alpha(x)\Omega(x)], \tag{3.138}$$

$$\Omega(x) = -\frac{N_c}{16\pi^2}\epsilon^{\alpha\beta\mu\nu}\Big[v_{\alpha\beta}v_{\mu\nu} + \frac{4}{3}(\nabla_\alpha a_\beta)(\nabla_\mu a_\nu) + \frac{2}{3}i\{v_{\alpha\beta}, a_\mu a_\nu\} + \frac{8}{3}ia_\mu v_{\alpha\beta}a_\nu + \frac{4}{3}a_\alpha a_\beta a_\mu a_\nu\Big] \tag{3.139}$$

$$v_{\alpha\beta} = \partial_\alpha v_\beta - \partial_\beta v_\alpha - i[v_\alpha, v_\beta] \tag{3.140}$$

$$\nabla_\alpha a_\beta = \partial_\alpha a_\beta - i[v_\alpha, a_\beta], \tag{3.141}$$

where $N_c = 3$ is the number of colors. Note that this is independent of the quark and gluon fields. The initials in the subscript stand for Wess, Zumino and Witten, who studied how to generate this term in chiPT.

Example: the $\mathrm{U}(1)_A$ Anomaly

Now is a good time to pause and check that this generating function machinery gives the right Ward identity for a small $\mathrm{U}(1)_A$ transformation applied to QCD with electromagnetism. In this case, $\alpha(x) = a(x)$ is proportional to the identity and $\beta(x) = 0$. The external fields are $s = M_q$, $v_\mu = eQ_qA_\mu$ with $p = a_\mu = 0$. The quark masses must be treated as a spurion since it explicity breaks $\mathrm{U}(1)_A$: I will pretend it transforms under $\mathrm{U}(1)_A$, write the result, and substitute $s = M_q$ at the end. Using the transformation law from eq. 3.79 and dropping $\mathcal{O}(a^2)$ terms gives

$$s + ip \to (1 + ia)(s + ip)(1 + ia) = (s - 2ap) + i(p + 2as) \tag{3.142}$$

$$\implies M_q \to M_q, \ p \to 2aM_q, \tag{3.143}$$

[9]Note that higher-order polygonal diagrams do not contribute since they are not divergent.

which changes the Lagrangian by

$$\delta\mathcal{L}_p = 2ia\bar{\mathbf{q}}M_q\gamma_5\mathbf{q}. \tag{3.144}$$

The theta term transforms to $\theta - 2\,\mathrm{tr}\,\alpha = \theta - 6a$, changing the Lagrangian by

$$\delta\mathcal{L}_\theta = -\frac{6g_s^2 a}{32\pi^2}G^a_{\mu\nu}\tilde{G}^{a\mu\nu}. \tag{3.145}$$

Using $v_{\alpha\beta} = eQ_qF_{\alpha\beta}$, the Wess-Zumino-Witten contribution is found to be

$$\delta\mathcal{L}_{\mathrm{WZW}} = -\frac{3e^2\,\mathrm{tr}[Q_q^2]a}{8\pi^2}F_{\mu\nu}\tilde{F}^{\mu\nu}. \tag{3.146}$$

Putting this all together with the earlier discussion of Noether's theorem gives the divergence of the $\mathrm{U}(1)_A$ current:

$$\partial_\mu J^\mu_{\mathrm{U}(1)_A} = \frac{\partial\delta\mathcal{L}}{\partial a(x)} = 2i\bar{\mathbf{q}}M_q\gamma_5\mathbf{q} - \frac{3g_s^2}{16\pi^2}G^a_{\mu\nu}\tilde{G}^{a\mu\nu} - \frac{3e^2\,\mathrm{tr}[Q_q^2]}{8\pi^2}F_{\mu\nu}\tilde{F}^{\mu\nu}. \tag{3.147}$$

This is exactly the expression derived in chapter 19 of Peskin and Schroeder [118] and chapter 30 of Schwartz [127].

3.6.2 The Generating Functional for the Anomaly in ChiPT

Now that we understand how $\mathcal{L}_{\mathrm{QCD}}$ transforms under $\mathrm{U}(3)_L \times \mathrm{U}(3)_R$, we need to extend the chiral Lagrangian. More specifically, the field $\theta(x)$ needs to appear in the chiral Lagrangian and have the correct transformation law (eq. 3.137). The generating function for the effective action also needs a term whose variation gives the anomalous terms $\delta S[s,p,v,a,\theta]_{\mathrm{WZW}}$.

As I showed in Sec. 3.3, under $(L(x), R(x)) \in \mathrm{SU}(3)_L \times \mathrm{SU}(3)_R$ the $\Sigma(x)$ field

transforms as

$$\Sigma \to R \cdot \Sigma \cdot L^\dagger. \tag{3.148}$$

The generalization to $\mathrm{U}(3)_L \times \mathrm{U}(3)_R$ is obtained by substituting $\Sigma(x) \to \bar{\Sigma}(x) = e^{-i\theta/3}\Sigma(x)$:[10]

$$\bar{\Sigma} \to \bar{R} \cdot \bar{\Sigma} \cdot \bar{L}^\dagger, \qquad (\bar{L}, \bar{R}) = \left(e^{i(b-a)}L, e^{i(b+a)}R\right) \in \mathrm{U}(3)_L \times \mathrm{U}(3)_R, \tag{3.149}$$

where $a(x), b(x) \in \mathbb{R}$ are the $\mathrm{U}(1)_B$ and $\mathrm{U}(1)_A$ parts of the transformation.[11] Expanding the transformation law out to see how $\theta(x)$ changes, we find

$$\bar{\Sigma} \to e^{i[6a-\theta]/3} R \cdot \Sigma \cdot L^\dagger \tag{3.150}$$

$$\implies \theta \to \theta - 6a, \tag{3.151}$$

$$\implies \Sigma \to R \cdot \Sigma \cdot L^\dagger. \tag{3.152}$$

Since $\arg\det \bar{R}\bar{L}^\dagger = 6a$, the transformation law for $\theta(x)$ is in accordance with eq. 3.137. The covariant derivative also must be modified so that it transforms in

[10] As I mentioned above, the complex logarithm is multivalued, which means this expansion is only well-defined for small field values (ie, near $\bar{\Sigma} = 1$). Care must be taken in performing finite $\mathrm{U}(3)_L \times \mathrm{U}(3)_R$ transformations on the effective Lagrangian. These ambiguities are discussed in detail by several authors [82, 61], but are not important for this work since I will be working to leading order in θ.

[11] Note that I have used BCH to write $\bar{R}$ and $\bar{L}$ as products of elements of U(1) and SU(3). The U(1) factors are not actually uniquely defined by $\bar{R}$ and $\bar{L}$, since eg. $\exp(i(a+b)) = [\det \bar{R}]^{1/3}$ is multivalued. It is not hard to see that the actual isomorphism is $\mathrm{U}(N) \cong \mathrm{SU}(N) \times \mathrm{U}(1)/\mathbb{Z}_N$. This doesn't affect the discussion, and the more important subtlety is that the generating function is periodic in θ with period 2π.

the same way as $\bar{\Sigma}$. This is achieved by taking

$$D_\mu \bar{\Sigma} \equiv e^{-i\theta/3}\left[D_\mu \Sigma - \frac{i}{3}(D_\mu\theta)\Sigma\right], \tag{3.153}$$

$$D_\mu \Sigma \equiv \partial_\mu \Sigma - i\hat{r}_\mu \Sigma + i\Sigma \hat{l}_\mu \tag{3.154}$$

$$D_\mu \theta = \partial_\mu \theta + 2\,\mathrm{tr}\, a_\mu. \tag{3.155}$$

where the covariant derivative only involves the traceless external fields $\hat{r}_\mu \equiv r_\mu - \frac{1}{3}\,\mathrm{tr}\, r_\mu$, $\hat{l}_\mu \equiv l_\mu - \frac{1}{3}\,\mathrm{tr}\, l_\mu$, coinciding with the original definition (see eq. 3.91). I confirm this transforms correctly in Appendix C. Putting these ingredients together, the locally invariant $\mathrm{U}(3)_L \times \mathrm{U}(3)_R$ leading order chiral Lagrangian is [61]

$$\begin{aligned}\mathcal{L}^{(2)}_{\mathrm{chiPT}}[s,p,v,a,\theta] &= \frac{f_\pi^2}{4}\,\mathrm{tr}\left[D_\mu\bar{\Sigma}\cdot(D^\mu\bar{\Sigma})^\dagger\right] + \frac{Bf_\pi^2}{2}\,\mathrm{tr}\left[(s-ip)\bar{\Sigma} + (s+ip)\bar{\Sigma}^\dagger\right] \\ &\quad + \frac{1}{12}(H_\theta - f_\pi^2)(D_\mu\theta)(D^\mu\theta) \qquad (3.156)\\ &= \frac{f_\pi^2}{4}\,\mathrm{tr}\left[D_\mu\Sigma\cdot(D^\mu\Sigma)^\dagger\right] \\ &\quad + \frac{Bf_\pi^2}{2}\,\mathrm{tr}\left[e^{-i\theta/3}(s-ip)\Sigma + e^{i\theta/3}(s+ip)\Sigma^\dagger\right] \\ &\quad + \frac{1}{12}H_\theta(D_\mu\theta)(D^\mu\theta), \qquad (3.157)\end{aligned}$$

where I used $\mathrm{tr}[\Sigma^\dagger D_\mu \Sigma] = 0$ to expand in terms of $\Sigma(x)$ and $\theta(x)$. Since the last term only leads to mediator-mediator interactions and $f_\pi^2 \sim \mathcal{O}(N_c)$ while the low energy constant H_θ is $\mathcal{O}(1)$ [81], I will ignore it from now on.

Wess and Zumino were the first to derive the $\mathrm{U}(3)_L \times \mathrm{U}(3)_R$-variant generating functional that reproduces the change in the effective action in eq. 3.138 [142]. Ignoring $\theta(x)$ briefly, the idea is to find a functional $S_{\mathrm{WZW}}[v,a]$ depending on Σ such that its variation under an infinitesimal chiral transformation $R = 1 + i(\beta + \alpha)$,

$L = 1 + i(\beta - \alpha)$ is given by eq. 3.138:

$$D(\beta, \alpha) S_{\rm WZW}[v, a] = \int d^4x \ \ {\rm tr}[\alpha(x)\Omega(x)], \tag{3.158}$$

where $D(\beta, \alpha)$ is the generator of infinitesimal chiral transformations. [12] This is a differential equation for $S_{\rm WZW}[v, a]$ and thus requires a boundary condition. The correct one is

$$S_{\rm WZW}[1, v, a] = 0, \tag{3.160}$$

since this is consistent with $S_{\rm WZW}[v, a]$ being invariant under the subgroup of vector transformations. Then if we choose matrices β_Σ and α_Σ satisfying

$$R_\Sigma \cdot \Sigma \cdot L_\Sigma^\dagger = e^{i(\beta_\Sigma + \alpha_\Sigma)} \Sigma e^{-i(\beta_\Sigma - \alpha_\Sigma)} = 1 \tag{3.161}$$

we have

$$e^{D(\beta_\Sigma, \alpha_\Sigma)} S_{\rm WZW}[v, a] = 0. \tag{3.162}$$

The solution to eq. 3.161 is clearly not unique [81], but Wess and Zumino derived consistency conditions demonstrating that the final result for the action is independent of this choice. A convenient solution is to take $\alpha_\Sigma = -\beta_\Sigma$ (or $R = 1$, $L = \Sigma$), which implies $e^{-2i\alpha_\Sigma} = \Sigma$. Then using eq. 3.158 along with the identity

[12] While we will not need it, the explicit form of the generator is found to be

$$D(\beta, \alpha) = \int d^4x \ \ \left[i[\alpha, a_\mu] \frac{\delta}{\delta v_\mu} + (\partial_\mu \alpha + i[\alpha, v_\mu]) \frac{\delta}{\delta a_\mu} - \{\alpha, p\} \frac{\delta}{\delta s} + \{\alpha, s\} \frac{\delta}{\delta p} - 2 \, {\rm tr} \, \alpha \frac{\delta}{\delta \theta} + \ldots \right], \tag{3.159}$$

where I omitted similar terms for the vector part of the transformation. It can be verified that this reproduces the transformation laws of the fields under finite chiral transformations, eqs. 3.77-3.79.

$1/n = \int_0^1 dt\ t^{n-1}$ and linearity of the generator in α and β, the above equation becomes

$$\begin{aligned}
S_{\rm WZW}[v,a] &= \left(1 - e^{D(\beta_\Sigma,\alpha_\Sigma)}\right) S_{\rm WZW}[v,a] \\
&= -\sum_{n=1}^{\infty} \frac{1}{n!}[D(\beta_\Sigma,\alpha_\Sigma)]^n S_{\rm WZW}[v,a] \\
&= -\sum_{n=1}^{\infty} \frac{1}{n}\frac{1}{(n-1)!}\int d^4x\ \ {\rm tr}\left\{\alpha(x)[D(\beta_\Sigma,\alpha_\Sigma)]^{n-1}\Omega(x)\right\} \\
&= -\sum_{n=1}^{\infty} \int_0^1 dt\ t^{n-1}\frac{1}{(n-1)!}\int d^4x\ \ {\rm tr}\left\{\alpha(x)[D(\beta_\Sigma,\alpha_\Sigma)]^{n-1}\Omega(x)\right\} \\
&= -\sum_{n=0}^{\infty} \int_0^1 dt\ t^{n}\frac{1}{n!}\int d^4x\ \ {\rm tr}\left\{\alpha(x)[D(\beta_\Sigma,\alpha_\Sigma)]^{n}\Omega(x)\right\} \\
&= -\int_0^1 dt\ \ \int d^4x\ \ {\rm tr}\{\alpha(x) e^{D(t\beta_\Sigma,t\alpha_\Sigma)}\Omega(x)\}. \qquad (3.163)
\end{aligned}$$

The operator e^D replaces v_μ and a_μ with their transformed values

$$e^{D(t\beta_\Sigma,t\alpha_\Sigma)}\Omega[v,a] = \Omega[v_t,a_t], \qquad (3.164)$$

where

$$v_t{}^\mu + a_t{}^\mu = v^\mu + a^\mu \qquad (3.165)$$

$$v_t{}^\mu - a_t{}^\mu = \Sigma_t(v^\mu - a^\mu)\Sigma_t^\dagger + i\Sigma_t\partial_\mu\Sigma_t^\dagger, \qquad (3.166)$$

$$\Sigma_t \equiv e^{-2it\alpha_\Sigma} = (\Sigma)^t. \qquad (3.167)$$

These can be substituted into eq. 3.163 and the integral over t can be performed explicitly, giving an action containing only odd numbers of mesons, in contrast with the invariant piece of the chiral Lagrangian [125]. Letting $\Xi_\mu^L = \Sigma^\dagger\partial_\mu\Sigma$ and

$\Xi_\mu^R = \Sigma\partial_\mu\Sigma^\dagger$, the piece of the Lagrangian depending on the external fields is

$$\mathcal{L}_{\mathrm{WZW}}[v,a] = -\frac{3i}{48\pi^2}\epsilon^{\mu\nu\rho\sigma}\,\mathrm{tr}[Z_{\mu\nu\rho\sigma}[v,a]], \tag{3.168}$$

$$Z_{\mu\nu\rho\sigma}[v,a] = \frac{1}{2}\Sigma l_\mu\Sigma^\dagger r_\nu\Sigma l_\rho\Sigma^\dagger r_\sigma \tag{3.169}$$

$$+\,\Sigma l_\mu l_\nu l_\rho\Sigma^\dagger r_\sigma - \Sigma^\dagger r_\mu r_\nu r_\rho\Sigma l_\sigma \tag{3.170}$$

$$+\,i\Sigma(\partial_\mu l_\nu)l_\rho\Sigma^\dagger r_\sigma - i\Sigma^\dagger(\partial_\mu r_\nu)r_\rho\Sigma l_\sigma \tag{3.171}$$

$$+\,i(\partial_\mu r_\nu)\Sigma l_\rho\Sigma^\dagger r_\sigma - i(\partial_\mu l_\nu)\Sigma^\dagger r_\rho\Sigma l_\sigma \tag{3.172}$$

$$-\,i\Xi_\mu^L l_\nu\Sigma^\dagger r_\rho\Sigma l_\sigma + i\Xi_\mu^R r_\nu\Sigma l_\rho\Sigma^\dagger r_\sigma \tag{3.173}$$

$$-\,i\Xi_\mu^L l_\nu l_\rho l_\sigma + i\Xi_\mu^R r_\nu r_\rho r_\sigma \tag{3.174}$$

$$+\,\frac{1}{2}\left[\Xi_\mu^L\Sigma^\dagger(\partial_\nu r_\rho)\Sigma l_\sigma - \Xi_\mu^R\Sigma(\partial_\nu l_\rho)\Sigma^\dagger r_\sigma\right] \tag{3.175}$$

$$+\,\frac{1}{2}\left[\Xi_\mu^L\Sigma^\dagger r_\nu\Sigma(\partial_\rho l_\sigma) - \Xi_\mu^R\Sigma l_\nu\Sigma^\dagger(\partial_\rho r_\sigma)\right] \tag{3.176}$$

$$-\,\Xi_\mu^L\Xi_\nu^L\Sigma^\dagger r_\rho\Sigma l_\sigma + \Xi_\mu^R\Xi_\nu^R\Sigma l_\rho\Sigma^\dagger r_\sigma \tag{3.177}$$

$$+\,\Xi_\mu^L[l_\nu(\partial_\rho l_\sigma) + (\partial_\nu l_\rho)l_\sigma] - \Xi_\mu^R[r_\nu(\partial_\rho r_\sigma) + (\partial_\nu r_\rho)r_\sigma] \tag{3.178}$$

$$+\,\frac{1}{2}\Xi_\mu^L l_\nu\Xi_\rho^L l_\sigma - \frac{1}{2}\Xi_\mu^R r_\nu\Xi_\rho^R r_\sigma \tag{3.179}$$

$$-\,i\Xi_\mu^L\Xi_\nu^L\Xi_\rho^L l_\sigma + i\Xi_\mu^R\Xi_\nu^R\Xi_\rho^R r_\sigma. \tag{3.180}$$

This describes processes such as $\pi^0 \to \gamma\gamma$. Interestingly, $S_{\mathrm{WZW}}[0,0]$ is nonzero, and was studied in detail by Witten in [143]. The leading order term contains five-meson interactions, accounting for $K^+K^- \to \pi^0\pi^+\pi^-$; this will not be relevant for this thesis.

Importantly for my work, the singlet part of the external axial field $\mathrm{tr}\,a_\mu$ does not appear in $S_{\mathrm{WZW}}[v,a]$. This means we are free to perform a $\mathrm{U}(1)_A$ transformation to eliminate $\theta(x)$ from $S_{\mathrm{WZW}}[v,a]$.[13] The scalar and pseudoscalar external

[13] In fact, SWZW$[v,a]$ is only defined up to contact terms involving θ along with two or more factors of a_μ [81, 82]. These terms are not relevant for this work.

fields also do not appear in $S_{\rm WZW}[v,a]$, which makes sense because s and p do not appear in $\Omega(x)$.

3.7 Matching for the Pseudoscalar Model

By comparing the Lagrangians $\mathcal{L}_{>1\text{ GeV}}|_P$ and $\mathcal{L}_{\rm QCD}[s,p,v,a,\theta]$ (see eqs. 2.16 and 3.134), we see that the external fields should be set to

$$s = M_q \tag{3.181}$$

$$p = g_{Pq} P \tag{3.182}$$

$$v_\mu = eQ_q A_\mu \tag{3.183}$$

$$a_\mu = 0 \tag{3.184}$$

$$\theta = g_{PG}\frac{P}{v}. \tag{3.185}$$

The leading-order chiral Lagrangian is obtained by substituting these into eq. 3.157:

$$\mathcal{L}^{(2)}_{<1\text{ GeV}}\Big|_P \approx \mathcal{L}_{P,\rm free} + \mathcal{L}_{\chi,\rm free} + \mathcal{L}_{\rm QED} + \mathcal{L}_{P,\rm int} \tag{3.186}$$

$$+ \frac{f_\pi^2}{4}\,\mathrm{tr}\left[D_\mu\tilde{\Sigma}\cdot(D^\mu\tilde{\Sigma})^\dagger\right] \tag{3.187}$$

$$+ \frac{Bf_\pi^2}{2}\,\mathrm{tr}\left\{\left[M_q - i\left(g_{Pq}+\frac{g_{PG}}{v}M_q\right)P\right]\tilde{\Sigma}\right. \tag{3.188}$$

$$\left. + \left[M_q + i\left(g_{Pq}+\frac{g_{PG}}{v}M_q\right)P\right]\tilde{\Sigma}^\dagger\right\}, \tag{3.189}$$

$$\mathcal{L}_{P,\rm free} = \frac{1}{2}(\partial_\mu\tilde{P})(\partial^\mu\tilde{P}) - \frac{1}{2}m_{\tilde{P}}^2\tilde{P}^2, \tag{3.190}$$

where I expanded to leading order in $g_{PG}P/v$ to be consistent with the microscopic model. [14] The matching for this theory and the axion are very similar [70].

[14] This avoids several other complications. For example, the external fields θ and p have different transformation laws, which means P does not transform in a well-defined way if we do not make this expansion. Additionally, the potential for P and π^0 contains a cosine term (as

While P does not acquire a vev, we must find the mass eigenstates (P, π^0) in terms of the interaction eigenstates $(\tilde{P}, \tilde{\pi^0})$, since these mix via[15]

$$\mathcal{L}^{(2)}_{<1\text{ GeV}}\Big|_P \supset \frac{Bf_\pi}{v_h}[(g_{Pu}+g_{PG})m_u-(g_{Pd}+g_{PG})m_d]\tilde{P}\tilde{\pi^0} \equiv \epsilon\tilde{P}\tilde{\pi^0}. \tag{3.192}$$

I will assume the mixing is small ($\epsilon \ll m^2_{\tilde{P}} - m^2_{\pi^0}$). Setting the effective mediator mass to

$$m^2_{\tilde{P}} = m^2_P + \frac{\epsilon^2}{m^2_\pi - m^2_P} \tag{3.193}$$

ensures P has the same mass in the EFT and microscopic model. The neutral pion-like mass eigenstate's mass is shifted the leading order chiPT value $m^2_\pi \equiv 2B(m_u+m_d)$ to

$$m^2_\pi + \frac{\epsilon^2}{m^2_\pi - m^2_P}. \tag{3.194}$$

While this certainly puts constraints on the pseudoscalar's couplings to matter, a full analysis requires a next-to-leading order chiPT analysis, taking into account eg. the electromagnetic contribution to $m^2_{\pi^0} - m^2_{\pi^+}$. This is beyond the scope of this work, and instead I avoid parameters for which $\epsilon^2/(m^2_\pi - m^2_P) > 5$ MeV.

with the axion) as well as a sine term which is not bounded below nor periodic. A way to avoid these issues would have been to define P's couplings to fermions using

$$\mathcal{L}_{>1\text{ GeV}}|_P \supset \sum_f m_f \bar{f} e^{ig_{Pf}P\gamma^5/v} f, \tag{3.191}$$

as with the axion [9]. I will leave these issues for future study since the resulting DM annihilation cross sections depend only on the $\mathcal{O}(P/v)$ part of the Lagrangian and are thus the same in this framework and the one I have chosen.

[15]Note that $\langle\pi^0\rangle$ remains zero, as it should since it is a PNGB. The pseudoscalar mediator also mixes with the η. I will ignore this since the η is above the 500 MeV cutoff for this analysis.

The mass and interaction eigenstates are related by

$$\begin{pmatrix} \pi^0 \\ P \end{pmatrix} = \begin{pmatrix} \cos\theta_{P\pi^0} & \sin\theta_{P\pi^0} \\ -\sin\theta_{P\pi^0} & \cos\theta_{P\pi^0} \end{pmatrix} \begin{pmatrix} \tilde{\pi^0} \\ \tilde{P} \end{pmatrix}, \tag{3.195}$$

where $\theta_{P\pi^0} = \epsilon/(m_P^2 - m_\pi^2)$ and I will work to $\mathcal{O}(\theta_{P\pi^0})$. As a result, P inherits the neutral pion's interactions, which contribute to $P \to \gamma\gamma$ as well as $P \to \pi^0\pi^0\pi^0$ through $\mathcal{L}_{\rm WZW}$.

3.7.1 Branching Fractions

Since P has odd parity it cannot annihilate into two-pion final states: instead, $\gamma\gamma$, $3\pi^0$ and $\pi^0\pi^+\pi^-$ are the dominant annihilation channels. The first has a tree-level contribution from the effective interaction in the microscopic model as well as a contribution from P mixing with the neutral pion in the Wess-Zumino-Witten action. The coupling to the other two channels comes from the mass term in the chiral Lagrangian. The cross sections are given in App. D.2.1. Ignoring the coupling g_{PF}, all of the cross sections are proportional to the mixing angle $\theta_{P\pi^0}$. The annihilation into these final states as well as leptonic ones is s-wave.

The resulting branching fractions are shown in Figure 3.2, with $m_P > m_\chi$ and the couplings set to $g_{Pu} = -g_{Pd}$ and g_{PG}, g_{PF} given by eqs. 2.21-2.22. The branching fraction into neutral pions dominates almost immediately when that final state is accessible. Using couplings inspired by the type II 2HDM UV completion ($g_{Pd} = g_{P\ell} = 0$) effectively stretches out the x-axis of this plot, with $\mathrm{Br}(\bar{\chi}\chi \to \gamma\gamma)$ dropping below $\mathrm{Br}(\bar{\chi}\chi \to 3\pi^0)$ at $m_\chi \sim 212$ MeV rather than $m_\chi \sim 207$ MeV. This will change the resulting gamma ray spectra and resulting constraints very slightly. If the coupling to leptons is nonzero, its branching fraction into hadronic states is ~ 5 orders of magnitude smaller than into leptonic

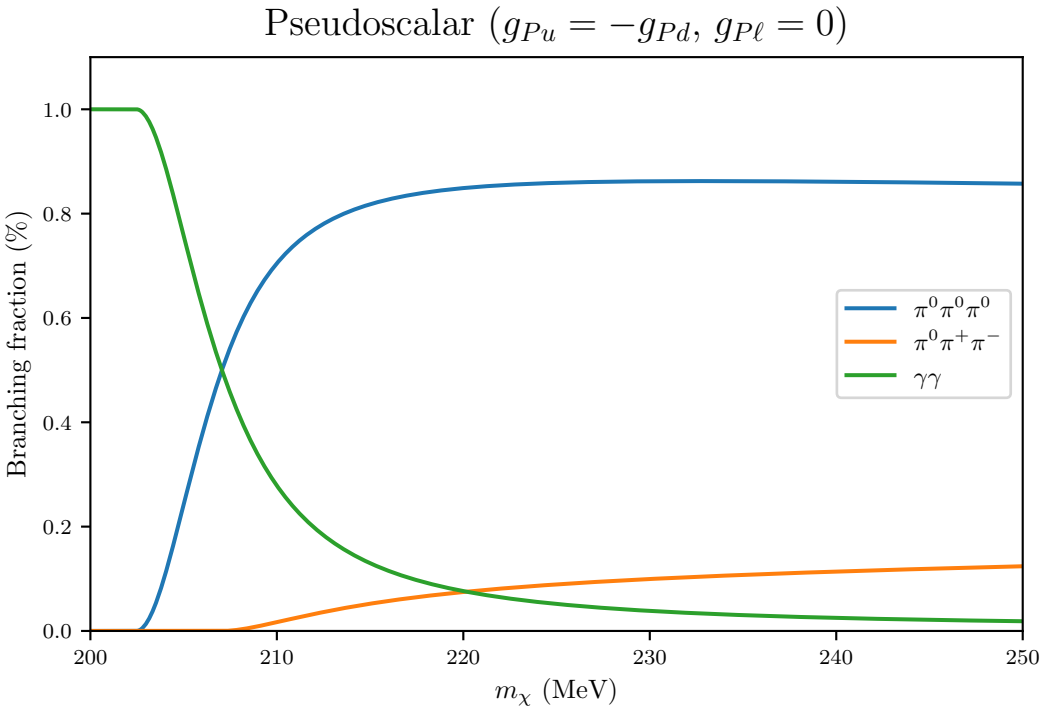

Figure 3.2: Branching fractions for DM annihilation in the pseudoscalar simplified model, with the benchmark couplings $g_{Pu} = -g_{Pd}$ and g_{PG}, g_{PF} given by the MFV relations in eqs. 2.21-2.22. The pseudoscalar's mass is set to a value larger than m_χ.

ones, so I will ignore this scenario.

3.8 Matching for the Vector Model

The matching for the vector theory is very simple at this point. Setting $r_\mu = l_\mu = eQ_q A_\mu + g_{Vq} V_\mu$ gives the leading order effective sub-GeV Lagrangian:

$$\mathcal{L}^{(2)}_{<1\text{ GeV}}\Big|_V = \mathcal{L}_{V,\text{free}} + \mathcal{L}_{\chi,\text{free}} + \mathcal{L}_{\text{QED}} + \mathcal{L}_{V,\text{int}} + \mathcal{L}_{\text{WZW}}|_V \tag{3.196}$$

$$+ \frac{f_\pi^2}{4}\,\text{tr}\left[D_\mu\Sigma \cdot D^\mu\Sigma^\dagger\right] + \frac{B f_\pi^2}{2}\,\text{tr}\left[M_q\Sigma^\dagger + M_q\Sigma\right], \tag{3.197}$$

$$\mathcal{L}_{\text{WZW}}|_V = \mathcal{L}_{\text{WZW}}[eQ_qA_\mu + g_{Vq}V_\mu, eQ_qA_\mu + g_{Vq}V_\mu] \tag{3.198}$$

$$\mathcal{L}_{V,\text{free}} = -\frac{1}{4}V_{\mu\nu}V^{\mu\nu} + \frac{1}{2}m_V^2 V_\mu V^\mu, \tag{3.199}$$

where the covariant derivatives are

$$D_\mu \ell = (\partial_\mu + ieA_\mu)\ell, \qquad D_\mu\Sigma = \partial_\mu\Sigma + ieA_\mu[\Sigma, Q_q] + iV_\mu[\Sigma, g_{Vq}]. \tag{3.200}$$

3.8.1 Branching Fractions

The expressions for the DM annihilation cross sections are collected in App. D.3.1. Figure 3.3 shows the branching fractions for DM annihilating into hadronic final states through V as a function of the ratio of the vector's couplings to light quarks. The couplings between the vector and leptons are set to zero for this plot, and the plot does not change significantly for different values of m_χ.

The coupling dependence of these cross sections can be understood without performing detailed calculations. Since the vector model can be recast as an abelian gauge theory like QED (see Sec. 2.3), the coupling of V to a composite state is the sum of its couplings to its consituents. As a consequence, the vector's couplings to pions and the proton are $g_{V\pi^+} = g_{Vu} - g_{Vd}$, $g_{V\pi^0} = 0$ and $g_{Vp} = 2g_{Vu} + g_{Vd}$, respectively. The cross section $\sigma_{\bar{\chi}\chi\to\pi^+\pi^-}$ is thus proportional to

$(g_{Vu} - g_{Vd})^2$. The interaction producing $V \to \pi^0\gamma$ comes from the anomalous terms in the Wess-Zumino-Witten Lagrangian. Since the anomaly is exact at one loop, the relevant triangle diagrams can be evaluated with a proton running in the loop, making it easy to see that $\sigma_{\bar{\chi}\chi\to\pi^0\gamma} \propto g_{Vp}^2$. The coupling dependence for these cross sections is the same to all orders in perturbation theory.

The branching fraction into $\pi^0\gamma$ is orders of magnitude smaller than the branching fraction into $\pi^+\pi^-$ over all but a narrow region around $g_{Vdd} = g_{Vuu}$. This is because the anomalous triangle diagrams are highly suppressed. This will have consequences for the DM annihilation spectrum in this theory as $\pi^0\gamma$ produces more photons than the $\pi^+\pi^-$ final state, and emphasizes the importance of considering realistic particle physics models rather than examining observational constraints on specific annihilation final states.

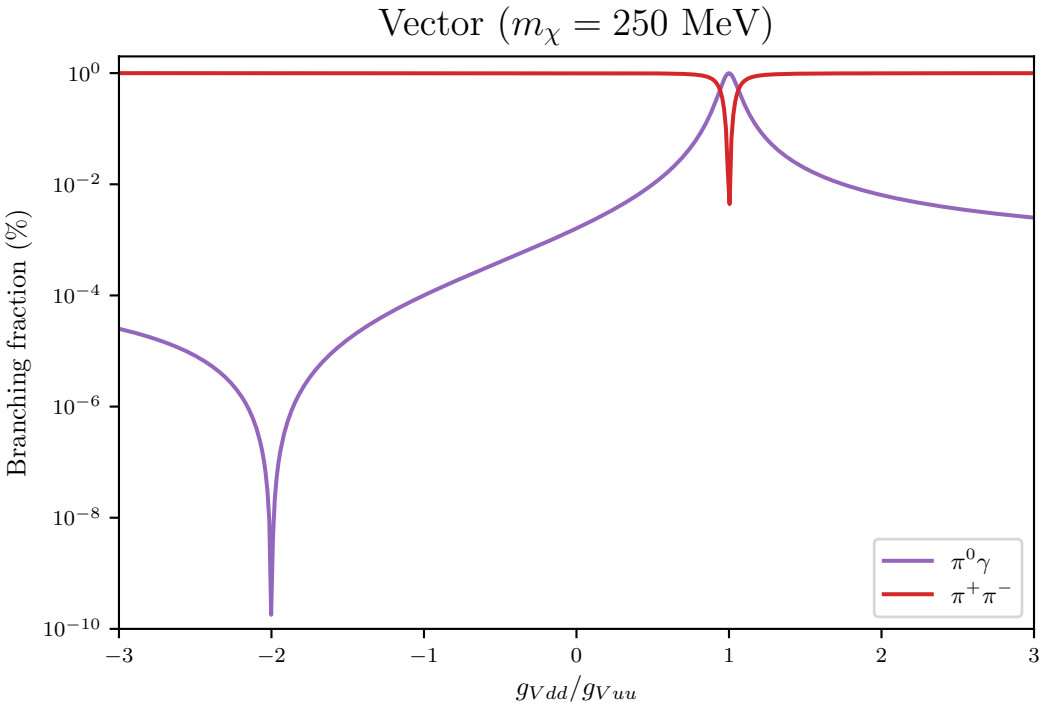

Figure 3.3: Branching fractions for DM annihilation through the vector mediator, with $g_{Vee} = g_{V\mu\mu} = 0$. The vector's mass is taken to be larger than the dark matter mass.

Chapter 4

Gamma Ray Spectra from Dark Matter Annihilation

The total spectrum for DM annihilation into light SM particles is the sum of three pieces:

$$\left.\frac{dN}{dE_\gamma}\right|_{\bar{\chi}\chi} = \left.\frac{dN}{dE_\gamma}\right|_{\bar{\chi}\chi,\text{dec.}} + \left.\frac{dN}{dE_\gamma}\right|_{\bar{\chi}\chi,\text{line}} + \left.\frac{dN}{dE_\gamma}\right|_{\bar{\chi}\chi,\text{FSR}}. \tag{4.1}$$

The first contribution comes from DM annihilating into an SM particle (or particles) A that subsequently undergoes radiative decay (or decays) $A \to B\gamma$:

$$\left.\frac{dN}{dE_\gamma}\right|_{\bar{\chi}\chi,\text{dec.}}(E_\gamma) = \sum_A \text{Br}(\bar{\chi}\chi \to A)\left.\frac{dN}{dE_\gamma}\right|_A (E_\gamma). \tag{4.2}$$

The second term is a sum over final states with a monochromatic gamma ray (or rays). Only two such states are relevant in this work:

$$\left.\frac{dN}{dE_\gamma}\right|_{\bar{\chi}\chi,\text{line}}(E_\gamma) = \text{Br}(\bar{\chi}\chi \to \pi^0\gamma)\ \delta(E_{\pi^0\gamma} - E_\gamma) \tag{4.3}$$

$$+ 2\,\text{Br}(\bar{\chi}\chi \to \gamma\gamma)\ \delta(E_{\text{CM}}/2 - E_\gamma), \tag{4.4}$$

where the energy of the line from the $\pi^0\gamma$ final state is $E_{\pi^0\gamma} \equiv (E_{\rm CM}^2 - m_{\pi^0}^2)/(2E_{\rm CM})$ and $E_{\rm CM}$ is the center of mass energy. The last term term in eq. 4.1 is the contribution from final state radiation (FSR) off of charged annihilation products:

$$\left.\frac{dN}{dE_\gamma}\right|_{\bar{\chi}\chi,\rm FSR} = \frac{1}{\sigma_{\bar{\chi}\chi}} \sum_A \frac{d\sigma_{\bar{\chi}\chi\to A\gamma}}{dE_\gamma}(E_\gamma) = \sum_A \mathrm{Br}(\bar{\chi}\chi \to A) \left.\frac{dN}{dE_\gamma}\right|_{\bar{\chi}\chi\to A}(E_\gamma). \quad (4.5)$$

The purpose of this chapter is to explain how to take these various contributions into account using the effective Lagrangians I derived in the previous chapter. This requires performing integrations over the phase space of three or more particles. Some of these integrations are standard (eg, integrating over matter fields' momenta to find the spectrum for the FSR process $\bar{\chi}\chi \to S^*, V^* \to \pi^+\pi^-\gamma$) [99]. Determining the spectra for the pseudoscalar simplified model is more challenging. For example, determining the spectrum for $\bar{\chi}\chi \to P^* \to 3\pi^0$ requires "convolving" the neutral pions' decay spectra with the matrix element squared for this process. I will begin this chapter by briefly explaining an algorithm for performing such phase space integrations.

Next, I exactly compute the FSR spectra for annihilation into e^+e^- and $\mu^+\mu^-$ in all my simplified models as well as for $\pi^+\pi^-$ in the scalar and vector models, which has not been done before. While less distinctive than photon lines or the π^0 decay spectrum, the resulting spectra scale with photon energy as $dN/dE_\gamma \propto E_\gamma^{-1}$ at low photon energies, in accordance with Low's theorem [98, 33] and in contrast with the softer $dN/dE_\gamma \propto E_\gamma^{-2}$ astrophysical background. I also review the box-shaped neutral pion spectrum and the muon and charged pion radiative decay spectra, which also scale as E_γ^{-1}. The contribution of charged pion radiative decay to DM gamma ray spectra has not been considered in previous work on indirect detection of sub-GeV DM. I conclude by presenting the total annihilation spectra for each of the simplified models.

4.1 Multiparticle Final State

Consider the process $\bar{\chi}\chi \to A_n$. Let $\{p_i\}_{i=1}^2$ denote the $\bar{\chi}$ and χ momenta. The final state A_n denotes a set of n particles $\{a_j\}_{j=1}^n$ with momenta $\{q_j\}_{j=1}^n$ and masses $\{m_j\}_{j=1}^n$. The contribution to the spectrum from the final state particles' radiative decays is determined by averaging their spectra over n-body phase space:

$$\left.\frac{dN}{dE}\right|_{\bar{\chi}\chi,\text{dec}}(E_\gamma) = \frac{1}{\sigma_{\bar{\chi}\chi}} \int d\Pi_{A_n} \frac{d\sigma_{\bar{\chi}\chi\to A_n}(\{p_i\},\{q_j\})}{d\Pi_{A_n}} \left[\sum_{j=1}^n \left.\frac{dN}{dE_\gamma}\right|_{a_j,\text{dec}}(E_\gamma; E_j)\right],$$
$$d\Pi_{A_n} \equiv \left[\prod_{j=1}^n \frac{d^3q_j}{(2\pi)^3 2E_j}\right](2\pi)^4\delta^{(4)}\left(\sum_i p_i - \sum_j q_j\right).$$

The jth final state particle's radiative decay spectrum is denoted by $dN/dE_\gamma|_{a_j,\text{dec}}$, and is a function of photon energy as well as the particle's energy, as I have made explicit. The total self-annihilation cross section is $\sigma_{\bar{\chi}\chi}$.

It is easy to check that this reduces to eq. 4.2 in the $n = 2$ case, but is generally analytically intractable for non-constant differential cross sections. In these cases I perform the integration using a Monte Carlo algorithm called RAMBO [88].[1] As input, RAMBO requires the center of mass energy $\sqrt{s} = |\sum_i p_i|$ and the masses of the final state particles. Its output is a list of 4-momenta $\{q_j\}_{j=1}^n$ such that $\sum_i p_i = \sum_j q_j$ and $|q_j| = m_j$, as well as a weight w used to correct for the algorithm's bias toward over- and undersampling different regions of phase space.

Algorithm 1 demonstrates the simplest way to use RAMBO to perform the phase space integral. In practice this approach is quite slow since it requires computing $dN/dE_\gamma|_{a_j,\text{dec}}$ for each phase space point, which involves computing various numerical integrations to boost into the lab frame. Instead, I perform the reweighting in line 11 and use the resulting $\overline{w}^{(k)}$s to create a weighted histogram of each final state particles' energies. The total spectrum is obtained by evaluating

[1] Note that equation 4.11 in this reference should have $1/w^{2n-4}$ rather than $1/w^{2n-3}$.

$dN/dE_\gamma|_{a_j,\mathrm{dec}}$ at each bin energy and using the bin weights to average the results. I have found that using 25 bins with $\mathcal{O}(10^5)$ RAMBO phase space points leads to a significant speedup with negligible loss in accuracy.

Similar phase space integrals are required for deriving the FSR spectra for multiparticle final states. The generalization of the procedure I have just described is to histogram the photon energies generated by RAMBO rather than performing a sum. Both of these approaches also apply to determining S, P and V's decay spectra.

Algorithm 1 Procedure to compute radiative decay spectra using RAMBO.

$N \leftarrow$ number of phase space points to generate
$E_\gamma \leftarrow$ photon energy

$\left\{\{q_j^{(k)}\}, w^{(k)}\right\}_{k=1}^{N} \leftarrow \mathrm{RAMBO}\left(\sqrt{s}, \{m_j\}, N\right)$ ▷ Run RAMBO N times

$w^{(\mathrm{tot})} \leftarrow \sum_{k=1}^{N} w^{(k)}$ ▷ Sum weights

$\left.\widehat{\frac{dN}{dE_\gamma}}\right|_{\bar{\chi}\chi\to A_n,\mathrm{dec}} \leftarrow 0$ ▷ Total spectrum

for $k = 1, \ldots, N$ **do**
    $\overline{w}^{(k)} \leftarrow \frac{w^{(k)}}{w^{(\mathrm{tot})}} \times \frac{d\sigma_{\bar{\chi}\chi\to A_n}(\{p_i\},\{q_j\})}{d\Pi_{A_n}}$ ▷ Reweight
    $\left.\widehat{\frac{dN}{dE_\gamma}}\right|_{\bar{\chi}\chi\to A_n,\mathrm{dec}} \leftarrow \left.\widehat{\frac{dN}{dE_\gamma}}\right|_{\bar{\chi}\chi\to A_n,\mathrm{dec}} + \overline{w}^{(k)} \times \sum_j \left.\frac{dN}{dE_\gamma}\right|_{a_j,\mathrm{dec}} (E_\gamma; E_j)$
end for

return $\left.\widehat{\frac{dN}{dE_\gamma}}\right|_{\bar{\chi}\chi\to A_n,\mathrm{dec}}$

4.2 Final State Radiation

Dark matter annihilating into charged SM particles generically produces photons via final state radiation (FSR). Most previous works on indirect detection of sub-GeV DM apply the Altarelli-Parisi (AP) splitting function to compute the FSR spectrum for the e^+e^- and $\mu^+\mu^-$ final states [17, 19, 103, 28, 56]: [2]

$$\left.\frac{dN}{dE_\gamma}\right|_{\bar{\chi}\chi\to\bar{\ell}\ell} = \frac{2\alpha}{\pi Q}\cdot\frac{1}{x}\left[1+(1-x)^2\right]\cdot\left[-1+\log\left(\frac{(1-x)}{\mu_\ell^2}\right)\right], \tag{4.6}$$

where $\mu_\ell \equiv m_\ell/Q$, $x \equiv 2E_\gamma/Q$ and Q is the center of mass energy. However, the AP approximation is not sufficient for our applications since it was derived under the assumption that $m_\ell \ll Q$. This assumption breaks down for the $\mu^+\mu^-$ final state, since the DM and muon masses are of the same order. An important consequence is that the AP spectrum cuts off for E_γ above $(Q^2 - em_\ell^2)/(2Q^2)$, which is different from the true kinematic threshold $(Q^2 - m_\ell^2)/(2Q^2)$. Furthermore, since the particles radiating are fermions, the AP approximation is inapplicable to FSR from pions.

To determine the FSR spectra exactly, I used the Lagrangians $\mathcal{L}^{(2)}_{<1\text{ GeV}}\Big|_S$, $\mathcal{L}^{(2)}_{<1\text{ GeV}}\Big|_P$ and $\mathcal{L}^{(2)}_{<1\text{ GeV}}\Big|_V$ to calculate

$$\left.\frac{dN}{dE_\gamma}\right|_{\bar{\chi}\chi\to A} \equiv \frac{1}{\sigma_{\bar{\chi}\chi\to A}}\frac{d\sigma_{\bar{\chi}\chi\to A\gamma}}{dE_\gamma}, \tag{4.7}$$

where the relevant final states are $A = e^+e^-, \mu^+\mu^-, \pi^+\pi^-$ for the scalar and vector models and $A = e^+e^-, \mu^+\mu^-$ for the pseudoscalar model.

The Feynman diagrams for FSR from the $\pi^+\pi^-$ final state have the same topologies as the lepton ones in the case of the vector simplified model. For the scalar model, there is an additional contribution from the $S\pi^+\pi^-\gamma$ vertex. This

[2] Note that DarkSUSY [30] and the PPPC4DMID [40] use the AP approximation.

can be traced back to the coupling between S and the divergence of the dilatation current $\partial_\mu D^\mu$, which contains the kinetic piece of the chiral Lagrangian whose covariant derivative contains the photon. All of the resulting FSR spectra are given in appendices D.1.2, D.2.2 and D.3.2. In the limit $m_f \ll Q$ ($\mu_\ell \ll 1$), the leptonic FSR reduce to the AP approximation, up to an additional term proportional to x for the scalar and pseudoscalar.

Figure 4.1 shows the spectra for FSR in the scalar and vector simplified models as well as the AP spectrum (blue, red and yellow curves respectively). The specific values of the couplings, mediator masses and DM mass do not impact the shape of the spectrum since they cancel when dividing by $\sigma_{\bar{\chi}\chi\to\bar{\ell}\ell}$. As expected, the AP approximation performs poorly near the dimuon threshold (upper left panel). The photon energy at which the spectrum cuts off is an order of magnitude too large, and while the normalization is within a factor of two for the scalar model's spectrum, it is an order of magnitude larger than the vector model's one. The situation improves at larger center of mass energies, and just above the $\pi\pi$ threshold the spectra all agree to within a factor of two. The pion FSR spectra are shown in Figure 4.2, again with the AP approximation for comparison.

In the pseudoscalar model, the only hadronic final state that produces FSR is $\pi^0\pi^+\pi^-$. This spectrum is computationally demanding to determine since it requires integrating over the pions' phase space using RAMBO. I have checked that the resulting spectrum is about 10% as large as the radiative decay spectrum for this final state, so I will ignore it for the rest of this thesis.

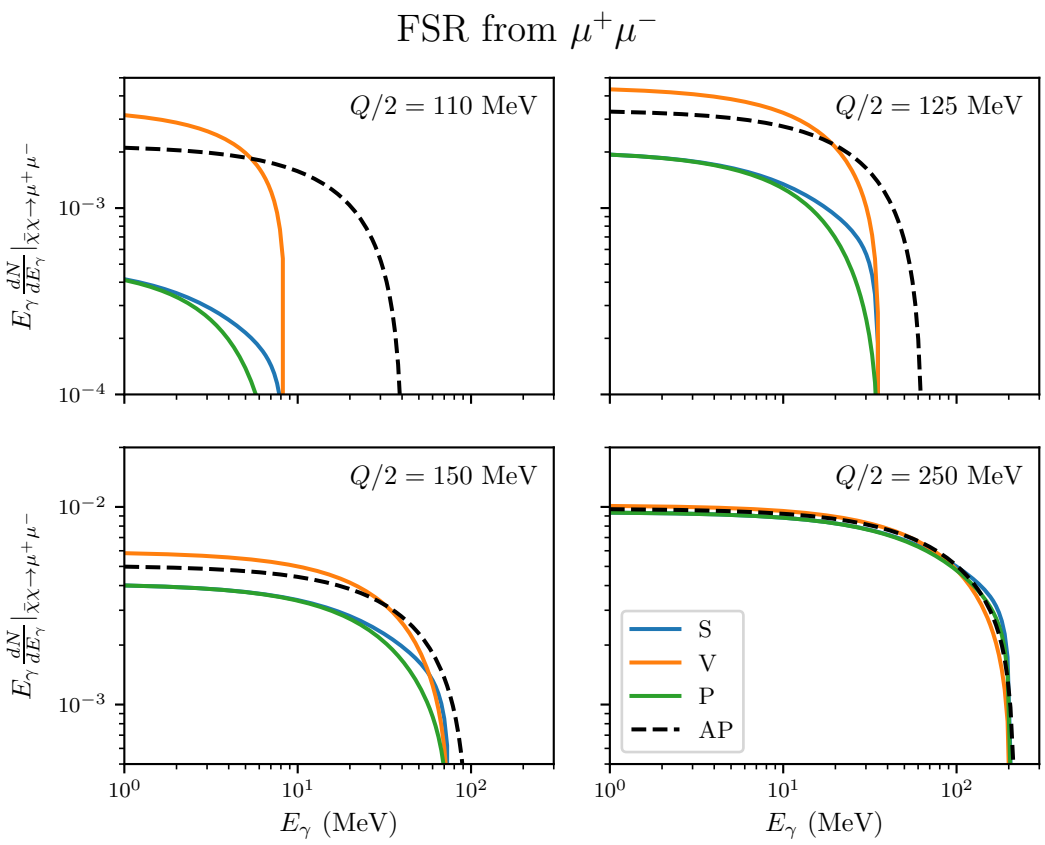

Figure 4.1: Muon FSR spectra for the scalar (blue curve), vector (orange) and pseudoscalar (green) simplified models, where each subplot is labeled by the center of mass energy. The Altarelli-Parisi spectrum from eq. 4.6 is also shown (black dashed curve), illustrating the limiting behavior of the spectra as Q becomes much larger than m_μ.

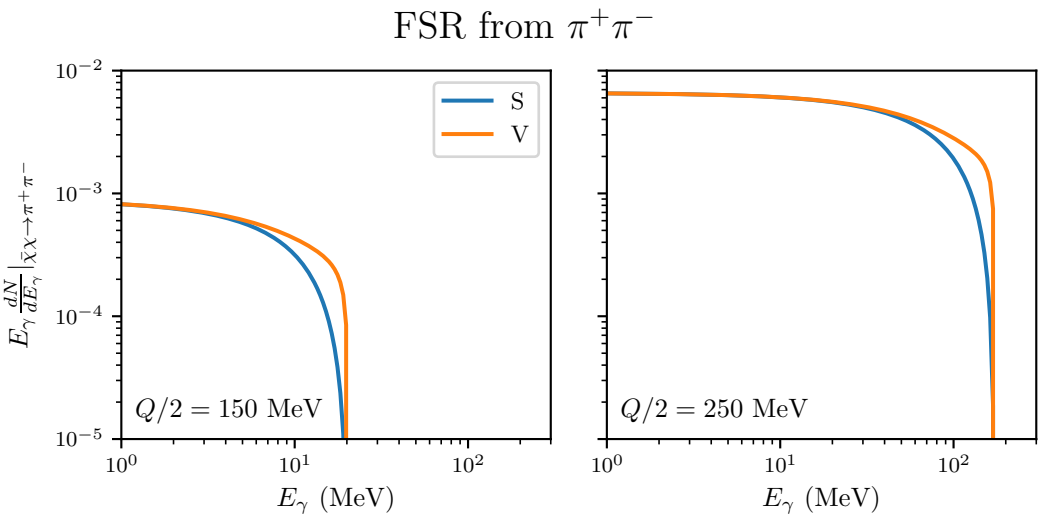

Figure 4.2: Pion FSR spectra for the scalar (blue curve) and vector (orange curve) simplified models, where the relative velocity in the title was used to compute the center of mass energy.

4.3 Radiative Decay Spectra

4.3.1 Decay Spectra in Different Frames

Before computing the radiative decay spectra for the $\mu^\pm$, π^0 and $\pi^\pm$, I will review how to boost a spectrum $dN/dE_{\gamma,R}$ from the parent particle's rest frame to the obtain the "lab frame" spectrum dN/dE_γ where the particle has a boost $\gamma \equiv E/m$ along the z-axis. Let the photon phase space coordinates be $(E_{\gamma,R}, \cos\theta_{\gamma,R})$ in the rest frame and $(E_\gamma, \cos\theta_\gamma)$ in the lab frame, where $\theta_{\gamma,R}$ and θ_γ are the angles with respect to the z axis and I have assumed azimuthal symmetry. Then since the number of photons in a small patch of phase space does not depend on which

coordinates we choose, we have

$$dN = f(E_{\gamma,R}, \cos\theta_{\gamma,R})\ dE_{\gamma,R}\ d\cos\theta_{\gamma,R} \tag{4.8}$$

$$= \begin{vmatrix} \frac{dE_{\gamma,R}}{dE_\gamma} & \frac{dE_{\gamma,R}}{d\cos\theta_\gamma} \\ \frac{d\cos\theta_{\gamma,R}}{dE_\gamma} & \frac{d\cos\theta_{\gamma,R}}{d\cos\theta_\gamma} \end{vmatrix} f(E_{\gamma,R}(E_\gamma, \cos\theta_\gamma), \cos\theta_{\gamma,R}(E_\gamma, \cos\theta_\gamma))dE_\gamma\ d\cos\theta_\gamma, \tag{4.9}$$

where we recognize the partial phase space density as $f(E, \cos\theta) \equiv dN/(dE\ d\cos\theta)$ and the term with the two vertical lines is the Jacobian factor for the change of variables. If the $f(E_{\gamma,R}, \cos\theta_{\gamma,R})$ is independent of $\cos\theta_{\gamma,R}$ (which is the case for all the spectra I will consider), then we can write:

$$f(E_{\gamma,R}, \cos\theta_{\gamma,R}) = \frac{1}{2}\frac{dN}{dE_{\gamma,R}} \tag{4.10}$$

The variables $E_1, E_2, \cos\theta_1$ and $\cos\theta_2$ are related via a lorentz boost. The relationships are

$$E_{\gamma,R} = \gamma E_\gamma(1 - \beta\cos\theta_\gamma), \qquad \cos\theta_{\gamma,R} = \frac{\beta - \cos\theta_\gamma}{1 - \beta\cos\theta_\gamma} \tag{4.11}$$

where $\beta = \sqrt{1 - 1/\gamma^2}$ is the particle's velocity. The Jacobian factor can be computed using these relations, yielding

$$J = \begin{vmatrix} \frac{dE_{\gamma,R}}{dE_\gamma} & \frac{dE_{\gamma,R}}{d\cos\theta_\gamma} \\ \frac{d\cos\theta_{\gamma,R}}{dE_\gamma} & \frac{d\cos\theta_{\gamma,R}}{d\cos\theta_\gamma} \end{vmatrix} = \frac{1}{\gamma(\beta\cos\theta_\gamma - 1)}. \tag{4.12}$$

The gamma ray spectrum in the lab frame is then obtained by integrating eq. 4.8 over $\cos\theta_\gamma$:

$$\frac{dN}{dE_\gamma} = \int \cos\theta_\gamma \frac{1}{2\gamma(\beta\cos\theta_\gamma - 1)} \frac{dN}{dE_{\gamma,R}}. \tag{4.13}$$

In the remainder of this section I will present the radiative decay spectra for the neutral pion, muon and charged pion as a function of the decaying particle's energy and E_γ. The integral in eq. 4.13 can only be performed analytically for the the neutral pion: the other rest frame decay spectra must be boosted by performing the integral numerically.

4.3.2 Neutral Pions

The dominant decay mode for neutral pions is $\pi^0 \to \gamma\gamma$ with a branching fraction of about 99% [116]. Due to this decay modes' large branching fraction and the fact that it has two photons in the final state, I will ignore the π^0's other decay modes. In the pion's rest frame, the gamma-ray spectrum is trivial:

$$\left.\frac{dN}{dE_\gamma}\right|_{\pi^0} (E_{\gamma,R}, m_{\pi^0}) = 2\ \delta\left(E_{\gamma,R} - \frac{m_\pi}{2}\right) \tag{4.14}$$

where the factor of 2 comes from the fact that there are two photons in the final state. Applying eq. 4.13 and 4.11 gives that the gamma ray spectrum in the laboratory frame is

$$\begin{aligned}\left.\frac{dN}{dE_\gamma}\right|_{\pi^0} (E_\gamma, E_{\pi^0}) &= \int \cos\theta_\gamma \frac{1}{2\gamma(\beta\cos\theta_\gamma - 1)} 2\ \delta\left(E_{\gamma,R} - \frac{m_{\pi^0}}{2}\right) \\ &= \frac{2}{\gamma\beta m_{\pi^0}} \left[\theta(E_{\pi^0} - E_-) - \theta(E_{\pi^0} - E_+)\right]\end{aligned} \tag{4.15}$$

with $E_\pm = m_{\pi^0}/2\gamma(1 \mp \beta)$. This is the characteristic box spectrum centered at $m_{\pi^0}/2$.

4.3.3 Muons

In the muon's rest frame, the radiative decay spectrum is given by [93]

$$\left.\frac{dN}{dE_\gamma}\right|_{\mu^\pm}(E_{\gamma,R}, m_\mu) = \frac{\alpha(1-x_R)}{36\pi E_\gamma}\left[12(3-2x_R(1-x_R)^2)\log\left(\frac{1-x_R}{r}\right)\right.$$
$$\left. +x_R(1-x_R)(46-55x_R)+102\right], \quad (4.16)$$

where $r \equiv (m_e/m_\mu)^2$, $x_R \equiv 2E_{\gamma,R}/m_\mu$ and the kinematic bounds on E_γ translate into $0 \leq x_R \leq (1+r)m_\mu/2$.

4.3.4 Charged Pions

The dominant pion decay is $\pi^+ \to \ell^+\nu_\ell$, where $\ell = e, \mu$ and ℓ is produced approximately on shell, thanks to the narrow width approximation when $\ell = \mu$. Contributions to the pion's radiative decay spectrum come from initial state radiation (ISR) from the photon, FSR from the lepton, and photon emission from virtual states in the $\pi\ell\nu$ vertex. An expression for the differential decay width in the pion's rest frame, $d^2\Gamma_{\pi^+\to\ell^+\nu\gamma}/dxdy$, is given in equation 4 of [31], where $x \equiv 2E_{\gamma,R}/m_{\pi^+}$ and $y \equiv 2E_{\ell,R}/m_{\pi^+}$. After changing to the Mandelstam variables

$$s \equiv (p_\pi - p_\gamma)^2 = m_{\pi^+}^2(1-x),$$
$$t \equiv (p_\pi - p_\ell)^2 = m_{\pi^+}^2\left(1 - y + \frac{m_\ell^2}{m_{\pi^+}^2}\right),$$

integrating over $0 \leq t \leq (m_{\pi^+}^2 - s)(s - m_\ell^2)/s$ and dividing by the total π^+ decay width yields an analytic expression for this channel's contribution to the π^+ decay

spectrum:

$$\mathrm{Br}(\pi^+ \to \ell^+\nu_\ell) \cdot \left.\frac{dN}{dE_\gamma}\right|_{\pi^+\to\ell^+\nu_\ell} (E_{\gamma,R}, m_{\pi^+}) = \frac{2}{m_{\pi^+}\Gamma_{\pi^+}} \cdot \frac{\alpha(f(x)+g(x))}{24\pi f_\pi^2 (r-1)^2(x-1)^2 rx}, \tag{4.17}$$

where $r \equiv m_\ell^2/m_{\pi^+}^2$ and

$$\begin{aligned} f(x) = (r+x-1)\Big[&m_{\pi^+}^2 x^4 (A^2+V^2)(r^2 - rx + r - 2(x-1)^2) \\ &- 12 f_\pi m_{\pi^+} r(x-1)x^2(A(r-2x+1)+Vx) \\ &-12 f_\pi^2 r(x-1)(4r(x-1)+(x-2)^2)\Big] \end{aligned} \tag{4.18}$$

$$\begin{aligned} g(x) = 12 f_\pi r(x-1)^2 \log\left(\frac{r}{1-x}\right)\Big[&m_{\pi^+} x^2(A(x-2r)-Vx) \\ &+ f_\pi(2r^2 - 2rx - x^2 + 2x - 2)\Big]. \end{aligned} \tag{4.19}$$

When $\ell = \mu$, the muon's subsequent radiative decay also contributes significantly to the pion's decay spectrum. Since we can take the muon to be on shell by the narrow width approximation, this decay path's contribution is simply the product of the branching fraction for $\pi^+ \to \mu^+\nu_\mu$ and the muon decay spectrum eq. 4.16 evaluated at the muon's energy. Our final expression for the charged pion decay spectrum is thus

$$\begin{aligned} \left.\frac{dN}{dE_\gamma}\right|_{\pi^+} (E_{\gamma,R}, m_{\pi^+}) = &\sum_{\ell=e,\mu} \mathrm{Br}(\pi^+ \to \ell^+\nu_\ell) \cdot \left.\frac{dN}{dE_\gamma}\right|_{\pi^+\to\ell^+\nu_\ell} (E_{\gamma,R}, m_{\pi^+}) \\ &+ \mathrm{Br}(\pi^+ \to \mu^+\nu_\mu) \cdot \left.\frac{dN}{dE_\gamma}\right|_{\mu^\pm} \left(E_{\gamma,R}, E_\mu = \frac{m_{\pi^+}^2 - m_\mu^2}{2m_{\pi^+}}\right). \end{aligned} \tag{4.20}$$

Figure 4.3 shows the contributions of each term and the total spectrum in the pion's rest frame. The muon's radiative decay is the most important component

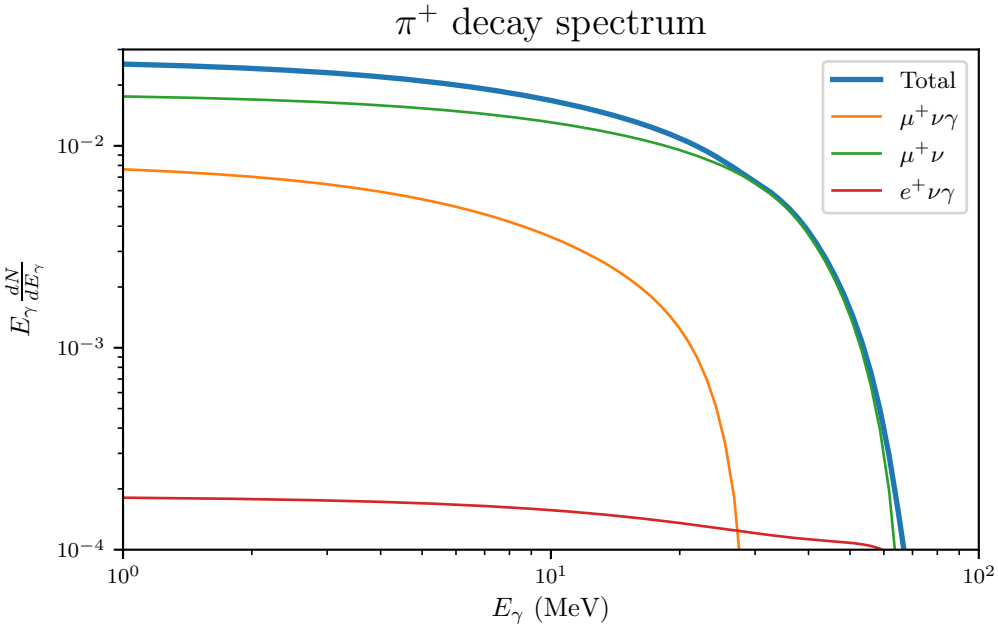

Figure 4.3: Different contributions to the charged pion radiative decay spectrum. The curve labeled $\mu^+\nu$ is the contribution from the radiative decay of the muon which is produced on-shell in $\pi^+ \to \mu^+\nu$. The other two curves are the contributions captured by eq. 4.17.

since nearly every pion decay produces a muon. There is also more phase space available for the photon in comparison with $\pi^+ \to \mu^+\nu_\mu\gamma$ since the other final state particles are massless: the former spectrum cuts off at ~ 69 MeV and the latter at $(m_{\pi^+}^2 - m_\mu^2)/(2m_{\pi^+}) \approx 27$ MeV. The contribution from $\pi^+ \to e^+\nu\gamma$ is smaller than the others due to the $\sim 2 \times 10^{-5}$ helicity suppression.

4.4 Simplified Model Annihilation Spectra

The FSR and radiative decay contributions to the DM annihilation spectrum for the scalar, pseudoscalar and vector simplified models can be calculated using the methods described in this chapter. In the plots that follow, the total spectra have been convolved with a Gaussian whose standard deviation is equal to 5%

of its mean, the energy resolution of the EGRET telescope. This is the only meaningful way to show the gamma ray line spectrum, which is a delta function. The gamma ray line energies are indicated with vertical dashed lines. The center of mass energy is set to $Q = 2m_\chi\left(1 + \frac{1}{2}v_\chi\right)$, where $v_\chi = 10^{-3}$ is the velocity dispersion in the Milky Way. The mediator is taken to be heavier than the DM.

The different annihilation final states' contributions to the scalar model's spectrum are shown in Figure 4.4. The top subpanel was computed by fixing the relations between the couplings to agree with the Higgs portal UV completion ($g_{Sf} = g_{SG} = g_{SF}$). The spectrum is dominated by the heaviest kinematically accessible final state until the $2\pi^0$ channel becomes accessible, which has a distinctive shape and produces orders of magnitude more photons than the charged final states. The gamma ray line spectrum is negligible to the others above the muon threshold due to its tiny branching fraction. The bottom subpanel was determined with $g_{Sf} = g_{SF} = 0$ and $g_{SG} \neq 0$. In this case there are no final states available below the pion threshold, but the spectra are not qualitatively different from the ones derived with Higgs portal couplings. For both benchmarks S's couplings to different fermions are related to their Yukawas by the same constant of proportionality, which leaves little model dependence in the spectra.

Figure 4.5 shows spectra in the pseudoscalar model for different DM masses and coupling choices inspired by the 2HDM UV completion presented in Section 2.2.1. When the coupling between P and leptons is nonzero, the muon completely dominates the total spectrum since the other cross sections are suppressed by phase space factors or the anomaly. In the other case the spectrum has two distinctive peaks for $m_\chi > 3m_\pi/2$, the larger coming from neutral pion decays and the smaller coming from annihilation into two photons. The spectrum is nearly independent of the DM mass above this threshold. When $m_\chi \sim 3m_\pi/2$,

the spectrum consists of two lines. The ratio between the normalizations of these components is dependent on g_{Pd}/g_{Pu}.

The components of the annihilation spectrum in the vector model are plotted in Figure 4.6. Figure 4.7 exhibits the total spectrum's mass and coupling dependence, with $g_{Ve} = g_{V\mu} = 0$. At low masses, only the $\pi^0\gamma$ final state is available, which produces a line centered at $m_\chi - m_{\pi^0}^2/(4m_\chi)$ and box centered at $m_{\pi^0}/2$. These look nearly indistinguishable for $m_\chi = 75$ MeV after the convolution and merge as the DM mass is increased. Above the $\pi^+\pi^-$ threshold, either final state can dominate the spectrum, depending on the ratio between the $\pi^0\gamma$ spectrum and its small branching fraction. This will lead to stronger coupling dependence of indirect detection limits than in the scalar or pseudoscalar models.

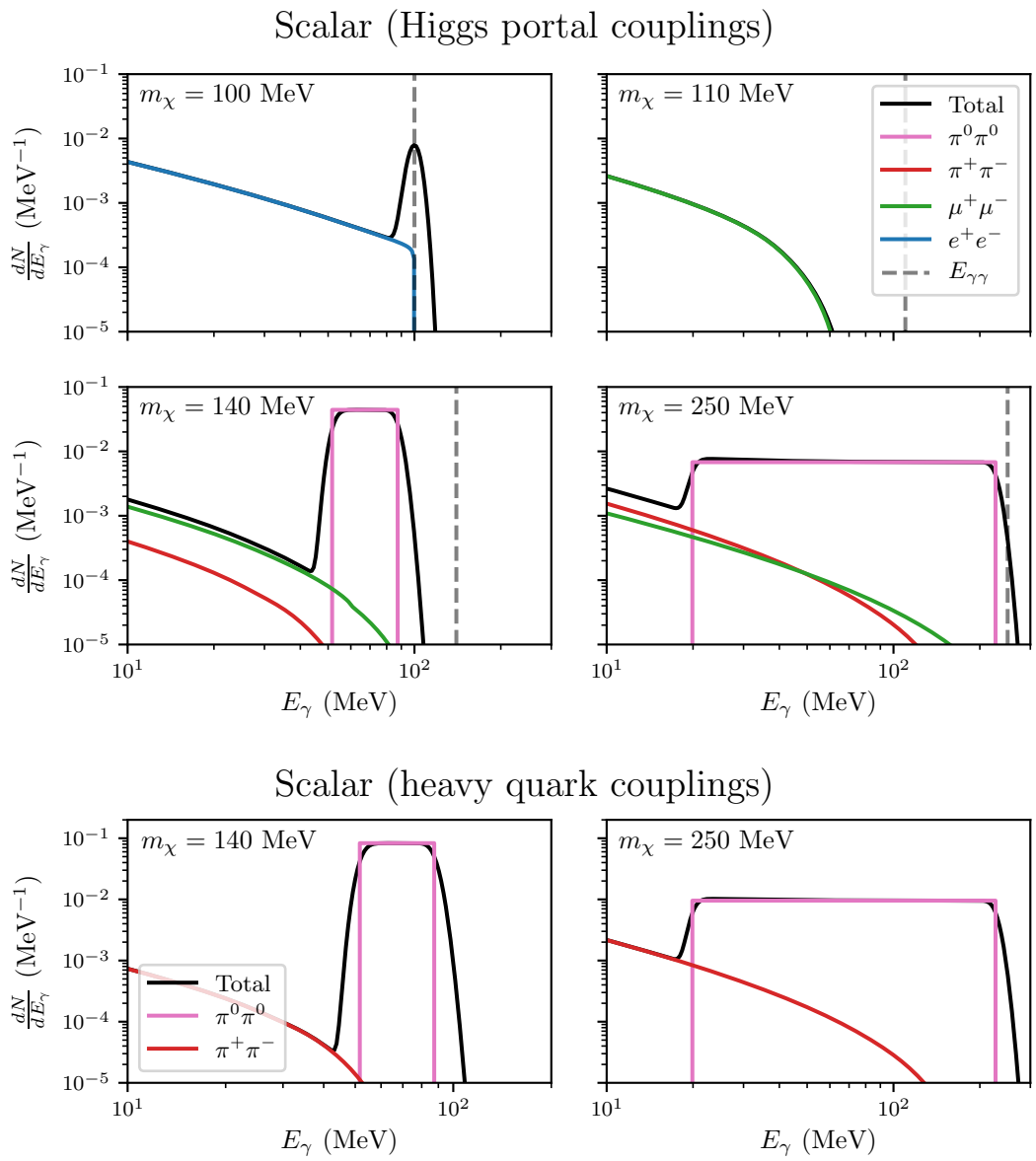

Figure 4.4: Different final states' contributions to the scalar simplified model's DM annihilation spectrum. The curve labeled "Total" is the spectrum as seen by an instrument with 5% energy resolution. Top panel: Higgs portal-type couplings ($g_{Sf} = g_{SG} = g_{SF}$). The vertical dashed line indicates the monochromatic gamma ray's energy. Bottom panel: heavy quark-type couplings ($g_{Sf} = g_{SF} = 0$, $g_{SG} \neq 0$).

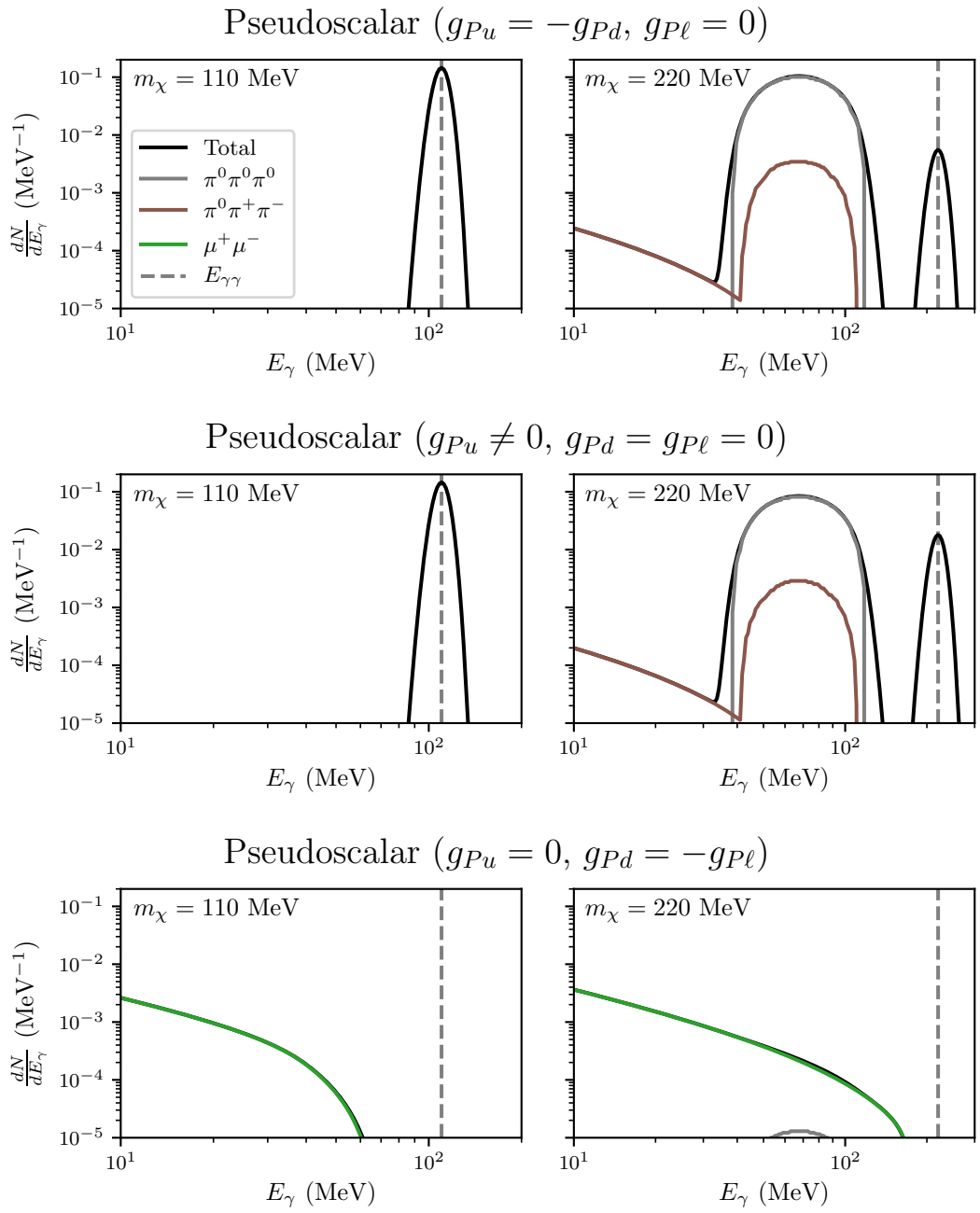

Figure 4.5: The same as Fig. 4.4, but for the pseudoscalar simplified model. The couplings in the different panels are inspired by variants of the 2HDM UV completion discussed in Sec. 2.2.1: type III with $\tan\beta \ll 1$ (top), type II with $\tan\beta \ll 1$ (middle) and type II with $\tan\beta \gg 1$. The couplings g_{PG} and g_{PF} are fixed by the MFV relations eqs. 2.21-2.22. FSR from the $\pi^0\pi^+\pi^-$ final state contributes $\lesssim 10\%$ and has been neglected. The e^+e^- spectrum has been excluded and the $\pi^0\pi^+\pi^-$ decay spectrum is not shown in the bottom panel since they are completely negligible. The "Total" and "$\mu^+\mu^-$" curves in the bottom panel overlap.

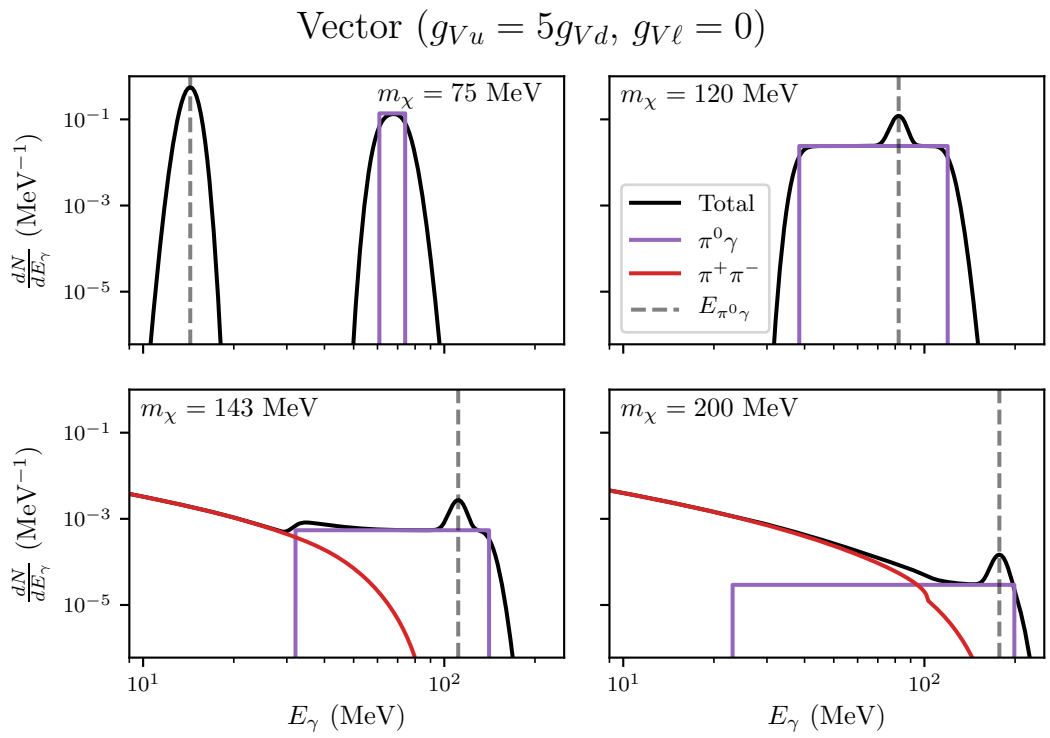

Figure 4.6: The same as Fig. 4.4 and 4.5, but for the vector simplified model. The coupling between V and electrons and muons is set to zero.

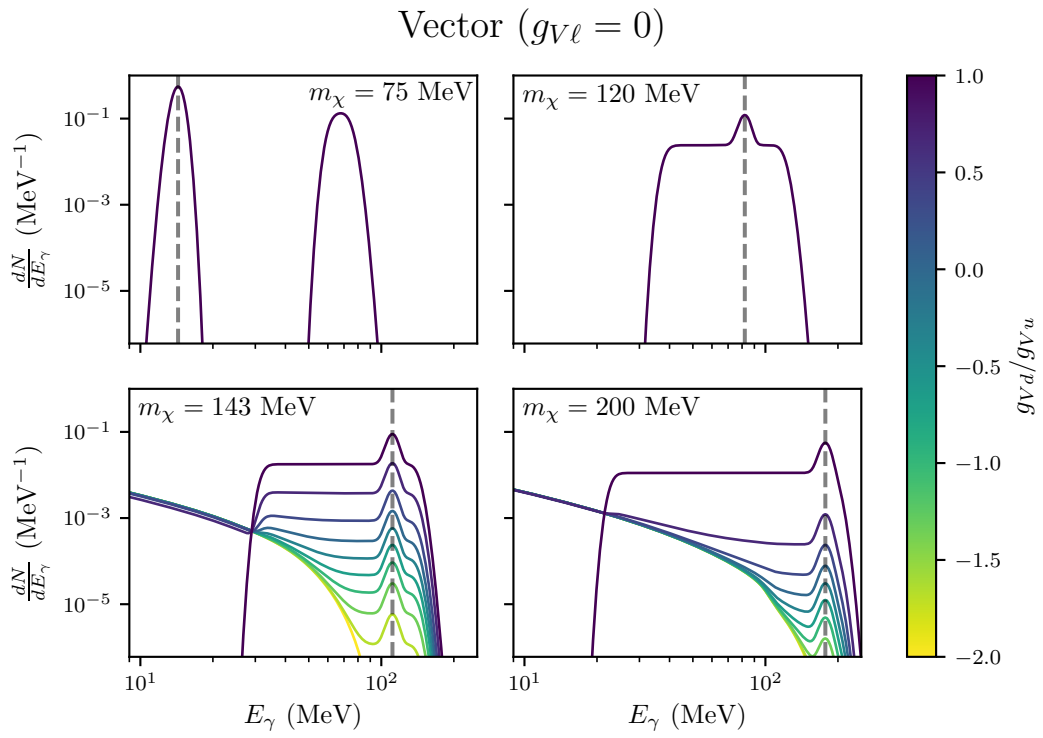

Figure 4.7: Dependence of total annihilation spectrum in the vector simplified model on the couplings to quarks, with the $\pi^0\gamma$ gamma ray line energy indicated by the vertical dashed line. All couplings to leptons have been set to zero. The total spectrum is again obtained by convolving the continuum and line components with the spectral resolution function for an instrument with 5% energy resolution.

Chapter 5

Observational Prospects

Now that the gamma ray spectra have been computed, the prospects for constraining the present-day DM self-annihilation cross section $\langle \sigma v \rangle_{\bar{\chi}\chi}$ using existing and planned gamma-ray detectors can be studied. The gamma ray flux from DM annihilating in a region of the sky subtending a solid angle $\Delta\Omega$ is

$$\left.\frac{d\Phi}{dE_\gamma}\right|_{\bar{\chi}\chi}(E) = \frac{\Delta\Omega}{4\pi}\frac{\langle \sigma v \rangle_{\bar{\chi}\chi}}{2 f_\chi m_\chi^2} J \left.\frac{dN}{dE_\gamma}\right|_{\bar{\chi}\chi}(E). \tag{5.1}$$

The factor f_χ in the first term is equal to 1 if the DM is self-conjugate and 2 otherwise ($f_\chi = 2$ in this thesis). The J factor counts the number of pairs of DM particles that can annihilate with each other in the observation region multiplied by the DM mass squared:

$$J \equiv \frac{1}{\Delta\Omega}\int_{\Delta\Omega} d\Omega \int_{\mathrm{LOS}} dl\ \rho(r(l,\psi))^2, \tag{5.2}$$

where $\rho(r)$ is the DM density profile. The annihilation spectrum $dN/dE_\gamma|_{\bar{\chi}\chi}$ is the precisely what was computed in the previous chapter.

The resulting number of photons observed by a detector with effective area

$A_{\rm eff}(E)$ and an energy-independent observing time $T_{\rm obs}$ over the energy range $[E_{\rm min}, E_{\rm max}]$ is

$$N_\gamma|_{\bar{\chi}\chi} = \int_{E_{\rm min}}^{E_{\rm max}} dE\ T_{\rm obs} \cdot A_{\rm eff} \cdot \left[\int dE'\ R_\epsilon(E|E')\ \frac{d\Phi}{dE_\gamma}\bigg|_{\bar{\chi}\chi}(E') \right] \tag{5.3}$$

The spectral resolution function $R_\epsilon(E|E')$ takes into account the finite energy resolution of gamma ray detectors. For a gamma ray with true energy E', $R_\epsilon(E|E')$ is the probability that it is reconstructed with energy E, which can be approximated as a Gaussian [29]:

$$R_\epsilon(E|E') \equiv \frac{1}{\sqrt{2\pi}\epsilon E'} \exp\left[-\frac{(E-E')^2}{2(\epsilon E')^2} \right]. \tag{5.4}$$

This equation defines ϵ.

In the next section a simple procedure is employed to set limits using current diffuse gamma ray measurements from the Imaging Compton Telescope (COMPTEL), the Energetic Gamma Ray Experiment Telescope (EGRET) and the Fermi Large Area Telescope (Fermi-LAT). I focus on e-ASTROGAM as a representative next-generation detector and determine projected limits below. In addition, constraints from the cosmic microwave background (CMB) are also derived. This involves determining the efficiency factor $f_{\rm eff}$ for energy injection by dark matter into the plasma at recombination, which is described in detail.

5.1 Limits from Existing Gamma-Ray Data

Data from COMPTEL, EGRET and Fermi-LAT furnish the strongest constraints on gamma ray production in the $\mathcal{O}(1\ \text{MeV} - 100\ \text{MeV})$ range by DM. Table 5.1 shows the approximate energy coverage and energy resolutions of these

Detector	Energy range	ϵ
COMPTEL[85]	$0.7 - 27$ MeV	5%
EGRET[136]	27 MeV $-$ 8.6 GeV	18%
Fermi-LAT[13]	150 MeV $-$ 95 GeV	7.5%
e-ASTROGAM[135]	0.3 MeV $-$ 3 GeV	$\lesssim$2%, E_γ<10 MeV 20$-$30%, $E_\gamma \geq$10 MeV

Table 5.1: Figures of merit for existing and planned gamma ray detectors. While the energy resolutions for COMPTEL, EGRET and Fermi-LAT are taken to be constant in this thesis, the energy-dependence described in the reference indicated for e-ASTROGAM is accounted for. Fig. 5.1 displays the effective areas for these detectors.

Detector	Latitude b	Longitute l	$\Delta\Omega$ (sr)	J (MeV^2 cm^{-5} sr^{-1})
COMPTEL[85]	$\lvert b\rvert < 20^\circ$	$\lvert l\rvert < 60^\circ$	1.433	3.725×10^{28}
EGRET[133]	$20^\circ < \lvert b\rvert < 60^\circ$	$\lvert l\rvert < 180^\circ$	6.585	3.79×10^{27}
Fermi-LAT[2]	$8^\circ < \lvert b\rvert < 90^\circ$	$\lvert l\rvert < 180^\circ$	10.817	4.698×10^{27}
e-ASTROGAM	$\lvert b\rvert < 10^\circ$	$\lvert l\rvert < 10^\circ$	0.121	1.795×10^{29}

Table 5.2: Target regions for different detectors' measurements of the diffuse gamma-ray flux. The region for e-ASTROGAM is used to compute projected constraints. The J-factors for COMPTEL, EGRET and Fermi-LAT are the values from [53] while the value for e-ASTROGAM is taken from [40]; all assume an NFW profile.

detectors [85, 136, 13, 135]; their effective areas are plotted in Figure 5.1. The J-factors and angular extents for each experiments' best-measured target region are gathered in Table 5.2 [85, 133, 2]. The Milky Way's DM density is taken to be an Navarro-Frenk-White (NFW) profile [108]. This is a traditional benchmark halo profile motivated by N-body simulations, with the functional form

$$\rho_{\rm NFW}(r) = \rho_s \frac{r_s}{r}\left(1 + \frac{r}{r_s}\right)^{-2}, \tag{5.5}$$

where the scale density is $\rho_s = 184\ \mathrm{MeV/cm^3}$ and the scale radius is $r_s = 24.42$ kpc [40].

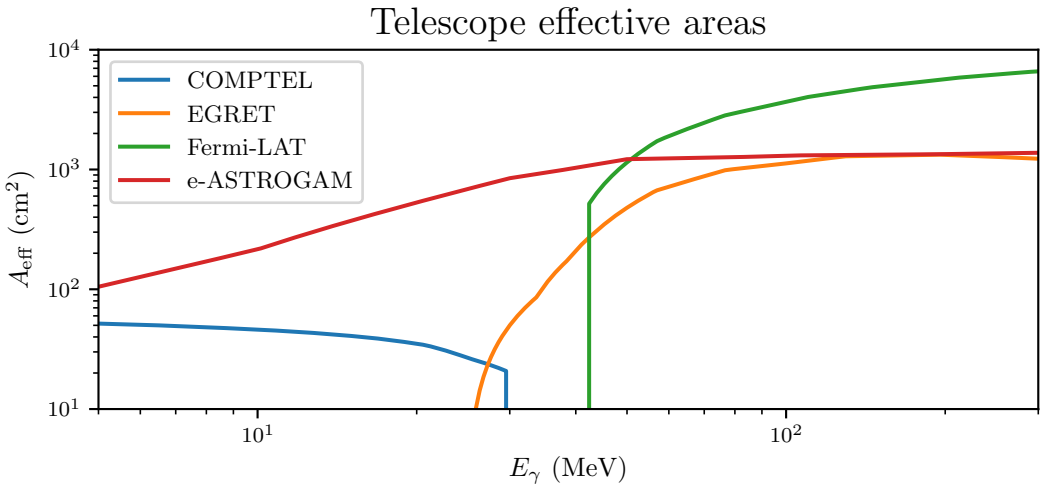

Figure 5.1: The energy-dependent effective areas of the detectors considered in this work. More details can be on the telescopes in [85], [136], [13] and [135], respectively.

There are several sources of uncertainty in the J factor calculation. Assuming an Einasto [52], Moore [86] or cored isothermal [15] profile only changes the J-factors for the EGRET and Fermi-Lat target regions by a factor of $\lesssim 1.5$. Since the COMPTEL region includes the Galactic Center where there is significant uncertainty about the DM halo profile, difference choices can affect its J-factor by a factor of ~ 2.7. It is also important to note that the local DM density $\rho_\odot$ is poorly constrained to 0.3 ± 0.1 GeV/cm^3 (see for example [26], though other groups have claimed more accurate determinations [37, 124]). This propagates to ρ_s and the J factor calculation, giving rise to an uncertainty of up to an order of magnitude.

As features of the prompt gamma ray spectrum from sub-GeV DM annihilation are the focus of this thesis with detailed calculation of secondary gamma ray emission left for future work, a simple procedure is employed to compute bounds using existing data. I require that the $\langle \sigma v \rangle_{\bar{\chi}\chi}$ is small enough that the integrated

photon flux from DM annihilations in bins $i = 1, \ldots, N$ not exceed the observed central value of the flux plus twice the upper error bar: $\Phi^{(i)}|_{\bar{\chi}\chi} < \Phi^{(i)}|_{\rm obs} + 2\sigma^{(i)}$. While better limits could be obtained by assuming a background model, this introduces significant systematic uncertainties and would improve our limits by less than an order of magnitude [53].

5.2 Projected Limits for e-ASTROGAM

A $10^\circ \times 10^\circ$ window centered on the Galactic Center is used as the target region and the diffuse gamma ray background model from Ref. [17] is employed. The background model was computed using `GALPROP` and fit to data in the window ($|b| < 10^\circ, |l| < 30^\circ$). The dwarf galaxy Draco was also considered as a target with an empirical power law background model fit to COMPTEL and EGRET data at higher latitudes, as in Ref. [22]. The limits in this case are weaker due to the simpler background model, and not shown here.

The number of signal photons in a fixed energy range $[E_{\rm min}, E_{\rm max}]$ is given by integrating the flux in eq. 5.1. Projected limits on $\langle \sigma v \rangle_{\bar{\chi}\chi}$ are computed by requiring that the signal-to-noise ratio is significant at the $n_\sigma = 5$ level: $N_\gamma|_{\bar{\chi}\chi} = n_\sigma \sqrt{N_\gamma|_{\rm bg}}$. N_γ is the number of photons in the energy range from DM annihilation or background and is computed by substituting the DM photon flux with the background one in eq. 5.3. This translates into

$$\langle \sigma v \rangle_{\bar{\chi}\chi} < \frac{4\pi \cdot 2 f_\chi m_\chi^2}{T_{\rm obs} \Delta\Omega J} \times n_\sigma \sqrt{N_\gamma|_{\rm bg}} \tag{5.6}$$

$$\times \left[\int_{E_{\rm min}}^{E_{\rm max}} dE \int dE' \; R_\epsilon(E|E') \left. \frac{dN}{dE} \right|_{\bar{\chi}\chi} (E') \right]^{-1} . \tag{5.7}$$

The best possible limit on $\langle \sigma v \rangle_{\bar{\chi}\chi}$ is found by optimizing over $E_{\rm min}$ and $E_{\rm max}$ to

minimize this expression. Note that the optimal $[E_{\min}, E_{\max}]$ does not completely align with spectral features. For example, in the case of a π^0 box spectrum setting $E_{\min}$ equal to the left boundary of the box would include too much of the $d\Phi/dE_\gamma|_{\rm bg} \propto E_\gamma^{-2}$ background flux.

5.3 Comparing Velocity-Dependent Annihilation Cross Sections

Before detailing the CMB limit calculations, it is important to review how to compare limits on the thermally averaged DM self-annihilation cross section in the Milky Way and at recombination.

Consider two dark matter particles with velocities $\mathbf{v}_1$ and $\mathbf{v}_2$. The nonrelativistic limit is valid in both these scenarios, and permits an expansion of the cross section times relative velocity in $\mathbf{v}_{\rm rel} = \mathbf{v}_1 - \mathbf{v}_2$:

$$\sigma(v_{\rm rel}) \cdot v_{\rm rel} \approx a + b v_{\rm rel}^2. \tag{5.8}$$

The quantities a and b depend only on the masses and couplings of the underlying theory. The case $a \gg b$ is called s-wave annihilation. The resulting thermally averaged cross section $\langle \sigma v \rangle_{\bar{\chi}\chi}$ is a temperature-independent constant, and so there is no trouble comparing cross section constraints derived from different systems or during different epochs.

If $b \gg a$, the annihilation is called p-wave. To proceed with the analysis, I will assume the dark matter is isothermal and that each of its components are

normally distributed.[1] Denoting the 3D velocity distribution function by

$$f_{\mathbf{v}}(\mathbf{v}) \equiv \left[\frac{m_\chi}{2\pi T}\right]^{3/2} \exp\left[-\frac{m_\chi |\mathbf{v}|^2}{2T}\right] \tag{5.9}$$

and the DM temperature by T, for p-wave DM the thermal average becomes

$$\begin{aligned}
\langle \sigma v \rangle_{\bar{\chi}\chi,T} &= b \int d^3\mathbf{v}_1 \; f_{\mathbf{v}}(\mathbf{v}_1) \int d^3\mathbf{v}_2 \; f_{\mathbf{v}}(\mathbf{v}_2) \; |\mathbf{v}_1 - \mathbf{v}_2|^2 && (5.10)\\
&= b \int d^3\mathbf{v}_1 \; f_{\mathbf{v}}(\mathbf{v}_1) \int d^3\mathbf{v}_2 \; f_{\mathbf{v}}(\mathbf{v}_2) \; \left[|\mathbf{v}_1|^2 + |\mathbf{v}_2|^2 - 2\mathbf{v}_1 \cdot \mathbf{v}_2\right] && (5.11)\\
&= b \left[2\,\mathrm{E}[|\mathbf{V}|^2] - 2\,\mathrm{E}[\mathbf{V}] \cdot \mathrm{E}[\mathbf{V}]\right] && (5.12)\\
&= 2b\,\mathrm{E}[|\mathbf{V}|^2]. && (5.13)
\end{aligned}$$

Here $\mathrm{E}[\cdot]$ denotes the expected value of a random variable with respect to $f_{\mathbf{v}}$. The last expectation value is the variance of the Maxwell-Boltzmann distribution describing the DM's speed, and is easily evaluated to give

$$\langle \sigma v \rangle_{\bar{\chi}\chi,T} = 6Tb/m_\chi = 3bv_T^2. \tag{5.14}$$

where the temperature in the Milky Way is defined through the relation $v_T \equiv \sqrt{2T/m}$ is the most probable DM speed. In the Milky Way, this is taken to be $v_0 \sim 220$ km/s, the circular velocity of the sun around the galaxy. The takeaway is that constraints derived on the cross section at recombination $\langle \sigma v \rangle_{\bar{\chi}\chi,\mathrm{CMB}}$ can be related to constraints from observations in the Milky Way by rescaling by $(v_0/v_{\mathrm{CMB}})^2$, where v_{CMB} is the DM speed at recombination.

[1] See refs. [58, 92, 23, 78] and the excellent lecture slides at `http://www.hep.ph.ic.ac.uk/susytalks/fairbairnimperialoneday.pdf` for discussion of the issues with these assumptions and how to address them, which is beyond the scope of this work.

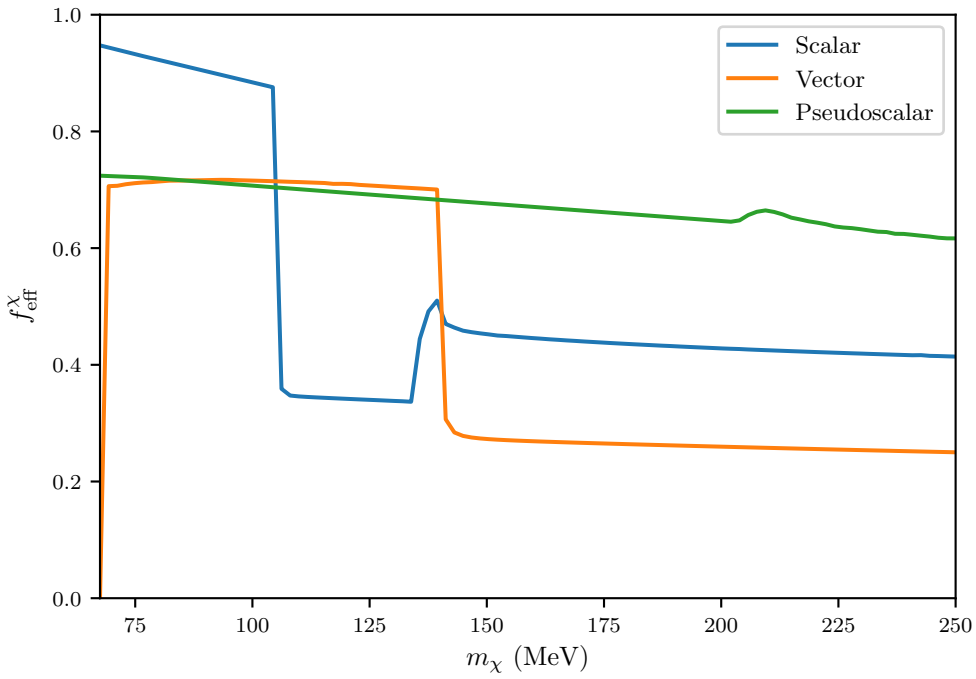

Figure 5.2: The efficiency factor $f_{\rm eff}$ for power injected into the plasma at recombination from DM annihilations for both our simplified models. The couplings are set to $g_{Sf} = g_{SG} = g_{SF}$ for the scalar, $g_{Pu} = -g_{Pd}$, $g_{P\ell} = 0$ for the pseudoscalar and $g_{Pu} = 5g_{Pd}$, $g_{P\ell} = 0$ for the vector simplified models.

5.4 Cosmic Microwave Background Constraints

Dark matter annihilations around the time of CMB formation can inject ionizing particles into the photon-baryon plasma [CITE: who thought of this? Find a good article.]. The resulting changes in the residual ionization fraction and baryon temperature modify the CMB temperature and polarization power spectra, particularly at small scales. The changes depend on the energy per unit volume per unit time imparted to the plasma, which is proportional to the DM annihilation

parameter

$$p_{\text{ann}} \equiv f_{\text{eff}}^{\chi} \cdot \frac{\langle \sigma v \rangle_{\bar{\chi}\chi,\text{CMB}}}{m_\chi}. \tag{5.15}$$

The thermal average is taken at the time of CMB formation.

The DM velocity at recombination depends on the kinetic decoupling temperature. While the DM velocity is thermal before kinetic decoupling, it redshifts more quickly afterwards, giving [53]

$$v_{\text{CMB}} = \sqrt{3T_\chi/m_\chi} \approx 2 \times 10^{-4} \left(\frac{T_\gamma}{1\text{ eV}}\right) \left(\frac{1\text{ MeV}}{m_\chi}\right) \left(\frac{10^{-4}}{x_{\text{kd}}}\right)^{1/2}, \tag{5.16}$$

where $x_{\text{kd}} \equiv T_\chi/m_\chi \approx 10^{-4}$–$10^{-6}$ and $T_\gamma = 0.235$ eV. Per the discussion in the previous section, this means that while the CMB bounds on $\langle \sigma v \rangle_{\bar{\chi}\chi,0}$ are quite stringent for s-wave annihilation, they are much weaker for p-wave annihilation since v_{CMB} is orders of magnitude smaller than v_0. The most recent Planck bound on the DM annihilation parameter [119], $p_{\text{ann}} < 4.1 \times 10^{-31}$ cm^3 s^{-1} MeV^{-1} is used to create the constraint plots later in this chapter.

The gamma-ray and positron spectra derived above are the key ingredients for calculating f_{eff}^{χ}, which encapsulates how efficiently DM annihilations inject energy into the plasma. It is computed by weighting the photon and e^+e^- spectra from DM annihilation by the energy injection efficiency factors f_{eff}^{γ} and $f_{\text{eff}}^{e^+e^-}$ [131]:

$$f_{\text{eff}}^{\chi} = \frac{1}{2m_\chi} \int_0^{m_\chi} dE\ E \left[2f_{\text{eff}}^{e^+e^-}(E) \cdot \left.\frac{dN}{dE_{e^+}}\right|_{\bar{\chi}\chi} + f_{\text{eff}}^{\gamma}(E) \cdot \left.\frac{dN}{dE_\gamma}\right|_{\bar{\chi}\chi} \right]. \tag{5.17}$$

The resulting f_{eff}^{χ} curves for the scalar, pseudoscalar and vector simplified models are shown in Figure 5.2.[2]

[2] f_{eff}^{χ} curves and CMB constraints for sub-GeV DM annihilating into specific final states can be found in [67], though the calculation has some differences noted in the Introduction to this

It is important to note that the CMB bound can be evaded. D'Eramo and Profumo [47] proposed a novel framework for thermally producing MeV-scale, s-wave DM that evades CMB constraints. The DM χ is thermally underproduced, but the dark sector is augmented by a new degee of freedom ψ that decays to χ after recombination. Assuming that ψ decays do not inject energy into the electron-photon plasma, this permits the DM to have a significant s-wave cross section at the present. The CMB constraints presented here are thus as conservative as possible.

5.5 Results

Figure 5.3 shows the current and projected limits on the scalar simplified model for Higgs portal-type couplings $g_{Sf} = g_{SG} = g_{SF}$. The scalar is taken to be heavier than the DM. As anticipated the CMB limits are very weak, even for $x_{\rm kd} = 10^{-6}$, since the DM annihilation cross section is p-wave suppressed. Since the coupling of S each SM field is proportional to the field's Yukawa, the constraints are determined by the $\mu^+\mu^-$ final state for $m_\mu < m_\chi < m_{\pi^0}$ and the $\pi^0\pi^0$ decay spectrum for $m_\chi > m_{\pi^0}$. The constraints weaken in the former mass range since there is little phase space available for the photon to be produced through FSR and strengthen significantly above the π^0 threshold. The $\pi^+\pi^-$ channel is nearly irrelevant to the constraint since approximate SU(2) isospin symmetry means the branching fractions are nearly identical, and the neutral pion spectrum is much more prominent. Due to its low energy range COMPTEL only observes the continuum part of the spectrum; as a result its limit does not strengthen for $m_\chi > m_{\pi^0}$.

The same constraints are applied to the pseudoscalar model in Figure 5.4. As

thesis.

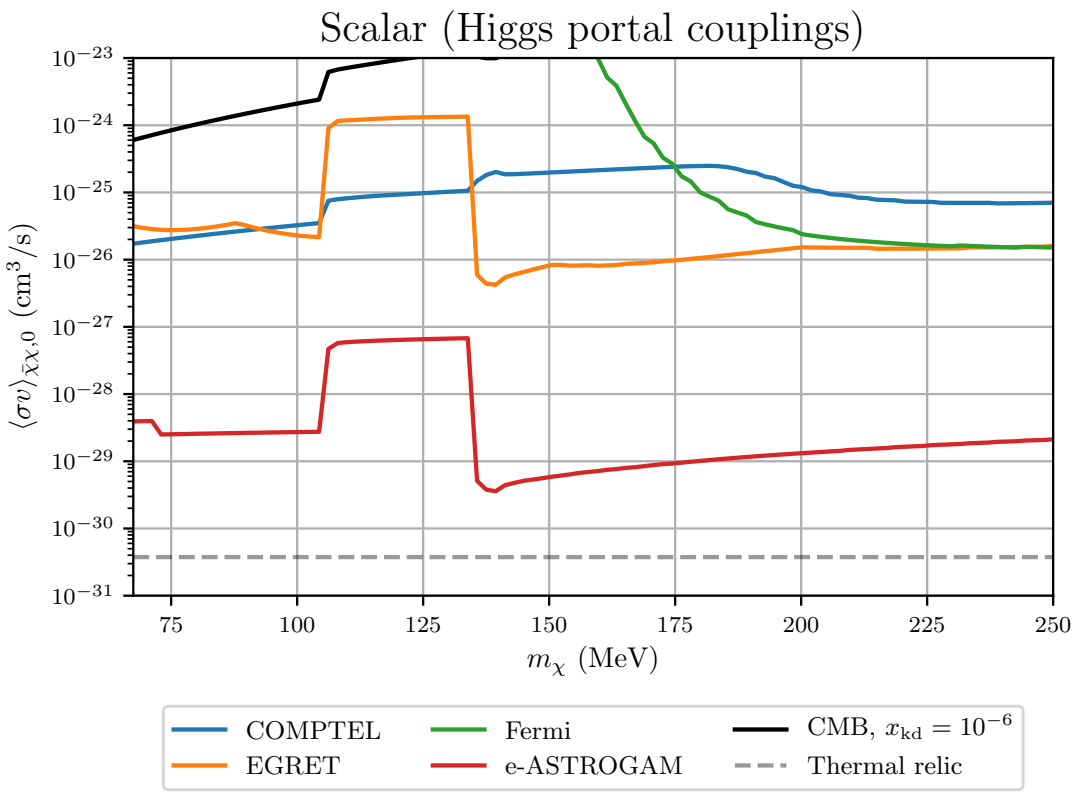

Figure 5.3: Current and projected limits on the DM self-annihilation cross section for the scalar mediator model. All the couplings of S to SM fields are taken to be equal. Since the annihilation is p-wave, the CMB and thermal relic constraints have been converted into constraints on the present-day self-annihilation cross section in the Milky Way by rescaling by $(v_0/v_{\rm CMB})^2$ and $(v_0/v_{\rm f.o.})^2$, respectively. Selecting a higher kinetic decoupling temperature $T_{\rm kd} = 10^{-4} m_\chi$ results in an even weaker CMB limit.

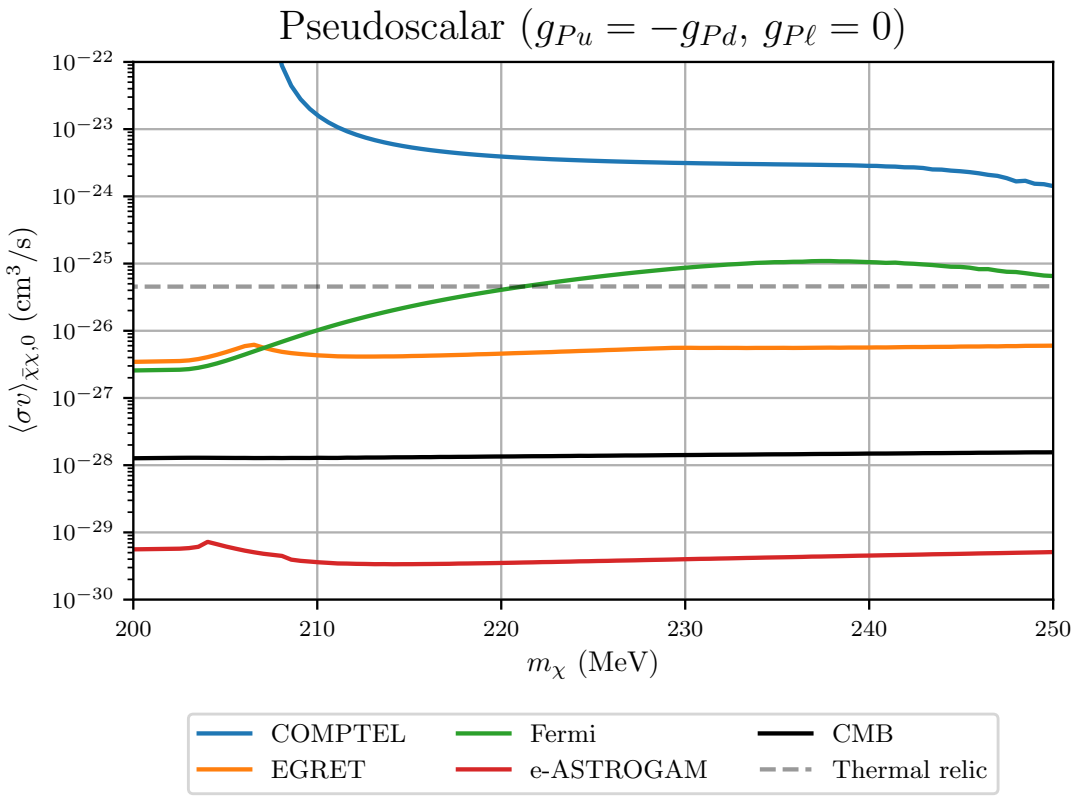

Figure 5.4: Current and projected limits on the DM self-annihilation cross section for the pseudoscalar mediator model. Since the annihilation is s-wave, the CMB limit can be plotted unambiguously with present-day indirect detection bounds.

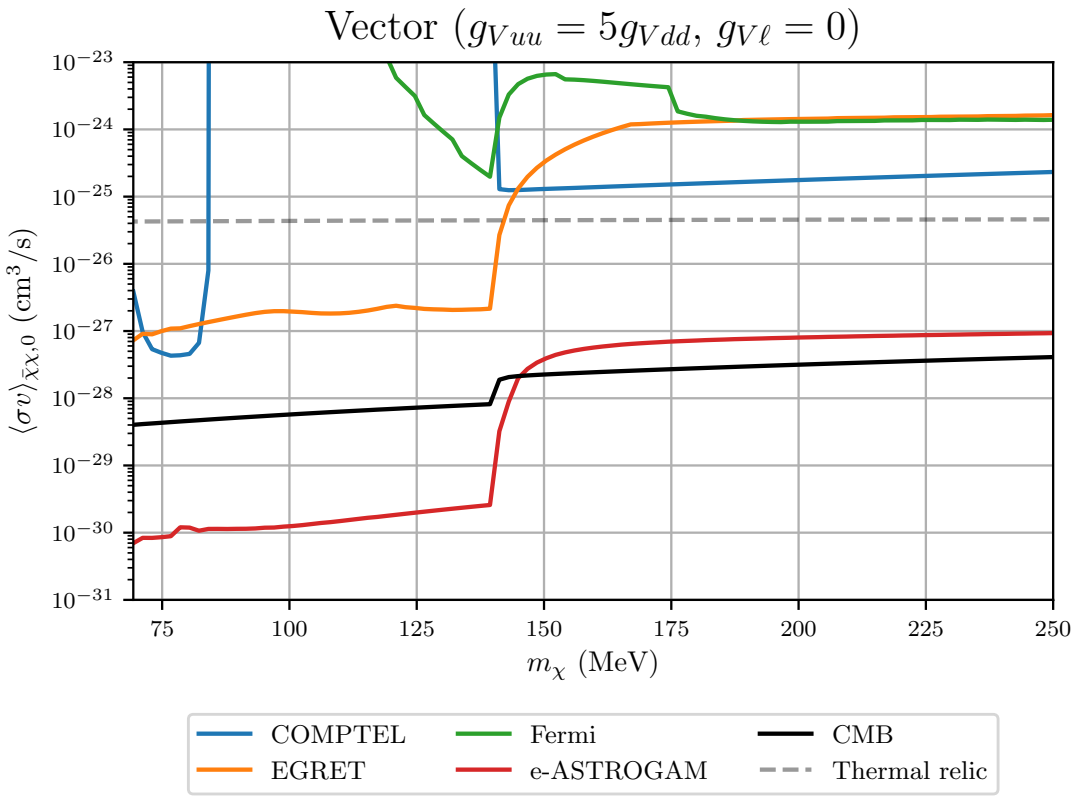

Figure 5.5: Current and projected limits on the DM self-annihilation cross section for the vector mediator model. Again, no rescaling is required to plot these limits together since the DM annihilation in this theory is s-wave.

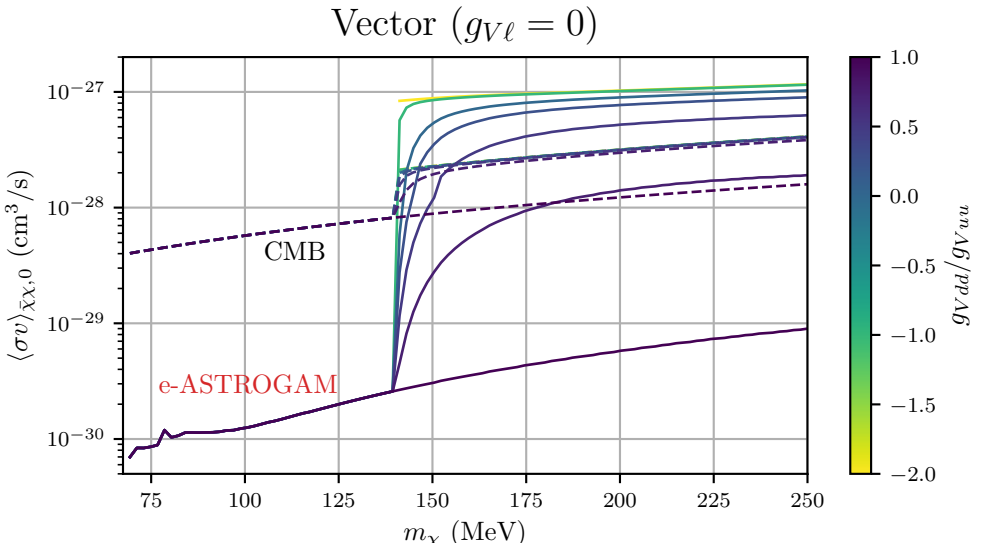

Figure 5.6: Dependence of e-ASTROGAM and CMB bounds for the vector simplified model on the light quark couplings.

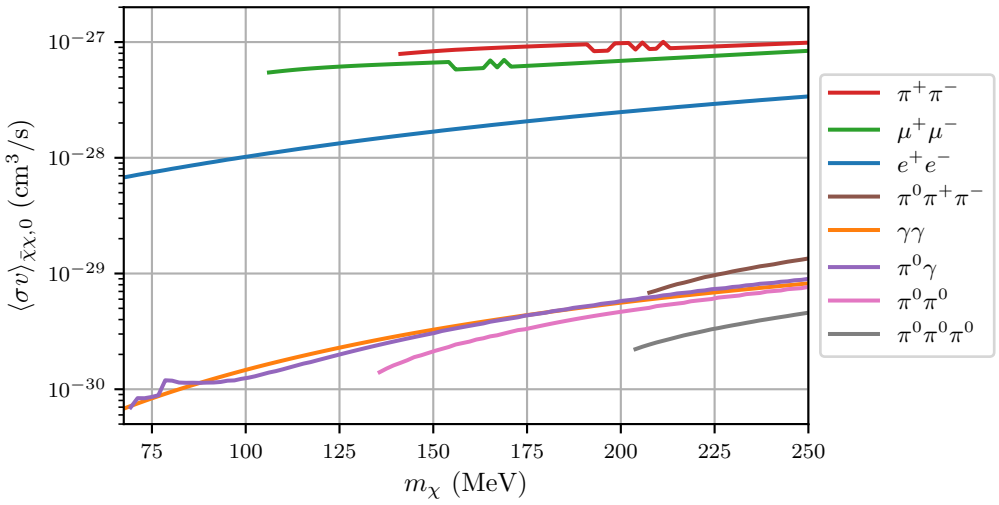

Figure 5.7: Projected limits for e-ASTROGAM for individual channels. The wiggles in the $\pi^+\pi^-$, $\mu^+\mu^-$ and $\pi^0\gamma$ bounds are noise from the optimizer's attempt to choose an energy window with the best signal-to-noise ratio.

before, the couplings are set to the type III 2HDM benchmark values: $g_{Pu} = -g_{Pd}$, $g_{P\ell} = 0$ and g_{PG}, g_{PF} are fixed by eqs. 2.21-2.22; P is taken heavier than χ. Remarkably, the projected constraint from e-ASTROGAM is a factor of ~ 40 stronger than the CMB bound. This is because the annihilation final states for this theory produce a significant number of photons. Existing constraints rule out the possibility that the DM is a standard thermal relic.

The kink in the EGRET and e-ASTROGAM bounds above ~ 205 MeV comes from crossing the kinematic threshold for the 3π final states. Fermi is incapable of observing the π^0 peak in the gamma ray spectrum since its lowest-energy bin covers $[153, 276]$ MeV; since the branching fraction for $\bar{\chi}\chi \to \gamma\gamma$ decreases above the 3π threshold the Fermi bound also becomes correspondingly weaker. The COMPTEL bound is the weakest by far since it cannot detect photons from π^0 decay or the diphoton line. The normalization of the continuum part of the spectrum from $\pi^\pm$ radiative decay increases with the DM mass, however, explaining why the COMPTEL limit becomes stronger for larger m_χ.

Note that the limit-setting procedure described in Sec. 5.2 does not try to optimize the signal-to-noise ratio over disjoint sets of energies. For m_χ above the 3π kinematic threshold, the optimizer selects a window that only encompasses the π^0 peak. This is clearly suboptimal since both the π^0 peak and gamma ray line portions of the spectrum have very high signal-to-noise ratios. A more dedicated analysis would integrate over both these energy ranges, which could increase the limit by a factor of ~ 2.

The constraints on the vector simplified model are shown in Figure 5.5. I have set $g_{Vuu} = 5g_{Vdd} = 1$, with all other couplings set to zero. Even though the DM annihilation cross section is s-wave, the CMB constraints are weaker than the e-ASTROGAM ones for $m_\chi < m_{\pi^+}$ and only a factor of two stronger for

$m_\chi > m_{\pi^+}$. Another interesting feature of this plot is the gap in the COMPTEL limits in the range ~ 85 MeV $< m_\chi < m_\pi$. For $m_\chi < m_\pi$, the only available final state is $\pi^0\gamma$, but this state's monochromatic gamma ray line is greater than the maximum energy COMPTEL can detect (30 MeV) for $m_\chi \gtrsim 85$ MeV. COMPTEL can constrain this model when $m_\chi > \pi$ since the $\pi^+\pi^-$ channel opens up, which produces low-energy gamma rays.

While the spectrum for and limits on the scalar mediator model are dictated almost solely by whichever channel is closest to threshold, this is not the case for the vector mediator. Figure 5.6 exhibits how the CMB and projected e-ASTROGAM bounds for this theory vary with the value of g_{Vdd}/g_{Vuu}. Depending on whether the $\pi^+\pi^-$ final state is accessible, the e-ASTROGAM constraint for $m_\chi > m_{\pi^+}$ can vary almost three orders of magnitude. The CMB constraints are less variable since f_{eff}^{χ} varies by at most a factor of $2-3$ over the range of values of g_{Vdd}/g_{Vuu}, which is itself a consequence of the fact that $f_{\text{eff}}^{e^+e^-}$ and f_{eff}^{γ} are nearly equal over the plotted mass range.

Experimental collaborations usually present limits on $\langle\sigma v\rangle_{\bar{\chi}\chi,0}$ assuming that DM can only annihilate into one final state. Projected e-ASTROGAM limits for all relevant final states are shown in Figure 5.7. The constraint on the $\pi^+\pi^-$ final state is slightly model-dependent since the FSR spectrum is somewhat different in the scalar and vector simplified models. Aside from this, uncertainties in the chiPT calculation of branching fractions completely factor out of the individual channel analysis. As I will discuss in the Conclusion, the uncertainties in the shape of the hadronic final states' spectra are less severe. On the other hand, no single channel agrees with the constraint curves for the scalar or vector simplified models, since the branching ratios are constrained by gauge invariance and chiral symmetry, highlighting the importance of our approach for setting realistic limits

on theories of sub-GeV DM.

Chapter 6

Conclusion

In this thesis I have performed a comprehensive analysis of the indirect detection prospects for three realistic simplified models of sub-GeV dark matter. The major results of Chapter 3 were the chiral Lagrangians for each of the models, which are valid for center of mass energies below ~ 500 MeV. These were used to analyze the branching fractions into different hadronic final states. In Chapter 4 the gamma ray spectra from DM annihilation were computed in detail. The final state radiation spectra for annihilation into leptons and charged pions were computed exactly, and the charged pion radiative decay spectrum was analyzed in detail. The positron spectra were also derived. In Chapter 5 constraints on the present-day DM self-annihilation cross section in the Milky Way were studied using a conservative procedure for existing and future gamma ray telescopes. The positron and gamma ray spectra were also used to compute f_{eff} in each simplified model, which in term permitted an accurate calculation of cosmic microwave background constraints on the DM self-annihilation cross section in the early universe. Notably, these were found to be weaker than the expected constraints from e-ASTROGAM over much of the parameter space in each of the models.

To conclude, I will briefly mention several further lines of inquiry.

6.1 Improving Indirect Detection Bounds

While the focus of this work was matching onto the chiral Lagrangian and computing the γ and e^+ spectra for several models, it would be interesting to perform a more rigorous statistical analysis of indirect detection prospects including secondary gamma rays. Secondary emission is produced through bremsstrahlung, inverse-Compton scattering of CMB photons and starlight, and synchrotron radiation from $e^\pm$ as well as in-flight annihilation of positrons with CR electrons. However, based on similar work taking these effects into account for DM annihilating into electrons and muons [17], this is likely to only improve the constraints less than an order of magnitude.

Another effect relevant to p-wave-annihilating DM that was not considered here is the enhancement of the velocity dispersion in the vicinity of the supermassive blackhole at the center of the Milky Way, Sagittarius A* [128]. In this high-density region the annihilation cross section the DM self-annihilation cross section could be 1-2 orders of magnitude larger than the standard value [129]. Given that this velocity "spike" region is very small, this is likely to correct the limits presented here by a factor of $\lesssim 10$.

6.2 Final State Interactions

It is well-known that the leading order chiral Lagrangian considered in isolation becomes less valid as the center of mass energy Q approaches the cutoff for the theory, $4\pi f_\pi \sim 1$ GeV, since tree-level next-to-leading order and leading-order loop corrections become increasingly important [125]. However, low-energy QCD contains particles besides the PNGBs with masses below this cutoff. The lowest-lying of these are the familiar vector meson ρ and the less well-understood $f_0(500)$

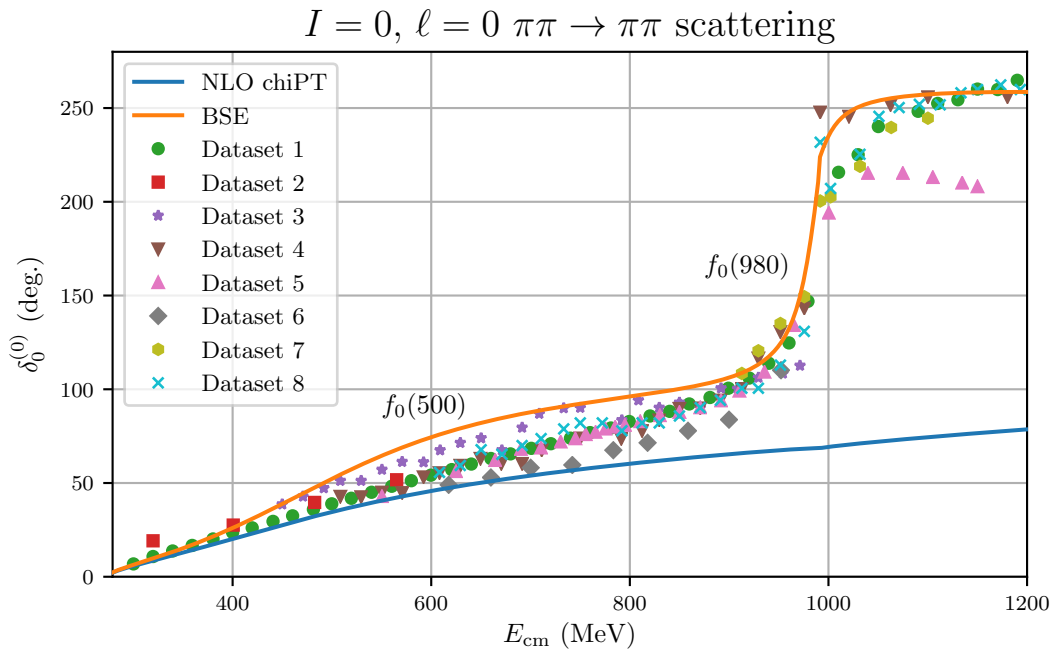

Figure 6.1: Phase shifts for elastic pion scattering in the isoscalar channel. The curve labeled "BSE" was computed using the Bethe-Salpeter unitarization procedure The datasets are those from Fig. 3 of [112].

(or σ) scalar meson [117]. Interactions between pions in DM annihilation final states therefore become important around 500 MeV for the scalar simplified model, since the scalar has the same quantum numbers (isospin $I = 0$, angular momentum $\ell = 0$) as the $f_0(500)$.[1]

This meson has mass similar to its width and thus cannot be understood as a Breit-Wigner resonance, in contrast to other unstable particles. σ was at one point thought to be the radial field associated with chiral perturbation theory thought of as a linear sigma model. This description of σ is incorrect, however, as integrating it out gives rise to completely incorrect values for the low energy constants in the NLO chiral Lagrangian; this necessitates a different treatement for the σ than for the vector resonances.

Resonances in QCD can be understood as a consequence of unitarity [117]. Various methods grounded in dispersion relations exist to correct calculations performed using the chiral Lagrangian to obey unitarity exactly [112, 110, 114, 64, 113, 73, 48, 109]. Focusing on the case of $I = 0$, $\ell = 0$ (isoscalar) elastic pion scattering, the simplest of these approaches is based on the Bethe-Salpeter equation (BSE), and involves resumming an infinite set of s-channel bubble diagrams involving only vertices from the leading-order chiral Lagrangian. The resulting amplitude has a pole corresponding to the $f_0(500)$. Related approaches give rise to a pole corresponding to the ρ meson, without introducing any parameters not present in the chiral Lagrangian.

Figure 6.1 exhibits the phase shift for isoscalar elastic pion scattering. The NLO chiPT prediction starts disagreeing with the data around 600 MeV while the BSE prediction reproduces it rather accurately up to 1.2 GeV. An advantage of the BSE unitarization procedure over others is that it is diagrammatic and

[1] I thank Michael Peskin for raising this point during a visit to UC Santa Cruz on Oct. 26, 2018.

can be applied straightforwardly to unitarizing the scalar simplified model in this thesis. For the vector theory, the ρ meson can be interpreted as resumming an analogous set of diagrams in the $I = 0$, $\ell = 1$ channel relevant for $\bar{\chi}\chi \to \pi^+\pi^-$, and can be included by adding a new octet of vector resonances to the chiral Lagrangian [51, 21, 121, 83].

As can be seen in Fig. 2 of [102], final state interactions have little impact on the photon spectrum from radiative ρ decay, and so should have little effect on the spectrum derived earlier for $\bar{\chi}\chi \to V^* \to \pi^+\pi^-\gamma$. Since this is related to the process $S \to \pi^+\pi^-\gamma$ by crossing symmetry, the same should hold there as well. In summary, I expect final state interactions to affect the branching fractions for the scalar and vector theories rather than the spectra for the individual final states. In the pseudoscalar model the story is sure to be more complicated since the final state interactions involve three pions. Fully accounting for these issues is left for future work.

6.3 Other Constraints

Numerous terrestrial, cosmological and astrophysical constraints apply to MeV-scale dark matter as well as the particle mediating its interactions with SM particles. These include rare and invisible meson decays [14], existing and proposed beam dumps [7], energy loss in the supernova SN1987A [80], stellar cooling, big bang nucleosynthesis, invisible Higgs decays, and direct detection, as mentioned in the Introduction. Overviews of these constraints and more references can be found in [90, 49, 89]. It remains to plot the indirect detection and CMB constraints along with these to determine which regions of parameter space are viable for the simplified models in this thesis. However, it is worth noting that many of these constraints depend on how the mediator interacts with leptons (for example, the

rare decays $B \to K e^+ e^-$ and $K \to \pi e^+ e^-$, which are relevant to the scalar simplified model), and can be easily evaded by making different assumptions about the couplings in the theories.

The effective Lagrangians derived in Chapter 3 are an important ingredient for determining these constraints. Supernova constraints are in particular need of revision. The current bounds come from a calculation of axion emission in nucleon-nucleon scattering [80]. Applying this to the mediators considered here is invalid since that analysis neglects the axion's mass and couplings to pions. Furthermore the one-pion exchange approximation used there is known to be inaccurate, as is the modeling of the supernova core temperature [89]. These effects will likely correct the current supernova constraints by an order of magnitude.

6.4 `hazma` version 1.0

The package `hazma` I have been developing with Logan Morrison was used to make all of the plots in this paper. Our goal has been to create a comprehensive, easy-to-use, extensible framework for performing any calculations related to MeV-scale dark matter, with a focus on indirect detection. The official release will become available this fall at `https://github.com/LoganAMorrison/Hazma`.

Appendix A

Conventions

I generally use the same conventions as Peskin and Schroeder and Schwartz since those are the books from which I learned field theory. These conventions often differ from the chiPT literature.

- $g_{\mu\nu} = \text{diag}(1, -1, -1, -1)$, the West Coast metric.
- $\epsilon^{0123} = +1$. This disagrees with much of the chiPT literature.
- $\gamma^5 = i\gamma^0\gamma^1\gamma^2\gamma^3$, as is used by much of the chiPT literature.
- In contrast to Peskin and Schroeder but in agreement with Schwartz, I take $e > 0$. This means the covariant derivative for the electron in QED is $D_\mu = \partial_\mu + ieA_\mu$.
- The Higgs vacuum expectation value is $v_h = 246$ GeV.

Appendix B

Baryon Number Conservation

This Appendix demonstrates that a global U(1) symmetry leads to conservation of a discrete quantum number. The simplest Lagrangian that demonstrates this is

$$\mathcal{L} = \bar{\psi}(i\gamma_\mu \partial^\mu - m)\psi, \tag{B.1}$$

and under the global U(1) $\psi \mapsto \exp(i\alpha)\psi \approx (1 + i\alpha)\psi$. By Noether's theorem, the conserved current associated with this symmetry is

$$j^\mu_{\mathrm{U}(1)} = i\frac{\partial \mathcal{L}}{\partial(\partial_\mu \psi)}\psi - i\bar{\psi}\frac{\partial \mathcal{L}}{\partial(\partial_\mu \bar{\psi})} = -\bar{\psi}\gamma^\mu \psi. \tag{B.2}$$

By integrating the continuity equation $\partial_\mu j^\mu_{\mathrm{U}(1)} = 0$ over space, the conservation law can be reexpressed as

$$Q_{\mathrm{U}(1)} \equiv \int d^3x \; j^0_{\mathrm{U}(1)} = -\int d^3x \; \psi^\dagger \psi \implies \frac{dQ_{\mathrm{U}(1)}}{dt} = 0. \tag{B.3}$$

The charge can be expanded in terms of fermion creation and annihilation operators, dropping terms that annihilate the vacuum:

$$Q = -\sum_{r,s} \int d^3x \int \frac{d^3p}{(2\pi)^3\sqrt{2E_p}} \frac{d^3k}{(2\pi)^3\sqrt{2E_k}} \tag{B.4}$$

$$\times \left(b_p^r v^{r\dagger}(p) e^{-ip\cdot x} + a_p^{r\dagger} u^{r\dagger}(p) e^{ip\cdot x} \right) \tag{B.5}$$

$$\times \left(a_k^s u^s(k) e^{-ik\cdot x} + b_k^{s\dagger} v^s(k) e^{ik\cdot x} \right) \tag{B.6}$$

$$= -\sum_{r,s} \int d^3x \int \frac{d^3p}{(2\pi)^3\sqrt{2E_p}} \frac{d^3k}{(2\pi)^3\sqrt{2E_k}} \tag{B.7}$$

$$\times \Big[v^{r\dagger}(p) v^s(k)\ b_p^r b_k^{s\dagger}\ e^{i(k-p)\cdot x} \tag{B.8}$$

$$+ u^{r\dagger}(p) u^s(k)\ a_p^{r\dagger} a_k^s\ e^{i(p-k)\cdot x} \Big] \tag{B.9}$$

$$= -\sum_{r,s} \int \frac{d^3p}{(2\pi)^3 2E_p} \left[v^{r\dagger}(p) v^s(p)\ b_p^r b_p^{s\dagger} + u^{r\dagger}(p) u^s(p)\ a_p^{r\dagger} a_p^s \right] \tag{B.10}$$

$$= -\sum_{s} \int \frac{d^3p}{(2\pi)^3} \left[b_p^s b_p^{s\dagger} + a_p^{s\dagger} a_p^s \right] \tag{B.11}$$

$$\sim -\sum_{s} \int \frac{d^3p}{(2\pi)^3} \left[a_p^{s\dagger} a_p^s - b_p^s b_p^{s\dagger} \right], \tag{B.12}$$

where I used $\{b_p^r, b_k^{s\dagger}\} = (2\pi)^3 \delta^{(3)}(\mathbf{p} - \mathbf{k}) \delta^{rs}$ and dropped the infinite constant in the last line. The two terms are just the number operators for fermions and antifermions, showing that the discrete quantum number counting U(1) charge is conserved.

Appendix C

The $\mathrm{U}(3)_L \times \mathrm{U}(3)_R$ Covariant Derivative in ChiPT

The covariant derivative of the field $\bar{\Sigma}(x) = e^{-i\theta(x)/3}\Sigma(x)$ is defined as

$$D_\mu \bar{\Sigma} \equiv e^{-i\theta/3}\left[D_\mu \Sigma - \frac{i}{3}(D_\mu\theta)\Sigma\right], \tag{C.1}$$

$$D_\mu \Sigma \equiv \partial_\mu \Sigma - i\hat{r}_\mu \Sigma + i\Sigma\hat{l}_\mu \tag{C.2}$$

$$D_\mu \theta = \partial_\mu \theta + 2\,\mathrm{tr}\, a_\mu. \tag{C.3}$$

In this appendix I will confirm that it transforms correctly. Under a $\mathrm{U}(3)_L \times \mathrm{U}(3)_R$ transformation

$$(\bar{L}, \bar{R}) = \left(e^{i(b-a)}L, e^{i(a+b)}R\right) \in \mathrm{U}(3)_L \times \mathrm{U}(3)_R \tag{C.4}$$

the fields transform as

$$\theta \to \theta - 6a \tag{C.5}$$

$$\Sigma \to R \cdot \Sigma \cdot \Lambda^\dagger \tag{C.6}$$

$$\operatorname{tr} a_\mu \to \operatorname{tr} a_\mu + \frac{1}{2} \operatorname{tr}\left[\bar{R} \cdot (i\partial_\mu \bar{R}^\dagger) - \bar{L} \cdot (i\partial_\mu \bar{L}^\dagger)\right] \tag{C.7}$$

$$= \operatorname{tr} a_\mu + \frac{1}{2} \operatorname{tr}\left[L\left(L^\dagger \partial_\mu (a+b) + \partial_\mu L^\dagger\right) - L\left(L^\dagger \partial_\mu (b-a) + \partial_\mu L^\dagger\right)\right] \tag{C.8}$$

$$= \operatorname{tr} a_\mu + 3\partial_\mu a + \frac{1}{2} \operatorname{tr}\left[R\partial_\mu R^\dagger - L\partial_\mu L^\dagger\right] \tag{C.9}$$

$$= \operatorname{tr} a_\mu + 3\partial_\mu a. \tag{C.10}$$

The last equality comes from the fact that $R\partial_\mu R^\dagger$ is proportional to the Maurer-Cartan form for $\mathrm{SU}(3)_R$, which is an element of the Lie algebra and is therefore traceless (and similarly for the L term). The covariant derivative therefore transforms as

$$D_\mu \bar{\Sigma} \to e^{-i(\theta-6a)/3}\left[R \cdot (D_\mu \Sigma) \cdot L^\dagger - \frac{i}{3}(\partial_\mu - 6\partial_\mu a + 2\operatorname{tr} a_\mu + 6\partial_\mu a) R \cdot \Sigma \cdot L^\dagger\right] \tag{C.11}$$

$$= \bar{R} \cdot (D_\mu \bar{\Sigma}) \cdot \bar{L}^\dagger, \tag{C.12}$$

which is the same transformation law as for $\bar{\Sigma}(x)$, as was desired.

Appendix D

Cross sections, Widths and Spectra

This chapter is a repository for the DM annihilation cross sections, mediator decay widths and final state radiation spectra for the theories studied in this thesis. Since expanding the chiral Lagrangian is error-prone, I used the Mathematica packages FeynRules [8], FeynArts [75] and FeynCalc [130, 106] to automate the calculations. These packages are available from `http://feynrules.irmp.ucl.ac.be/`, `http://www.feynarts.de` and `https://github.com/FeynCalc/feyncalc`. An excellent treatment of three-body phase space integrations can be found in [99, p. 171].

In what follows, I use Q to denote the center of mass energy, $r_a \equiv m_a/Q$, as well as

$m_\pi^2 \equiv B(m_u + m_d)$	pion mass at leading order
$\lambda(a,b,c) \equiv (a-b-c)^2 - 4bc$	three body phase space factor
$\mathcal{D}_M(Q^2) \equiv (Q^2 - m_M^2)^2 + m_M^2\Gamma_M^2$	propagator denominator factor.

It is convenient to express photon spectra in terms of the dimensionless variable $x \equiv 2E_\gamma/Q$, where E_γ is the photon energy.

D.1 Scalar Simplified Model

D.1.1 Cross sections

$$
\begin{aligned}
\sigma_{\bar{\chi}\chi\to\bar{\ell}\ell} &= -\frac{g_{Sf}^2 g_{S\chi}^2 r_\ell^2 (2r_\ell - 1)(2r_\ell + 1)\sqrt{(1-4r_\ell^2)(1-4r_\chi^2)}}{8\pi v_h^2}\frac{Q^4}{\mathcal{D}_S(Q^2)} \\
\sigma_{\bar{\chi}\chi\to\gamma\gamma} &= \frac{\alpha^2 g_{SF}^2 g_{S\chi}^2\sqrt{1-4r_\chi^2}}{256\pi^3 v_h^2}\frac{Q^4}{\mathcal{D}_S(Q^2)} \\
\sigma_{\bar{\chi}\chi\to SS} &= \frac{g_{S\chi}^4 (c_{SS}^{(1)} + c_{SS}^{(2)})}{32\pi(1-4r_\chi^2)}\frac{1}{Q^2} \\
c_{SS}^{(1)} &= \frac{2\sqrt{(1-4r_S^2)(1-4r_\chi^2)}(r_S^2 - 4r_\chi^2)^2}{4r_S^2 r_\chi^2 - r_S^4 - r_\chi^2} - 4\sqrt{(1-4r_S^2)(1-4r_\chi^2)} \\
c_{SS}^{(2)} &= \frac{6r_S^4 - 4r_S^2(4r_\chi^2+1) - 32r_\chi^4 + 16r_\chi^2 + 1}{1-2r_S^2} \\
&\qquad \times \log\left[\left(\frac{1-2r_S^2+\sqrt{(1-4r_S^2)(1-4r_\chi^2)}}{1-2r_S^2-\sqrt{(1-4r_S^2)(1-4r_\chi^2)}}\right)^2\right] \\
\sigma_{\bar{\chi}\chi\to\pi^+\pi^-} &= \frac{g_{S\chi}^2\sqrt{(1-4r_{\pi^+}^2)(1-4r_\chi^2)}}{729\cdot 2^4\pi v_h^2(4g_{SG}v_S + 9v_h)^2(3g_{Sf}v_S + 2g_{SG}v_S + 3v_h)^2} \\
&\qquad \times \frac{(c_{\pi\pi}^{(Q)}Q^2 + c_{\pi\pi}^{(m)}m_\pi^2)^2}{\mathcal{D}_S(Q^2)}, \\
c_{\pi\pi}^{(Q)} &= 54 g_{SG}(1-2r_{\pi^+}^2)v_h(3g_{Sf}v_S + 2g_{SG}v_S + 3v_h) \\
c_{\pi\pi}^{(m)} &= (4g_{SG}v_S + 9v_h)(27v_h(3g_{Sf} + 2g_{SG}) + 16 g_{SG}v_S(9g_{Sf} - 2g_{SG})) \\
\sigma_{\bar{\chi}\chi\to\pi^0\pi^0} &= \frac{1}{2}\sigma_{\bar{\chi}\chi\to\pi^+\pi^-} \text{ with } \pi^\pm \to \pi^0.
\end{aligned}
$$

D.1.2 Final State Radiation Spectra

$$\left.\frac{dN}{dE_\gamma}\right|_{\bar{\chi}\chi\to\bar{\ell}\ell} = \frac{2\alpha}{\pi E_\gamma (1-4r_\ell)^{3/2}} \times \left[-(1-4r_\ell^2)(1-x)\sqrt{1-\frac{4r_\ell^2}{1-x}} + \left[2-x(2-x)-4r_\ell^2(3-2x-4r_\ell^2)\right]\tanh^{-1}\left[\sqrt{1-\frac{4r_\ell^2}{1-x}}\right]\right]$$

$$\left.\frac{dN}{dE_\gamma}\right|_{\bar{\chi}\chi\to\pi^+\pi^-} = \frac{2\alpha}{\pi E_\gamma (1-4r_{\pi^+}^2)^{1/2}} \times \left[(1-x)\sqrt{1-\frac{4r_{\pi^+}^2}{1-x}} - 2(1-x-2r_{\pi^+}^2)\tanh^{-1}\left[\sqrt{1-\frac{4r_{\pi^+}^2}{1-x}}\right]\right].$$

D.2 Pseudoscalar Simplified Model

D.2.1 Cross sections

$$\sigma_{\bar{\chi}\chi\to\bar{\ell}\ell} = \frac{(1-2\theta_{P\pi^0}^2)g_{P\ell}^2 g_{P\chi}^2\sqrt{1-4r_\ell^2}}{16\pi\sqrt{1-4r_\chi^2}}\frac{Q^2}{\mathcal{D}_M(Q^2)}$$

$$\sigma_{\bar{\chi}\chi\to\gamma\gamma} = \frac{\alpha^2 g_{P\chi}^2[(1-2\theta_{P\pi^0}^2)f_\pi^2 g_{PF}^2 - 2\theta_{P\pi^0}f_\pi g_{PF}v_h + \theta_{P\pi^0}^2 v_h^2]}{256\pi^3 f_\pi^2\sqrt{1-4r_\chi^2}v_h^2}\frac{Q^4}{\mathcal{D}_M(Q^2)}$$

$$\sigma_{\bar{\chi}\chi\to PP} = \frac{(1-2\theta_{P\pi^0}^2)g_{P\chi}^4\left(c_{PP}^{(1)}+c_{PP}^{(2)}\right)}{64\pi(1-4r_\chi^2)}\frac{1}{Q^2},$$

$$c_{PP}^{(1)} \equiv \frac{2\sqrt{(1-4r_P^2)(1-4r_\chi^2)}(3r_P^4-8r_P^2r_\chi^2+2r_\chi^2)}{4r_P^2r_\chi^2-r_P^4-r_\chi^2}$$

$$c_{PP}^{(2)} \equiv \frac{(6r_P^4-4r_P^2+1)}{1-2r_P^2}\log\left[\left(\frac{1-2r_P^2+\sqrt{(1-4r_P^2)(1-4r_\chi^2)}}{1-2r_P^2-\sqrt{(1-4r_P^2)(1-4r_\chi^2)}}\right)^2\right]$$

$$\frac{d\sigma_{\bar{\chi}\chi\to\pi^0\pi^0\pi^0}}{ds} = \frac{c_{000}\theta_{P\pi^0}^2 g_{P\chi}^2}{512\pi^3 f_\pi^4}\frac{\lambda^{1/2}(Q^2,m_{\pi^0}^2,s)\sqrt{s-4m_{\pi^0}^2}}{Q\sqrt{s(Q^2-4m_\chi^2)}\mathcal{D}_M(Q^2)},$$

$$c_{000} \equiv (m_P^2+m_\pi^2-m_{\pi^0}^2)^2$$

$$\frac{d\sigma_{\bar{\chi}\chi\to\pi^0\pi^+\pi^-}}{ds} = \frac{c_{0+-}\theta_{P\pi^0}^2 g_{P\chi}^2}{4608\pi^3 f_\pi^4}\frac{\lambda^{1/2}(Q^2,m_{\pi^0}^2,s)\sqrt{s-4m_{\pi^+}^2}}{Q\sqrt{s(Q^2-4m_\chi^2)}\mathcal{D}_M(Q^2)},$$

$$c_{0+-} \equiv (m_P^2-2m_{\pi^+}^2+m_\pi^2-2m_{\pi^0}^2+3s)^2,$$

where the $P-\pi^0$ mixing angle is

$$\theta_{P\pi^0} = \frac{Bf_\pi}{(m_P^2-m_{\pi^0}^2)v_h}[(g_{Pu}+g_{PG})m_u-(g_{Pd}+g_{PG})m_d],$$

which I have assumed is small. The last two expressions are functions of $s = (p_\chi + p_{\bar{\chi}} - p_{\pi^0})^2$, the Mandelstam variable associated with the (or one of the)

neutral pions. To obtain the cross section, these expressions must be numerically integrated:

$$\sigma_{\bar{\chi}\chi\to\pi^0\pi^0\pi^0} = \int_{4m_{\pi^0}^2}^{(Q-m_{\pi^0})^2} ds\ \frac{d\sigma_{\bar{\chi}\chi\to\pi^0\pi^0\pi^0}}{ds} \tag{D.1}$$

$$\sigma_{\bar{\chi}\chi\to\pi^0\pi^+\pi^-} = \int_{4m_{\pi^+}^2}^{(Q-m_{\pi^0})^2} ds\ \frac{d\sigma_{\bar{\chi}\chi\to\pi^0\pi^+\pi^-}}{ds}. \tag{D.2}$$

D.2.2 Final State Radiation Spectra

$$\left.\frac{dN}{dE_\gamma}\right|_{\bar{\chi}\chi\to\bar{\ell}\ell} = \frac{2\alpha}{\pi E_\gamma\sqrt{1-4r_\ell^2}} \times\left[(1-x)\sqrt{1-\frac{4r_\ell^2}{1-x}} -(2-x(2-x)-4r_\ell^2)\tanh^{-1}\left[\sqrt{1-4r_\ell^2}\right]\right]$$

D.3 Vector Simplified Model

D.3.1 Cross sections

$$\left.\frac{dN}{dE_\gamma}\right|_{\bar{\chi}\chi\to\bar{\ell}\ell} = \frac{2\alpha}{\pi E_\gamma(1-4r_\ell^2)^{1/2}(1+2r_\ell^2)}$$

$$\sigma_{\bar{\chi}\chi\to\bar{\ell}\ell} = \frac{g_{V\ell}^2 g_{V\chi}^2 \sqrt{1-4r_\ell^2}(1+2r_\ell^2)(1+2r_\chi^2)}{12\pi\sqrt{1-4r_\chi^2}} \frac{Q^2}{\mathcal{D}_V(Q^2)}$$

$$\sigma_{\bar{\chi}\chi\to\pi^0\gamma} = \frac{\alpha g_{V\chi}^2 (2g_{Vu}+g_{Vd})^2 (1-r_{\pi^0}^2)^3 (1+2r_\chi^2)}{27\cdot 2^7\pi^4 f_\pi^2 \sqrt{1-4r_\chi^2}} \frac{Q^4}{\mathcal{D}_V(Q^2)}$$

$$\sigma_{\bar{\chi}\chi\to\pi^+\pi^-} = \frac{g_{V\chi}^2 (1-4r_{\pi^+}^2)^{3/2}(1+2r_\chi^2)(g_{Vu}-g_{Vd})^2}{48\pi\sqrt{1-4r_\chi^2}} \frac{Q^2}{\mathcal{D}_V(Q^2)}$$

$$\sigma_{\bar{\chi}\chi\to VV} = \frac{g_{V\chi}^4 \sqrt{1-4r_V^2}\left(c_{VV}^{(1)}+c_{VV}^{(2)}\right)}{16\pi\sqrt{1-4r_\chi^2}},$$

$$c_{VV}^{(1)} \equiv \frac{2\sqrt{(1-4r_V^2)(1-4r_\chi^2)}(2r_V^4+4r_\chi^4+r_\chi^2)}{4r_V^2 r_\chi^2 - r_V^4 - r_\chi^2}$$

$$c_{VV}^{(2)} \equiv \frac{4r_V^4+4(1-2r_V^2)r_\chi^2-8r_\chi^4+1}{1-2r_V^2}\log\left[\left(\frac{1-2r_V^2+\sqrt{(1-4r_V^2)(1-4r_\chi^2)}}{1-2r_V^2-\sqrt{(1-4r_V^2)(1-4r_\chi^2)}}\right)^2\right]$$

D.3.2 Final State Radiation Spectra

Explain factorization (see Schwartz)!

$$\left.\frac{dN}{dE_\gamma}\right|_{\bar{\chi}\chi\to\bar{\ell}\ell} = \frac{2\alpha}{\pi E_\gamma (1-4r_\ell^2)^{1/2}(1+2r_\ell^2)} \times\left[\left[2-x(2-x)+4r_\ell^2(1-x)\right]\sqrt{1-\frac{4r_\ell^2}{1-x}} -2\left[2-x(2-x)-4r_\ell^2(x+2r_\ell^2)\right]\tanh^{-1}\left[\sqrt{1-\frac{4r_\ell^2}{1-x}}\right]\right]$$

$$\left.\frac{dN}{dE_\gamma}\right|_{\bar{\chi}\chi\to\pi^+\pi^-} = \frac{2\alpha}{\pi E_\gamma (1-4r_{\pi^+}^2)^{3/2}} \times\left[-\left[1-x(1+x)-4r_{\pi^+}^2(1-x)\right]\sqrt{1-\frac{4r_{\pi^+}^2}{1-x}} +2(1-4r_{\pi^+}^2)(1+x-2r_{\pi^+}^2)\tanh^{-1}\left[\sqrt{1-\frac{4r_{\pi^+}^2}{1-x}}\right]\right]$$

Bibliography

[1] Tomohiro Abe, Ryosuke Sato, and Kei Yagyu. Lepton-specific two Higgs doublet model as a solution of muon g 2 anomaly. *JHEP*, 07:064, 2015.

[2] M. Ackermann et al. Fermi-lat observations of the diffuse -ray emission: Implications for cosmic rays and the interstellar medium. *The Astrophysical Journal*, 750(1):3, 2012.

[3] M. Ackermann et al. Searching for Dark Matter Annihilation from Milky Way Dwarf Spheroidal Galaxies with Six Years of Fermi Large Area Telescope Data. *Phys. Rev. Lett.*, 115(23):231301, 2015.

[4] R. Agnese et al. New Results from the Search for Low-Mass Weakly Interacting Massive Particles with the CDMS Low Ionization Threshold Experiment. *Phys. Rev. Lett.*, 116(7):071301, 2016.

[5] R. Agnese et al. Projected Sensitivity of the SuperCDMS SNOLAB experiment. *Phys. Rev.*, D95(8):082002, 2017.

[6] M. E. Albrecht, Th. Feldmann, and Th. Mannel. Goldstone Bosons in Effective Theories with Spontaneously Broken Flavour Symmetry. *JHEP*, 10:089, 2010.

[7] Sergey Alekhin et al. A facility to Search for Hidden Particles at the CERN SPS: the SHiP physics case. *Rept. Prog. Phys.*, 79(12):124201, 2016.

[8] Adam Alloul, Neil D. Christensen, Céline Degrande, Claude Duhr, and Benjamin Fuks. FeynRules 2.0 - A complete toolbox for tree-level phenomenology. *Comput. Phys. Commun.*, 185:2250–2300, 2014.

[9] Daniele S. M. Alves and Neal Weiner. A viable QCD axion in the MeV mass range. *JHEP*, 07:092, 2018.

[10] G. Angloher et al. Results on light dark matter particles with a low-threshold CRESST-II detector. *Eur. Phys. J.*, C76(1):25, 2016.

[11] Giorgio Arcadi, Maíra Dutra, Pradipta Ghosh, Manfred Lindner, Yann Mambrini, Mathias Pierre, Stefano Profumo, and Farinaldo S. Queiroz. The waning of the WIMP? A review of models, searches, and constraints. *Eur. Phys. J.*, C78(3):203, 2018.

[12] Q. Arnaud et al. First results from the NEWS-G direct dark matter search experiment at the LSM. *Astropart. Phys.*, 97:54–62, 2018.

[13] W. B. Atwood et al. The large area telescope on the fermi gamma-ray space telescope mission. *The Astrophysical Journal*, 697(2):1071, 2009.

[14] Andriy Badin and Alexey A Petrov. Searching for light Dark Matter in heavy meson decays. *Phys. Rev.*, D82:034005, 2010.

[15] J. N. Bahcall and R. M. Soneira. The universe at faint magnitudes. I - Models for the galaxy and the predicted star counts. *Astrophysical Journal Supplement Series*, 44:73–110, Sep 1980.

[16] William A. Bardeen. Anomalous Ward identities in spinor field theories. *Phys. Rev.*, 184:1848–1857, 1969.

[17] Richard Bartels, Daniele Gaggero, and Christoph Weniger. Prospects for indirect dark matter searches with mev photons. *Journal of Cosmology and Astroparticle Physics*, 2017(05):001, 2017.

[18] Martin Bauer, Ulrich Haisch, and Felix Kahlhoefer. Simplified dark matter models with two Higgs doublets: I. Pseudoscalar mediators. *JHEP*, 05:138, 2017.

[19] John F. Beacom, Nicole F. Bell, and Gianfranco Bertone. Gamma-ray constraint on galactic positron production by mev dark matter. *Phys. Rev. Lett.*, 94:171301, May 2005.

[20] J. S. Bell. Current algebra and gauge variance. *Il Nuovo Cimento A (1965-1970)*, 50(1):129–134, Jul 1967.

[21] Johan Bijnens, Gilberto Colangelo, and Gerhard Ecker. The Mesonic chiral Lagrangian of order p^6. *JHEP*, 02:020, 1999.

[22] Kimberly K. Boddy and Jason Kumar. Indirect detection of dark matter using mev-range gamma-ray telescopes. *Phys. Rev. D*, 92:023533, Jul 2015.

[23] Kimberly K. Boddy, Jason Kumar, and Louis E. Strigari. The Effective J-Factor of the Galactic Center for Velocity-Dependent Dark Matter Annihilation. 2018.

[24] Paul Bode, Jeremiah P. Ostriker, and Neil Turok. Halo formation in warm dark matter models. *Astrophys. J.*, 556:93–107, 2001.

[25] Steven E. Boggs et al. The Advanced Compton Telescope Mission. *New Astron. Rev.*, 50:604–607, 2006.

[26] Jo Bovy and Scott Tremaine. On the local dark matter density. *Astrophys. J.*, 756:89, 2012.

[27] G. C. Branco, P. M. Ferreira, L. Lavoura, M. N. Rebelo, Marc Sher, and Joao P. Silva. Theory and phenomenology of two-Higgs-doublet models. *Phys. Rept.*, 516:1–102, 2012.

[28] Torsten Bringmann, Lars Bergström, and Joakim Edsjö. New gamma-ray contributions to supersymmetric dark matter annihilation. *Journal of High Energy Physics*, 2008(01):049, 2008.

[29] Torsten Bringmann, Michele Doro, and Mattia Fornasa. Dark matter signals from draco and willman 1: prospects for magic ii and cta. *Journal of Cosmology and Astroparticle Physics*, 2009(01):016, 2009.

[30] Torsten Bringmann, Joakim Edsjö, Paolo Gondolo, Piero Ullio, and Lars Bergström. DarkSUSY 6 : An Advanced Tool to Compute Dark Matter Properties Numerically. *JCAP*, 1807(07):033, 2018.

[31] DA Bryman, P Depommier, and C Leroy. $\pi \to e\nu$, $\pi \to e\nu\gamma$ decays and related processes. *Physics Reports*, 88(3):151–205, 1982.

[32] Ranny Budnik, Ori Chesnovsky, Oren Slone, and Tomer Volansky. Direct Detection of Light Dark Matter and Solar Neutrinos via Color Center Production in Crystals. *Phys. Lett.*, B782:242–250, 2018.

[33] T. H. Burnett and Norman M. Kroll. Extension of the low soft-photon theorem. *Phys. Rev. Lett.*, 20(2), January 1968.

[34] Curtis G. Callan, Sidney Coleman, J. Wess, and Bruno Zumino. Structure of phenomenological lagrangians. ii. *Phys. Rev.*, 177:2247–2250, Jan 1969.

[35] Junjie Cao, Liangliang Shang, Peiwen Wu, Jin Min Yang, and Yang Zhang. Interpreting the galactic center gamma-ray excess in the NMSSM. *JHEP*, 10:030, 2015.

[36] Junjie Cao, Liangliang Shang, Peiwen Wu, Jin Min Yang, and Yang Zhang. Supersymmetry explanation of the Fermi Galactic Center excess and its test at LHC run II. *Phys. Rev.*, D91(5):055005, 2015.

[37] Riccardo Catena and Piero Ullio. A novel determination of the local dark matter density. *JCAP*, 1008:004, 2010.

[38] R. S. Chivukula, Andrew G. Cohen, H. Georgi, Benjamin Grinstein, and A. V. Manohar. Higgs Decay Into Goldstone Bosons. *Annals Phys.*, 192:93–103, 1989.

[39] R. Sekhar Chivukula and Howard Georgi. Composite Technicolor Standard Model. *Phys. Lett.*, B188:99–104, 1987.

[40] Marco Cirelli, Gennaro Corcella, Andi Hektor, Gert Hütsi, Mario Kadastik, Paolo Panci, Martti Raidal, Filippo Sala, and Alessandro Strumia. Pppc 4 dm id: a poor particle physicist cookbook for dark matter indirect detection. *Journal of Cosmology and Astroparticle Physics*, 2011(03):051, 2011.

[41] G. Colangelo, J. Gasser, and H. Leutwyler. The quark condensate from k_{e_4} decays. *Phys. Rev. Lett.*, 86:5008–5010, May 2001.

[42] S. Coleman, J. Wess, and Bruno Zumino. Structure of phenomenological lagrangians. i. *Phys. Rev.*, 177:2239–2247, Jan 1969.

[43] J. Cooley. Overview of Non-Liquid Noble Direct Detection Dark Matter Experiments. *Phys. Dark Univ.*, 4:92–97, 2014.

[44] Nathaniel Craig and Scott Thomas. Exclusive Signals of an Extended Higgs Sector. *JHEP*, 11:083, 2012.

[45] Csaba Csáki and Philip Tanedo. Beyond the Standard Model. In *Proceedings, 2013 European School of High-Energy Physics (ESHEP 2013): Paradfurdo, Hungary, June 5-18, 2013*, pages 169–268, 2015.

[46] G. D'Ambrosio, G. F. Giudice, G. Isidori, and A. Strumia. Minimal flavor violation: An Effective field theory approach. *Nucl. Phys.*, B645:155–187, 2002.

[47] Francesco D'Eramo and Stefano Profumo. Sub-GeV Dark Matter Shining at Future MeV Gamma-Ray Telescopes. 2018.

[48] A. Dobado and J. R. Pelaez. The Inverse amplitude method in chiral perturbation theory. *Phys. Rev.*, D56:3057–3073, 1997.

[49] Matthew J. Dolan, Felix Kahlhoefer, Christopher McCabe, and Kai Schmidt-Hoberg. A taste of dark matter: Flavour constraints on pseudoscalar mediators. *JHEP*, 03:171, 2015. [Erratum: JHEP07,103(2015)].

[50] John F. Donoghue, J. Gasser, and H. Leutwyler. The Decay of a Light Higgs Boson. *Nucl. Phys.*, B343:341–368, 1990.

[51] G. Ecker, J. Gasser, A. Pich, and E. de Rafael. The Role of Resonances in Chiral Perturbation Theory. *Nucl. Phys.*, B321:311–342, 1989.

[52] J. Einasto. On the Construction of a Composite Model for the Galaxy and on the Determination of the System of Galactic Parameters. *Trudy Astrofizicheskogo Instituta Alma-Ata*, 5:87–100, 1965.

[53] Rouven Essig, Eric Kuflik, Samuel D. McDermott, Tomer Volansky, and Kathryn M. Zurek. Constraining light dark matter with diffuse x-ray and gamma-ray observations. *Journal of High Energy Physics*, 2013(11):193, Nov 2013.

[54] Rouven Essig, Eric Kuflik, Samuel D. McDermott, Tomer Volansky, and Kathryn M. Zurek. Constraining Light Dark Matter with Diffuse X-Ray and Gamma-Ray Observations. *JHEP*, 11:193, 2013.

[55] Rouven Essig, Jeremy Mardon, Oren Slone, and Tomer Volansky. Detection of sub-GeV Dark Matter and Solar Neutrinos via Chemical-Bond Breaking. *Phys. Rev.*, D95(5):056011, 2017.

[56] Rouven Essig, Neelima Sehgal, and Louis E. Strigari. Bounds on cross sections and lifetimes for dark matter annihilation and decay into charged leptons from gamma-ray observations of dwarf galaxies. *Phys. Rev. D*, 80:023506, Jul 2009.

[57] E. Fabri and L. E. Picasso. Quantum field theory and approximate symmetries. *Phys. Rev. Lett.*, 16:408–410, Mar 1966.

[58] Mads T. Frandsen, Ulrich Haisch, Felix Kahlhoefer, Philipp Mertsch, and Kai Schmidt-Hoberg. Loop-induced dark matter direct detection signals from gamma-ray lines. *JCAP*, 1210:033, 2012.

[59] Marat Freytsis, Zoltan Ligeti, and Jesse Thaler. Constraining the Axion Portal with $B \to K l^+ l^-$. *Phys. Rev.*, D81:034001, 2010.

[60] A. M. Galper et al. The GAMMA-400 space observatory: status and perspectives. 2014.

[61] J. Gasser and H. Leutwyler. Chiral perturbation theory: Expansions in the mass of the strange quark. *Nuclear Physics B*, 250(1):465 – 516, 1985.

[62] J. Goldstone. Field theories with superconductor solutions. *Il Nuovo Cimento (1955-1965)*, 19(1):154–164, Jan 1961.

[63] Jeffrey Goldstone, Abdus Salam, and Steven Weinberg. Broken symmetries. *Phys. Rev.*, 127:965–970, Aug 1962.

[64] A. Gomez Nicola and J. R. Pelaez. Meson meson scattering within one loop chiral perturbation theory and its unitarization. *Phys. Rev.*, D65:054009, 2002.

[65] Dorival Goncalves, Pedro A. N. Machado, and Jose Miguel No. Simplified Models for Dark Matter Face their Consistent Completions. *Phys. Rev.*, D95(5):055027, 2017.

[66] Paolo Gondolo and Graciela Gelmini. Cosmic abundances of stable particles: Improved analysis. *Nucl. Phys.*, B360:145–179, 1991.

[67] Alma X. Gonzalez-Morales, Stefano Profumo, and Javier Reynoso-Córdova. Prospects for indirect MeV Dark Matter detection with Gamma Rays in light of Cosmic Microwave Background Constraints. *Phys. Rev.*, D96(6):063520, 2017.

[68] J. Greiner et al. GRIPS - Gamma-Ray Imaging, Polarimetry and Spectroscopy. *Exper. Astron.*, 34:551–582, 2012.

[69] Kim Griest and Marc Kamionkowski. Unitarity Limits on the Mass and Radius of Dark Matter Particles. *Phys. Rev. Lett.*, 64:615, 1990.

[70] Giovanni Grilli di Cortona, Edward Hardy, Javier Pardo Vega, and Giovanni Villadoro. The QCD axion, precisely. *JHEP*, 01:034, 2016.

[71] Benjamin Grinstein and Lisa Randall. The Renormalization of g^2. *Phys. Lett.*, B217:335–340, 1989.

[72] Ben Gripaios. Lectures on Effective Field Theory. 2015.

[73] Francisco Guerrero and Jose Antonio Oller. $K\bar{K}$ scattering amplitude to one loop in chiral perturbation theory, its unitarization and pion form-factors. *Nucl. Phys.*, B537:459–476, 1999. [Erratum: Nucl. Phys.B602,641(2001)].

[74] Wei Guo and Daniel N. McKinsey. Concept for a dark matter detector using liquid helium-4. *Phys. Rev.*, D87(11):115001, 2013.

[75] Thomas Hahn. Feynman Diagram Calculations with FeynArts, FormCalc, and LoopTools. *PoS*, ACAT2010:078, 2010.

[76] S. D. Hunter et al. EGRET observations of the diffuse gamma-ray emission from the galactic plane. *Astrophys. J.*, 481:205–240, 1997.

[77] Stanley D. Hunter et al. A Pair Production Telescope for Medium-Energy Gamma-Ray Polarimetry. *Astropart. Phys.*, 59:18–28, 2014.

[78] Fabio Iocco, Miguel Pato, Gianfranco Bertone, and Philippe Jetzer. Dark Matter distribution in the Milky Way: microlensing and dynamical constraints. *JCAP*, 1111:029, 2011.

[79] Seyda Ipek, David McKeen, and Ann E. Nelson. A Renormalizable Model for the Galactic Center Gamma Ray Excess from Dark Matter Annihilation. *Phys. Rev.*, D90(5):055021, 2014.

[80] N. Ishizuka and M. Yoshimura. Axion and Dilaton Emissivity From Nascent Neutron Stars. *Prog. Theor. Phys.*, 84:233–250, 1990.

[81] Roland Kaiser. Anomalies and WZW term of two flavor QCD. *Phys. Rev.*, D63:076010, 2001.

[82] Roland Kaiser and H. Leutwyler. Large N_c in chiral perturbation theory. *Eur. Phys. J.*, C17:623–649, 2000.

[83] Karol Kampf, Jiri Novotny, and Jaroslav Trnka. On different lagrangian formalisms for vector resonances within chiral perturbation theory. *Eur. Phys. J.*, C50:385–403, 2007.

[84] David B. Kaplan. Five lectures on effective field theory. 2005.

[85] S. Cheenu Kappadath. *Measurement of the Cosmic Diffuse Gamma-Ray Spectrum from 800 keV to 30 MeV*. PhD thesis, University of New Hampshire, May 1993.

[86] Stelios Kazantzidis, Lucio Mayer, Chiara Mastropietro, Jürg Diemand, Joachim Stadel, and Ben Moore. Density profiles of cold dark matter substructure: Implications for the missing-satellites problem. *The Astrophysical Journal*, 608(2):663, 2004.

[87] Vardan Khachatryan et al. Searches for invisible decays of the Higgs boson in pp collisions at $\sqrt{s} = 7$, 8, and 13 TeV. *JHEP*, 02:135, 2017.

[88] R. Kleiss, W. James Stirling, and S. D. Ellis. A new monte carlo treatment of multiparticle phase space at high-energies. *Comput. Phys. Commun.*, 40:359, 1986.

[89] Simon Knapen, Tongyan Lin, and Kathryn M. Zurek. Light Dark Matter: Models and Constraints. *Phys. Rev.*, D96(11):115021, 2017.

[90] Gordan Krnjaic. Probing Light Thermal Dark-Matter With a Higgs Portal Mediator. *Phys. Rev.*, D94(7):073009, 2016.

[91] Bastian Kubis. An Introduction to chiral perturbation theory. In *Workshop on Physics and Astrophysics of Hadrons and Hadronic Matter Shantiniketan, India, November 6-10, 2006*, 2007.

[92] Michael Kuhlen, Neal Weiner, Jurg Diemand, Piero Madau, Ben Moore, Doug Potter, Joachim Stadel, and Marcel Zemp. Dark Matter Direct Detection with Non-Maxwellian Velocity Structure. *JCAP*, 1002:030, 2010.

[93] Yoshitaka Kuno and Yasuhiro Okada. Muon decay and physics beyond the standard model. *Rev. Mod. Phys.*, 73:151–202, Jan 2001.

[94] Paul Langacker. The Physics of Heavy Z' Gauge Bosons. *Rev. Mod. Phys.*, 81:1199–1228, 2009.

[95] Benjamin W. Lee and Steven Weinberg. Cosmological Lower Bound on Heavy Neutrino Masses. *Phys. Rev. Lett.*, 39:165–168, 1977. [,183(1977)].

[96] H. Leutwyler. On the foundations of chiral perturbation theory. *Annals of Physics*, 235(1):165 – 203, 1994.

[97] Xuewen Liu, Ligong Bian, Xue-Qian Li, and Jing Shu. Type-III two Higgs doublet model plus a pseudoscalar confronted with $h \to \mu\tau$, muon $g-2$ and dark matter. *Nucl. Phys.*, B909:507–524, 2016.

[98] F. E. Low. Bremsstrahlung of very low-energy quanta in elementary particle collisions. *Phys. Rev.*, 110:974–977, 1958.

[99] Michele Maggiore. *A Modern introduction to quantum field theory*. Oxford University Press, 2005.

[100] Aneesh V. Manohar. Introduction to Effective Field Theories. In *Les Houches summer school: EFT in Particle Physics and Cosmology Les Houches, Chamonix Valley, France, July 3-28, 2017*, 2018.

[101] William J. Marciano, Cen Zhang, and Scott Willenbrock. Higgs Decay to Two Photons. *Phys. Rev.*, D85:013002, 2012.

[102] E. Marco, S. Hirenzaki, E. Oset, and H. Toki. Radiative decay of rho0 and phi mesons in a chiral unitary approach. *Phys. Lett.*, B470:20–26, 1999.

[103] Jeremy Mardon, Yasunori Nomura, Daniel Stolarski, and Jesse Thaler. Dark matter signals from cascade annihilations. *Journal of Cosmology and Astroparticle Physics*, 2009(05):016, 2009.

[104] Stephen P. Martin. A Supersymmetry primer. pages 1–98, 1997. [Adv. Ser. Direct. High Energy Phys.18,1(1998)].

[105] C. McNeile, A. Bazavov, C. T. H. Davies, R. J. Dowdall, K. Hornbostel, G. P. Lepage, and H. D. Trottier. Direct determination of the strange and light quark condensates from full lattice qcd. *Phys. Rev. D*, 87:034503, Feb 2013.

[106] R. Mertig, M. Bohm, and Ansgar Denner. FEYN CALC: Computer algebraic calculation of Feynman amplitudes. *Comput. Phys. Commun.*, 64:345–359, 1991.

[107] Yoichiro Nambu. Quasi-particles and gauge invariance in the theory of superconductivity. *Phys. Rev.*, 117:648–663, Feb 1960.

[108] J. F. Navarro, C. S. Frenk, and S. D. M. White. The Structure of Cold Dark Matter Halos. *The Astrophysical Journal*, 462:563, May 1996.

[109] J. Nebreda and J. R. Pelaez. Strange and non-strange quark mass dependence of elastic light resonances from SU(3) Unitarized Chiral Perturbation Theory to one loop. *Phys. Rev.*, D81:054035, 2010.

[110] Juan Nieves and Enrique Ruiz Arriola. Bethe-Salpeter approach for unitarized chiral perturbation theory. *Nucl. Phys.*, A679:57–117, 2000.

[111] Yasunori Nomura and Jesse Thaler. Dark Matter through the Axion Portal. *Phys. Rev.*, D79:075008, 2009.

[112] J. A. Oller and E. Oset. Chiral symmetry amplitudes in the S wave isoscalar and isovector channels and the σ, $f_0(980)$, $a_0(980)$ scalar mesons. *Nucl. Phys.*, A620:438–456, 1997. [Erratum: Nucl. Phys.A652,407(1999)].

[113] J. A. Oller and E. Oset. N/D description of two meson amplitudes and chiral symmetry. *Phys. Rev.*, D60:074023, 1999. [,165(1998)].

[114] J. A. Oller, E. Oset, and J. R. Pelaez. Meson meson interaction in a nonperturbative chiral approach. *Phys. Rev.*, D59:074001, 1999. [Erratum: Phys. Rev.D75,099903(2007)].

[115] Giuliano Panico and Andrea Wulzer. *Goldstone Boson Higgs*, pages 17–75. Springer International Publishing, 2016.

[116] C. Patrignani et al. Review of Particle Physics. *Chin. Phys.*, C40(10):100001, 2016.

[117] J. R. Pelaez. From controversy to precision on the sigma meson: a review on the status of the non-ordinary $f_0(500)$ resonance. *Phys. Rept.*, 658:1, 2016.

[118] Michael E. Peskin and Daniel V. Schroeder. *An Introduction to quantum field theory*. Addison-Wesley, Reading, USA, 1995.

[119] Planck Collaboration. Planck 2015 results - xiii. cosmological parameters. *A&A*, 594:A13, 2016.

[120] Maxim Pospelov, Adam Ritz, and Mikhail B. Voloshin. Secluded WIMP Dark Matter. *Phys. Lett.*, B662:53–61, 2008.

[121] Joaquim Prades. Massive spin 1 field chiral Lagrangian from an extended Nambu-Jona-Lasinio model of QCD. *Z. Phys.*, C63:491–506, 1994. [Erratum: Z. Phys.C11,571(1999)].

[122] John Preskill. Gauge anomalies in an effective field theory. *Annals Phys.*, 210:323–379, 1991.

[123] Mauro Raggi and Venelin Kozhuharov. Results and perspectives in dark photon physics. *Riv. Nuovo Cim.*, 38(10):449–505, 2015.

[124] P. Salucci, F. Nesti, G. Gentile, and C. F. Martins. The dark matter density at the Sun's location. *Astron. Astrophys.*, 523:A83, 2010.

[125] Stefan Scherer. *Introduction to Chiral Perturbation Theory*, pages 277–538. Springer US, Boston, MA, 2003.

[126] Martin Schmaltz and David Tucker-Smith. Little higgs theories. *Annual Review of Nuclear and Particle Science*, 55(1):229–270, 2005.

[127] Matthew D. Schwartz. *Quantum Field Theory and the Standard Model*. Cambridge University Press, 2014.

[128] Stuart L. Shapiro and Jessie Shelton. Weak annihilation cusp inside the dark matter spike about a black hole. *Phys. Rev.*, D93(12):123510, 2016.

[129] Jessie Shelton, Stuart L. Shapiro, and Brian D. Fields. Black hole window into p-wave dark matter annihilation. *Phys. Rev. Lett.*, 115(23):231302, 2015.

[130] Vladyslav Shtabovenko, Rolf Mertig, and Frederik Orellana. New Developments in FeynCalc 9.0. *Comput. Phys. Commun.*, 207:432–444, 2016.

[131] Tracy R. Slatyer. Indirect dark matter signatures in the cosmic dark ages. i. generalizing the bound on s-wave dark matter annihilation from planck results. *Phys. Rev. D*, 93:023527, Jan 2016.

[132] A. W. Strong, H. Bloemen, R. Diehl, W. Hermsen, and V. Schoenfelder. Comptel skymapping: A New approach using parallel computing. *Astrophys. Lett. Commun.*, 39:209, 1999.

[133] Andrew W. Strong, Igor V. Moskalenko, and Olaf Reimer. Diffuse galactic continuum gamma rays: A model compatible with egret data and cosmic-ray measurements. *The Astrophysical Journal*, 613(2):962, 2004.

[134] Gerard 't Hooft. Naturalness, chiral symmetry, and spontaneous chiral symmetry breaking. *NATO Sci. Ser. B*, 59:135–157, 1980.

[135] M. Tavani et al. Science with e-ASTROGAM (A space mission for MeV-GeV gamma-ray astrophysics). 2017.

[136] D. J. Thompson et al. Calibration of the Energetic Gamma-Ray Experiment Telescope (EGRET) for the Compton Gamma-Ray Observatory. *Astrophys. J. Suppl.*, 86:629–656, 1993.

[137] Patrick Tunney, Jose Miguel No, and Malcolm Fairbairn. Probing the pseudoscalar portal to dark matter via $\bar{b}bZ(\to \ell\ell)+ \not{E}_T$: From the LHC to the Galactic Center excess. *Phys. Rev.*, D96(9):095020, 2017.

[138] C. Vafa and E. Witten. Restrictions on symmetry breaking in vector-like gauge theories. *Nuclear Physics B*, 234(1):173 – 188, 1984.

[139] M. Voloshin and V. Zakharov. Measuring quantum-chromodynamic anomalies in hadronic transitions between quarkonium states. *Phys. Rev. Lett.*, 45:688–691, Sep 1980.

[140] Steven Weinberg. A New Light Boson? *Phys. Rev. Lett.*, 40:223–226, 1978.

[141] Steven Weinberg. Phenomenological lagrangians. *Physica A: Statistical Mechanics and its Applications*, 96(1):327 – 340, 1979.

[142] J. Wess and B. Zumino. Consequences of anomalous Ward identities. *Phys. Lett.*, 37B:95–97, 1971.

[143] Edward Witten. Global aspects of current algebra. *Nuclear Physics B*, 223(2):422 – 432, 1983.

[144] Xin Wu, Meng Su, Alessandro Bravar, Jin Chang, Yizhong Fan, Martin Pohl, and Roland Walter. PANGU: A High Resolution Gamma-ray Space Telescope. *Proc. SPIE Int. Soc. Opt. Eng.*, 9144:91440F, 2014.